

# Recent Advances in Fluorinated Graphene from Synthesis to Applications: Critical Review on Functional Chemistry and Structure Engineering

Xinyu Chen, Kun Fan, Yang Liu, Yu Li, Xiangyang Liu,\* Wei Feng,\* and Xu Wang\*

Fluorinated graphene (FG), as an emerging member of the graphene derivatives family, has attracted wide attention on account of its excellent performances and underlying applications. The introduction of a fluorine atom, with the strongest electronegativity (3.98), greatly changes the electron distribution of graphene, resulting in a series of unique variations in optical, electronic, magnetic, interfacial properties and so on. Herein, recent advances in the study of FG from synthesis to applications are introduced, and the relationship between its structure and properties is summarized in detail. Especially, the functional chemistry of FG has been thoroughly analyzed in recent years, which has opened a universal route for the functionalization and even multifunctionalization of FG toward various graphene derivatives, which further broadens its applications. Moreover, from a particular angle, the structure engineering of FG such as the distribution pattern of fluorine atoms and the regulation of interlayer structure when advanced nanotechnology gets involved is summarized. Notably, the elaborated structure engineering of FG is the key factor to optimize the corresponding properties for potential applications, and is also an up-to-date research hotspot and future development direction. Finally, perspectives and prospects for the problems and challenges in the study of FG are put forward.

Nevertheless, the applications of graphene are usually limited by its inherent shortcomings. For example, the zero bandgap of pristine graphene prevents effective on-off state transition and thus hinders the straightforward application in field-effect transistor (FET).<sup>[10,12,13]</sup> The typical chemical inertness makes graphene exhibit low activity in catalysis as well as low selectivity in adsorption and separation.<sup>[9,14–16]</sup> The powerful van der Waals force between graphene nanosheets and the lack of active groups on the surface lead to its poor dispersibility and processability.<sup>[13,17–19]</sup> To solve these problems, various physicochemical modification methods have been employed, such as confined graphene nanoribbon,<sup>[20–23]</sup> graphene-based heterojunction,<sup>[24–27]</sup> and graphene derivatives engineering.<sup>[12,13]</sup>

Fluorinated graphene (FG;  $\text{CF}_x$ ,  $x = 0–1.1$ ) is achieved by covalently or ionically bonding fluorine atoms with a certain amount of carbon atoms in the graphene skeleton, which has obtained the increasing of attentions from synthesis


from application (Scheme 1).<sup>[28–33]</sup> As a significant and unique graphene derivative, FG was first prepared through fluorination of graphene and mechanical exfoliation of graphite fluoride by Geim et al.<sup>[28]</sup> and Otyepka et al.<sup>[29]</sup> in 2010, respectively. Due to the specific physicochemical properties of fluorine and corresponding C–F bonds, FG exhibits many exceptional properties compared with other graphene derivatives and thus attracts interdisciplinary attentions and interests.<sup>[29,30,34–44]</sup> Fluorine atoms have the strongest electronegativity (3.98) among all of the atoms, and the introduction of fluorine atom greatly changes electron distribution of pristine graphene, which results in a series of unique variations in optical and electric properties.<sup>[34–38]</sup> For instance, the introduced C–F bonds destroy the original 2D conjugated structure of graphene and largely open the bandgap, which brings about a tunable bandgap with the different F/C ratios in the range of 0–3.8 eV.<sup>[30,34,36–38]</sup> Fluorine atoms bound on the skeleton of graphene could augment the interlayer distance and limit the stacking of sheets, thus endowing FG with the excellent dispersibility and superb tribological properties as well as peculiar surface properties.<sup>[39,44]</sup> Furthermore, the introduction of fluorine atoms alters the hybridization of carbon atoms from  $\text{sp}^2$  to

## 1. Introduction

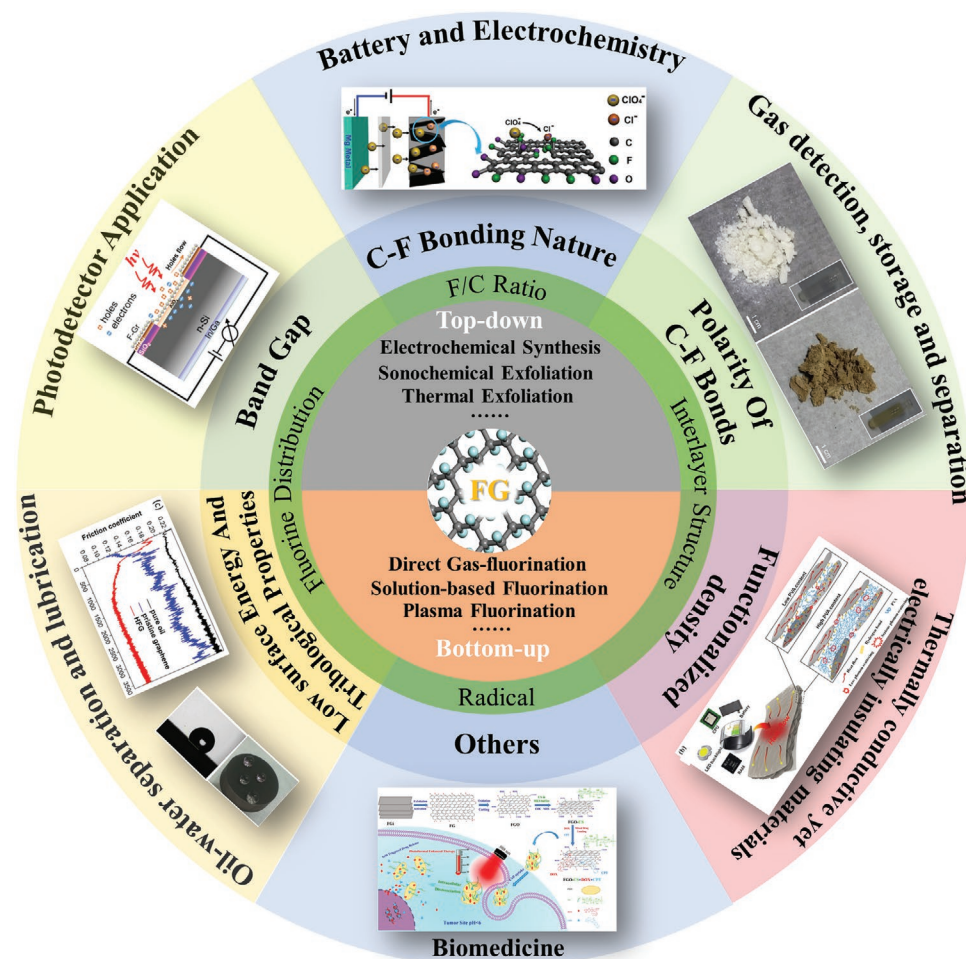
As the first truly 2D crystal material, the appearance of isolated high-quality graphene in 2004 brought the research upsurge of various 2D materials.<sup>[1–7]</sup> Due to the exceptional properties and performances of graphene and graphene-based materials, this carbon nanomaterial has been intensely investigated by numerous research groups with different backgrounds.<sup>[8–11]</sup>

X. Chen, K. Fan, Dr. Y. Liu, Prof. X. Liu, Prof. X. Wang  
College of Polymer Science and Engineering  
State Key Laboratory of Polymer Material and Engineering  
Sichuan University  
Chengdu 610065, P. R. China  
E-mail: lxy6912@sina.com; wangxu@scu.edu.cn

Prof. Y. Li, Prof. W. Feng  
School of Materials Science and Engineering  
Tianjin University  
Tianjin 300354, P. R. China  
E-mail: weifeng@tju.edu.cn

 The ORCID identification number(s) for the author(s) of this article can be found under <https://doi.org/10.1002/adma.202101665>.

DOI: 10.1002/adma.202101665



**Scheme 1.** Illustrative image of the synthesis strategies, peculiarities, and applications of fluorinated graphene. Image for “Battery and electrochemistry”: Reproduced with permission.<sup>[97]</sup> Copyright 2015, Wiley-VCH. Image for “Gas detection”: Reproduced with permission.<sup>[98]</sup> Copyright 2019, Elsevier. Image for “Thermally conductive yet electrically insulating material”: Reproduced with permission.<sup>[55]</sup> Copyright 2019, American Chemical Society. Image for “Biomedicine”: Reproduced with permission.<sup>[60]</sup> Copyright 2017, Wiley-VCH. Image for “Tribological performance”: Reproduced with permission.<sup>[47]</sup> Copyright 2018, American Chemical Society. Image for “Low surface energy”: Reproduced with permission.<sup>[99]</sup> Copyright 2013, Wiley-VCH. Image for “Photoelectric detection”: Reproduced with permission.<sup>[100]</sup> Copyright 2019, American Chemical Society.

$sp^3$  and simultaneously introduces defects in the lattice, which produces local magnetic moment and thus gives FG the adjustable magnetic properties.<sup>[42,43]</sup> In 2016, Feng et al. summarized the intrinsic physical properties of FG and the initial applications.<sup>[32]</sup> However, many new advances have been realized during the latest 5 years. For example, some novel applications of FG have been reported in lubrication,<sup>[45–50]</sup> ice resistance,<sup>[44]</sup> thermally conductive yet electrically insulating materials,<sup>[51–55]</sup> biomedicine,<sup>[56–62]</sup> and batteries.<sup>[63–71]</sup>

Apart from physical properties, chemical properties of FG have been thoroughly analyzed as one important direction in recent years.<sup>[33,72–83]</sup> Although classical organic chemistry generally believes that the C–F bond has a large bond energy and thus are chemical inert, the special nature of the C–F bond that originates from the 2D structure of this carbon material enhances its chemical reactivity significantly. For this aspect, Otyepka et al. introduced the derivative chemistry of FG in a mini review in 2017<sup>[33]</sup> Thereafter, the in-depth mechanism of derivative chemistry and its expansive applications were further

investigated.<sup>[77,84,85]</sup> Meanwhile, a variety of derivative reactions have been explored on FG surface recently, such as nucleophilic substitution,<sup>[72,73,76,81,82,86–90]</sup> free radical grafting,<sup>[80,91]</sup> and some classical organic chemistry processes like Friedel–Crafts reaction,<sup>[77]</sup> Suzuki–Miyaura reaction,<sup>[83]</sup> and Sonogashira C–C cross-coupling reaction.<sup>[78]</sup> This opens a universal route for the functionalization and even multifunctionalization of the graphene skeleton toward various graphene derivatives.

In addition, the advanced nanotechnology gets involved in recent years, and researchers have focused on the structure engineering of FG, such as pattern of fluorine distribution,<sup>[92–96]</sup> which pushes the investigations of FG to a new climax. The elaborated structure engineering of FG is the key factor to optimize the physicochemical performances, by which we could differentiate the specific contributions from different structures of FG to its properties. This would provide guidance for designing particular FGs so as to promote their practical applications. Notably, the structure engineering of FG largely depends on the study on its chemistry such as its synthesis

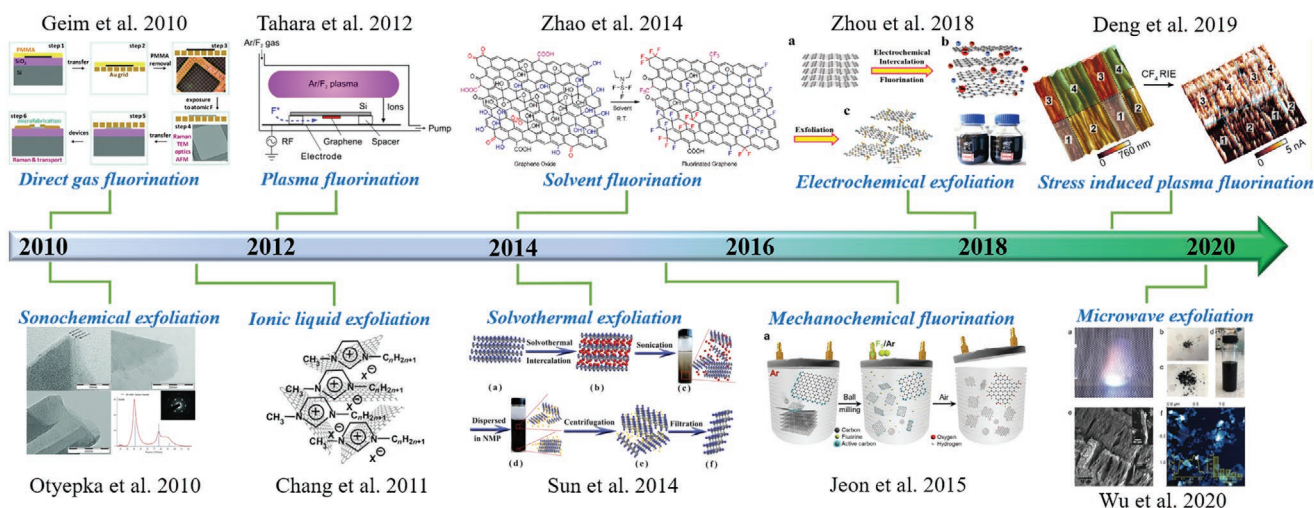


**Figure 1.** Timeline showing synthetic methods for FG in the past decade. Image for “Direct gas fluorination”: Reproduced with permission.<sup>[28]</sup> Copyright 2010, Wiley-VCH. Image for “Sonochemical exfoliation”: Reproduced with permission.<sup>[29]</sup> Copyright 2010, Wiley-VCH. Image for “Plasma fluorination”: Reproduced with permission.<sup>[132]</sup> Copyright 2012, American Institute of Physics. Image for “Ionic liquid fluorination”: Reproduced with permission.<sup>[103]</sup> Copyright 2011, Wiley-VCH. Image for “Solvent fluorination”: Reproduced with permission.<sup>[112]</sup> Copyright 2014, The Royal Society of Chemistry. Image for “Solvothermal exfoliation”: Reproduced with permission.<sup>[102]</sup> Copyright 2014, The Royal Society of Chemistry. Image for “Mechanochemical fluorination”: Reproduced with permission.<sup>[69]</sup> Copyright 2015, Wiley-VCH. Image for “Electrochemical fluorination”: Reproduced with permission.<sup>[120]</sup> Copyright 2018, American Chemical Society. Image for “Stress-induced plasma fluorination”: Reproduced with permission.<sup>[92]</sup> Copyright 2019, American Chemical Society. Image for “Microwave fluorination”: Reproduced with permission.<sup>[122]</sup> Copyright 2019, Wiley-VCH.

chemistry and derivative reactions, which provides the theoretical foundations and technical support for better completing the fine structure engineering of FG. Finally, this would realize to customize the FG products for meeting the needs of different application fields.<sup>[33,84,85]</sup>

Therefore, this review mainly focuses on the up-to-date research progress of FG and the introduction of FG would start from the following three aspects. 1) A comprehensive review of the synthesis methods, intrinsic physical properties, and applications, especially including new progress in the past 5 years. 2) Systematical descriptions of the functional chemistry of FG and the corresponding mechanism and applications. 3) Structure engineering of FG including the regulation of fluorine types, fluorine distribution, phase region, radical density, interlayer structure, etc. In addition, based on the present achievements, we also put forward our own views and prospects for the problems and challenges in the area. We hope such integral review of FG from synthesis to applications, especially including the critical review on its functional chemistry and structure engineering, can also offer a guidance for other 2D materials toward targeted and precise modifications.

## 2. Synthesis of FG

We summarize the development of synthetic methods for FG using a timeline, as shown in **Figure 1**. In general, the synthesis strategies of FG contain two approaches: the top-down synthesis and the bottom-up synthesis. The top-down approach shows universality and is frequently employed in the preparation of other 2D materials, such as boron nitride, black phosphorus, transition metal sulfide, and so on.<sup>[4–6]</sup> Here, the synthesis of FG chooses the commercially available fluorinated graphite

(FGi) as the raw material. The van der Waals force among the sheets is destroyed under the action of heat,<sup>[101,102]</sup> solvent,<sup>[103–105]</sup> or ultrasound,<sup>[29,106,107]</sup> thereby obtaining single-/few-layer FG. This method avoids the participation of poisonous fluorine sources (fluorine gas, xenon difluoride, etc.) and could be operated in the laboratory without special equipment. The latter one chooses graphene, graphene oxide (GO), and reduced graphene oxide (rGO) as the starting materials and utilizes the fluorine gas,<sup>[108,109]</sup> xenon difluoride,<sup>[28,30,31]</sup> and other organic/inorganic fluorine source<sup>[110–115]</sup> as the fluorine reagents. With the rapid development of graphene materials nowadays, this approach presents a great potential as a scalable production method. In addition, through optimizing its reaction conditions (solvent, temperature, pressure, reaction time, etc.), it is feasible to customize the special structure of FG, such as the C–F bonding nature and the distribution of fluorine atoms.

### 2.1. Top-Down Synthesis

Top-down exfoliation method is widely applied in preparing 2D materials because of its simplicity and nondestruction. In this way, some high-quality 2D materials have been prepared.<sup>[116–118]</sup> In the typical exfoliation process, under the action of external energy, some small molecules of the intercalation agent, such as sulfolane,<sup>[29]</sup> *N*-methyl-2-pyrrolidone (NMP),<sup>[107]</sup> ethylenediamine (EDA),<sup>[119]</sup> chloroform,<sup>[102]</sup> acetonitrile,<sup>[102]</sup> and ionic liquids<sup>[103,104,115]</sup> access the interlayer of the bulk materials and destroy the van der Waals force between the neighboring sheets, which isolates the 2D nanosheets with mono/multilayer structure. The top-down synthesis of FG is roughly divided into the following types: solvent-assisted sonochemical exfoliation, thermal exfoliation, and so on.



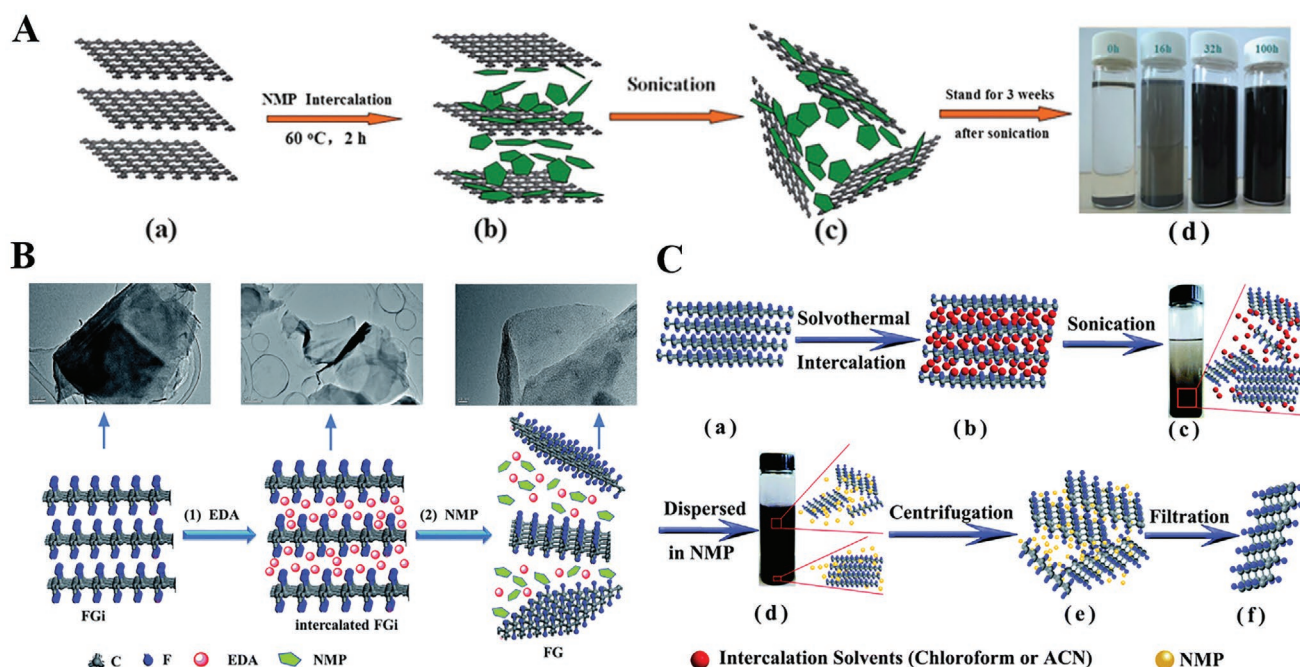


**Figure 2.** A) Schematic diagram of exfoliation process for FG dispersion by using NMP as the intercalation agent. Reproduced with permission.<sup>[107]</sup> Copyright 2012, The Royal Society of Chemistry. B) Illustrative image of preparation process for FG under ultrasonic using ethylenediamine an auxiliary intercalation agent. Reproduced with permission.<sup>[119]</sup> Copyright 2014, The Royal Society of Chemistry. C) Illustrative image of the preparation process of FG sheets under solvothermal condition by employing chloroform and acetonitrile as the intercalation agent. Reproduced with permission.<sup>[102]</sup> Copyright 2014, The Royal Society of Chemistry.

### 2.1.1. Solvent-Assisted Sonochemical Exfoliation

The solvent-assisted sonochemical exfoliation method has been well applied for a number of 2D nanomaterials.<sup>[5,6]</sup> Under the action of ultrasound, the shock wave generated by the collapse of bubbles in the liquid will pass through the layered bulk crystals, thus causing the bulk crystals exfoliated into thin layer of sheets with the assistance of solvent. Zbořil et al. utilized sulfolane as the intercalation agent to exfoliate the FGI (F/C = 1) in a 135 W ultrasonic bath and the monolayer FG sheets with a large bandgap of 3.1 eV were successfully obtained.<sup>[29]</sup> Chang et al. employed ionic liquid (1-butyl-3-methylimidazolium bromide) as the intercalation agent to accelerate exfoliation process and achieved some monolayer or few-layer FG sheets with an F/C ratio of about 0.25 or 0.50 and a 2–10 μm lamellar size.<sup>[103]</sup>

NMP is also extensively used for the exfoliation of FGI because of its high dipole moment (4.09 D), which can interact with C–F bonds and weaken the interaction between FGI layers. Gong et al. introduced NMP to intercalate FGI at 60 °C under a refluxing condition for the first time and the succedent exfoliation was promoted by an ultrasonication of 100 h to obtain the monolayer FG.<sup>[107]</sup> Meanwhile, it was confirmed that FG disposed by polar aprotic solvents showed a significant elimination of C–F bonds during the exfoliation (Figure 2A-d),<sup>[107]</sup> which proved the reactivity of the C–F bond in FG sheets. Based on this phenomenon, Hou et al. added EDA to the NMP solution as an auxiliary intercalation agent to synergistically exfoliate FGI under ultrasonic (Figure 2B). Compared with NMP, EDA not only promoted to the intercalation

process, but also in situ react with FG sheets due to its strong nucleophilicity.<sup>[119]</sup>

Overall, the laminar size and the fluorine content as well as the properties of FG can be regulated by changing the solvent system, the ultrasonic power and additives. But the yield of the single-layer nanosheets through the exfoliation suspension is always low, which would be not conducive to explore some extraordinary properties of FG based on corresponding single-layer form. In addition, the lateral size of the obtained FG sheets is small, which may be attributed to the high defect density in FGI (always prepared by F<sub>2</sub> fluorination at a high temperature of about 600 °C). Therefore, it is necessary to focus the further research on ascertaining the kinetics and dynamics in the exfoliation process, in order to prevent the defluorination and the fragmentation of FG nanosheets.

### 2.1.2. Solvothermal Exfoliation

Apart from ultrasonic exfoliation, solvothermal exfoliation was also widely used in the preparation of FG. During the exfoliation process, both high pressure and high temperature can weaken the van der Waals interaction between the adjacent lamellar, thus enable the intercalation agent molecules effectively intercalate into FGI layers. In order to avoid the destruction of FG at high temperature, Feng et al. employed chloroform and acetonitrile as the intercalation agent to exfoliate FGI under solvothermal condition<sup>[102]</sup> (Figure 2C). In general, the solvothermal exfoliation chiefly relied on the aeration of solvent with a liquid state. Compared with NMP, chloroform and acetonitrile



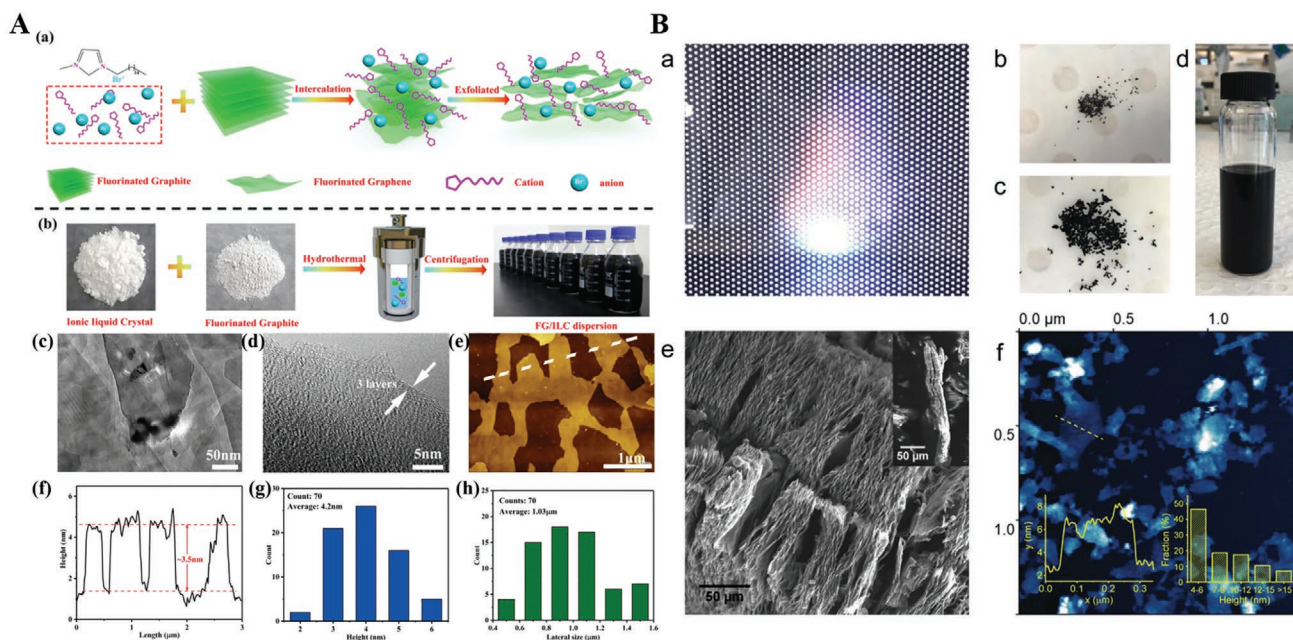


**Figure 3.** A) a,b) Schematic diagram of the ILC-assisted hydrothermal exfoliation process of FG. c,d) TEM and HRTEM images of the prepared FG nanosheets. e–h) AFM images and the corresponding height profiles, thickness histogram, and lateral size of FG, respectively. A) Reproduced with permission.<sup>[104]</sup> Copyright 2020, Elsevier. B) a) Photographs of the dazzling sparks generated by FG in microwave through microwave-induced plasma (MIP) treatment. b,c) Optical images of FG sheets before (b) and after (c) the MIP treatment, the latter exhibiting a significant color change and volume expansion. d) The formed steady FG suspension in NMP solution after moderate ultrasound and centrifugalization. e) SEM image of the gravely inflated FG and pristine FGi (inset). f) AFM photograph of the exfoliated FG nanosheets. B) Reproduced with permission.<sup>[122]</sup> Copyright 2019, Wiley-VCH.

with lower boiling point could fully gasify under a lower temperature, thus avoiding breaking the C–F bonds and reducing the corresponding F/C ratio.<sup>[102]</sup> Tian et al. developed an environment-friendly and effective hydrothermal exfoliation means using ionic liquids crystal (ILC) as the intercalator (Figure 3A). The essential rule of the method is to insert the cations with a small ion radius into the crystals' interlayer to form the ion intercalation compound, and then the ion intercalation can dramatically dilate the interlayer distance and reduce the van der Waals interactions between the neighboring sheets. Simultaneously, the noncovalent interactions fall in between made the obtained FG solution exhibit excellent dispersibility (more than 3 months without sediment).<sup>[104]</sup>

Solvothermal exfoliation method is a brief and efficient means to obtain the FG nanosheets. However, this method is a one-pot method under an airtight system, which thus lacks satisfactory explanations for the theoretical study, therefore, limitation continually occurs in the solvothermal exfoliation method. Also, how to accurately regulate the thickness and lateral size of the obtained FGs is still troublesome. Furthermore, avoiding the side reactions between solvents and FG sheets in solvothermal conditions is also crucial for the acquisition of high-quality FG sheets.

### 2.1.3. Other Exfoliation Methods

Recently, some more exfoliation methods have also been developed, which continuously enriched the synthesis strategies of FG. Jankovský et al. reported the direct thermal exfoliation of

FGi at a high temperature (400–1000 °C) in a quartz reactor. The thermal treatment of FGi enhanced the interlayer pressure because of the decomposition of fluorinated-related groups, thereby expanding its interlayer distance and subsequent forming partial reduced FG that exhibited an expanded “worm-like” morphology.<sup>[101]</sup> Zhou et al. demonstrated a productive electrochemical method to exfoliate graphite into highly solution-processable FG, but the products showed an extremely low fluorine content (only 3 at%).<sup>[120]</sup> Zhang et al. utilized melamine to exfoliate FGi by ball milling. This method avoided the use of solvent and produced monolayer FG in a high yield.<sup>[105]</sup> However, it is needed for further developing this approach to remove the destructive effect caused by the strong shear. Of course, from another angle, it can be considered as a conducive method for preparing fluorinated graphene quantum dots with smaller size.<sup>[121]</sup>

In addition, Wu et al. demonstrated an unconventional microwave-based means to obtain few-layer and partially fluorinated graphene recently (Figure 3B). The reaction occurred upon the generation of “microwave induced plasma” in seconds, which resulted in the decomposition and the volume expansion of FG during delamination.<sup>[122]</sup> With a small amount of graphite as catalyst, the heat generated by microwave irradiation on the graphite surface was converted into the input energy for exfoliating, which further accelerated the exfoliation process. Then, the highly fluffy FGi was dispersed in the icy NMP solution prior to sonication for about 20 min. During the microwave treatment, FGi had about 70% weight loss, which indicated the obvious defluorination and the restoration of aromatic regions. Notably, how to limit the defluorination behavior

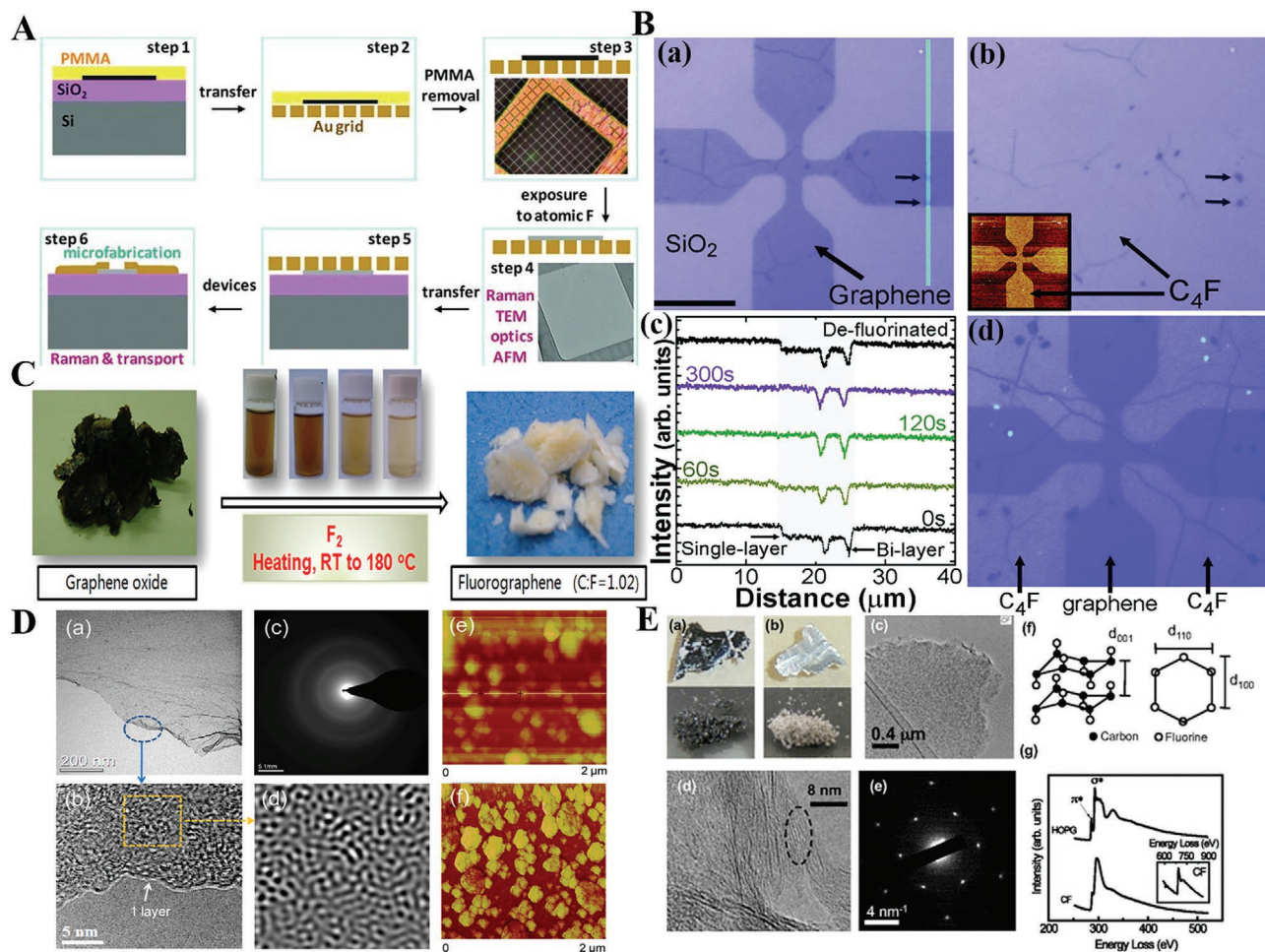


**Figure 4.** A) Schematic illustration of the fluorination process and the subsequent transfer and devices fabrication procedure. Reproduced with permission.<sup>[28]</sup> Copyright 2010, Wiley-VCH. B) Optical variation for graphene after fluorination. Reproduced with permission.<sup>[30]</sup> Copyright 2010, American Chemical Society. C) Photographs of the fluorinated (right) and nonfluorinated GO (left), the inset shows the ethanol dispersion of FGO with different fluorine content. D) a,b) TEM and HRTEM images of the FG samples with an F/C ratio of  $\approx 1.02$ , denoted as FGO-3 in (C). c) Selected-area electron diffraction pattern of FGO-3. d) Magnified image of the selected area in (b). e,f) AFM image and the corresponding phase diagram of FG sheets. C,D) Reproduced with permission.<sup>[108]</sup> Copyright 2013, American Chemical Society. E) a,b) Optical images before and after fluorination of HOPG (top) and conventional graphite (bottom). c) TEM image of the fluorinated HOPG sheets. e) Electron diffraction pattern of the fluorinated HOPG. f) Detailed parameters of the fluorinated sample. g) The K-edge of carbon atoms in the HOPG and fluorinated HOPG (electron energy loss spectroscopy data). E) Reproduced with permission.<sup>[109]</sup> Copyright 2010, The American Physical Society.

seems to be the general problem on the exfoliation methods of FG.<sup>[122]</sup>

## 2.2. Bottom-Up Synthesis

Alternative to top-down exfoliation, bottom-up approaches of producing FG allow for better control their fluorine content and C–F bonds' types with high efficiency and adjustability. Meanwhile, the gradual maturity and the industrialization of graphene preparation technology significantly promote the rising of this bottom-up synthesis strategy of FG.<sup>[10,13]</sup> By employing different kinds of raw materials/fluorine sources and various reaction conditions, FGs with diverse fluorinated degree were obtained and the bonding nature of C–F bond is controllable.<sup>[30,108,110,112,123,124]</sup> Herein, bottom-up synthesis is roughly

divided into the following several types: direct gas fluorination, solvent fluorination, plasma fluorination, mechanochemical fluorination, etc.

### 2.2.1. Direct Gas Fluorination

The direct gas fluorination is a common method for preparing carbon fluoride materials with gaseous fluorinating reagent, such as  $F_2$  and xenon difluoride ( $XeF_2$ ). Through controlling of the pressure, time, and temperature, the fluorinated degree can be easy to regulate. In 2010, Nair et al. used  $XeF_2$  as the fluorine source to prepare FG first (Figure 4A). They transferred the graphene film grown on silicon substrate to gold grid and then placed them in  $XeF_2$  atmosphere to obtain a double-sided fluorinated graphene by controlling reaction conditions.<sup>[28]</sup>



Robinson et al. prepared FG films with different fluorine contents through  $\text{XeF}_2$  direct fluorination, as well (Figure 4B). They, respectively, used copper and  $\text{SiO}_2/\text{Si}$  substrates to support the graphene sheets for fluorination and found  $\text{XeF}_2$  was difficult to etch the copper substrate, so the graphene on copper substrate only transformed into a single-sided fluorinated graphene with a fluorine content of 25% ( $\text{C}_4\text{F}$ ). While  $\text{F}_{1.0}\text{G}_{1.0}$  was obtained when  $\text{SiO}_2/\text{Si}$  substrate was applied thanks to that highly reactive  $\text{XeF}_2$  gas effectively etched the Si substrate.<sup>[30]</sup>

Fluorine gas ( $\text{F}_2$ ) is another vital reagent for preparing FG on account of the extremely high reactivity and the low cost. In 2013, Wang et al. first utilized  $\text{F}_2$  to react with honeycombed GO and successfully achieved a series of FGs with different C/F ratios (0.65, 0.84, and 1.02) at 180 °C through adjusting the concentration of  $\text{F}_2$  (Figure 4C,D). In the heating process, through the cleavage of the oxygen-related groups from GO sheets, the distance between stacked layers would be further enlarged by the inflated gas and more monolayer FG sheets were formed, which was conducive to obtain a high fluorinated degree by fluorinating both the sides of FG sheets. Furthermore, the cleaved oxygen-related groups facilitated the diffusion of the  $\text{F}_2$  and improved the uniformity degree of fluorination.<sup>[108]</sup> Cheng et al. established a method to synthesize multilayer FG by direct fluorinating highly ordered pyrolytic graphite (HOPG) with  $\text{F}_2$  at about 600 °C for 36–48 h, while the corresponding F/C ratio is about 0.7 (Figure 4E). Based on the crystal structure, it was found that the in-plane lattice distance of the corresponding FG was much larger than that of the original graphene (Figure 4E-f).<sup>[109]</sup> Mazánek et al. presented a simplified and direct fluorination method to synthesize FG from graphene powder materials using the autoclave under a  $\text{F}_2/\text{N}_2$  atmosphere with different times and temperatures (20, 180 °C), and multifarious FG with different fluorinated degree was obtained by their simple fluorination procedure.<sup>[123]</sup> In order to further reduce fluorinating temperature, Wang et al. used activated graphene with much porous structure as the starting material to prepare fluorinated porous graphene (FPG). Due to the introduction of meso- and micropores in graphene sheets, the fluorinated products were successfully obtained even at room temperature and it achieved a high F/C ratio of 0.67.<sup>[125]</sup> Obviously, defect structures (porous structure, oxygen-related groups, etc.) in the graphene sheets were proved to have activation effect on the direct fluorination and decrease the fluorination temperature.

As a typical gas–solid reaction, it is easy to trace and even in situ monitor the reaction process of the direct gas fluorination. This thus achieves to study the reaction mechanism meticulously and guide the preparation of FG with a fine structure, especially for the fluorination of single-layer graphene materials. Nevertheless, for the fluorination graphene powder materials, their gas–solid fluorination reaction is inevitably affected by diffusion of gaseous fluorinating reagent, which always leads to the heterogeneity structure and the nonuniform properties. Besides, the quality of FG products will be seriously impacted by the nondeterminacy of the graphene raw materials. Therefore, it is still a challenge to realize the large-scale synthesis of the highly qualified FG. Further investigations should aim at the improving of the raw material quality and the investigation of the fluorination reaction process and its mechanism, such as

clarifying the initial reaction sites, the fluorination dynamics, and the relationship between phase evolution and structure.

## 2.2.2. Solvent Fluorination

The solvent fluorination is also a feasible method to synthesize FG with the participation of different liquid fluorine-containing sources (HF, diethylaminosulfurtrifluoride (DAST),  $\text{BF}_3$ , etc.).<sup>[110–114]</sup> For this method, GO or rGO with a high reactivity was always employed as the raw materials. Compared with direct gas fluorination, the uniformity of solvent fluorination is better owing to homogenous solvent environment. Through changing the solvent types, it is feasible to further change the structure and property of FG. The use of mixed solvents can synergistically regulate the structure and property of FG and thus create the abundant reaction chemistry.<sup>[110–114]</sup> Wang et al. prepared FG through the reaction between dispersed GO and HF solution. By changing the amount of HF, the reaction time, and the temperature, the F/C ratio of FG was easily adjusted.<sup>[110]</sup> Zhao et al. demonstrated the preparation of FG in an acetonitrile solution at room temperature with GO as starting materials. After disposed by DAST, the oxygen-containing groups in GO was substituted by fluorine-related groups, which realized the conversion from GO into FG, and the fluorine content of FG can be tuned by altering the polarity of solvent.<sup>[112]</sup> Aguilar-Bolados et al. reported the solvent fluorination reaction of two different kinds of GOs. Tetrafluoroborate of diethylaminodifluorosulfonium was used as the fluorination reagent. It was found that the GO produced by Hummers' method showed a lower reactivity than that of Brodie's method. Their study showed that the types of oxygen-containing groups had a great influence on the fluorination process.<sup>[113]</sup> Samanta et al. reported the synthesis of FG from GO in  $\text{BF}_3$ -etherate solution in gram scale, and the maximum value of fluorine was up to 38 wt%, while the obtained FG nanosheets were still hydrophilic due to the coexistence of residual oxygen groups.<sup>[111]</sup> Recently, ionic liquids were selected as environmentally friendly reagent to substitute the volatile organic solvents.<sup>[104,114]</sup> Jahan-shahi et al. exploited a high-efficiency and eco-friendly means to prepare FG under moderate conditions by using  $\text{NH}_4\text{F}$  salt as the fluorine source and triethylammonium trifluoroacetate as an acidic ionic liquid. They preoxidized graphene first and converted it into GO to facilitate the fluorination process, and the subsequently obtained FG possessed an extremely high F/C ratio of 2.2. Moreover, their research further suggested that the protonated oxygen-related groups of GO were easily converted into fluorine-related groups of FG in acidic system.<sup>[114]</sup>

Compared with direct gas fluorination, the uniformity of solvent fluorination is better owing to homogenous solvent environment. Through changing the solvent types, we could further change the structure and property of FG. Of course, the use of mixed solvents may synergistically regulate the structure and property of FG, thereby creating the abundant reaction chemistry. However, existing solvents are a threat for natural environment. Meanwhile, the separation and purification processes between solvents and FG products are always complicated and power-wasting, thereby leading to the higher production cost. Notably, the unexpected anew stacking always occurs for



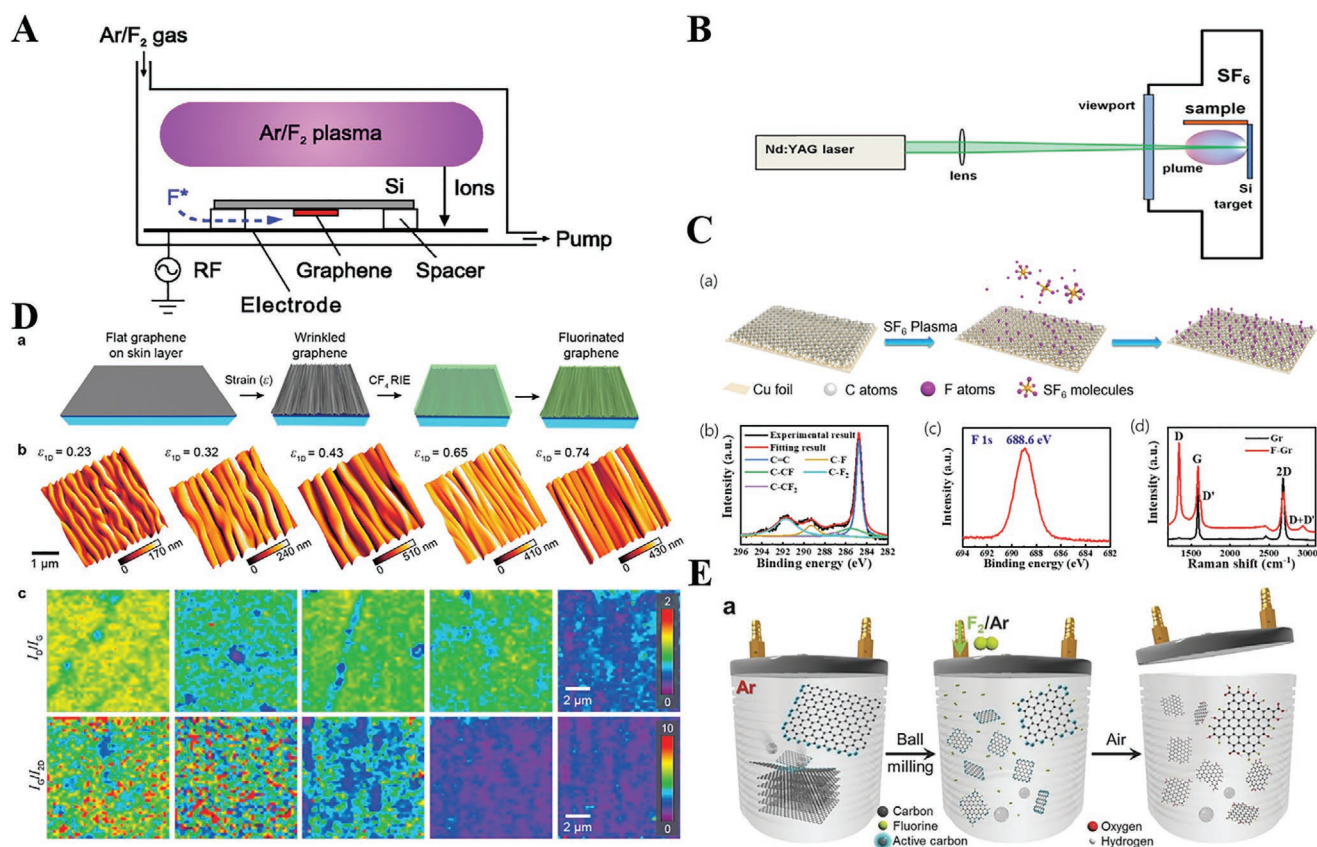


**Figure 5.** A) Schematic diagram of the reaction system utilized for the preparation of FG in Ar/F<sub>2</sub> plasma. Reproduced with permission.<sup>[132]</sup> Copyright 2012, American Institute of Physics. B) Schematic images of fluorination process under the SF<sub>6</sub> fluorine source. Reproduced with permission.<sup>[128]</sup> Copyright 2019, Elsevier. C) Schematic diagram of the fluorination procedure and the corresponding XPS spectra and Raman spectra. Reproduced with permission.<sup>[100]</sup> Copyright 2019, American Chemical Society. D) a) Schematic illustration of the fabrication and fluorination of wrinkled graphene. b) AFM photographs of the wrinkled graphene with different degree of strain relief. c)  $I_D/I_G$  mapping for wrinkled graphene with diverse strain. D) Reproduced with permission.<sup>[92]</sup> Copyright 2019, American Chemical Society. E) Schematic illustration of the preparation of the edge-fluorinated graphene nanoplatelets by ball-milling method. Reproduced with permission.<sup>[69]</sup> Copyright 2015, Wiley-VCH.

nanomaterials of FG accompanied by the separation of solvents, which seriously influence the corresponding structure and property.

### 2.2.3. Plasma Fluorination

Apart from direct gas fluorination and solution fluorination, plasma fluorination as another important approach is frequently used in the preparation of FG (Figure 5A). Compared with direct gas fluorination, plasma fluorination is considered to be a controllable and clean method for the preparation of FG. During the process of plasma fluorination, the formed fluorine radicals were adsorbed on graphene plane and then in situ produced miscellaneous fluorine-related groups. Recently, a series of plasma sources like SF<sub>6</sub>, CF<sub>4</sub>, and F<sub>2</sub> were employed in the plasma fluorination.<sup>[100,126–132]</sup> Wang et al. developed the synthesis of FG by using CF<sub>4</sub> plasma to fluorinate the unilaminar graphene nanosheets from chemical vapor deposition (CVD) method. By controlling the reaction conditions, FGs with different fluorine coverage were produced and the fluorine distribution on graphene was highly heterogeneous.<sup>[131]</sup> Zhou et al.

presented an effective way to synthesize fluorinated graphene oxide (FGO) with an alterable F/O ratio by employing CF<sub>4</sub> plasma and then the dispersibility of FGO in water reduced continuously while increased first and then dropped in *N,N*-dimethylacetamide with the increase of the plasma fluorination time, which was attributed to the competitive effect between the elimination of oxygen-related groups and the formation of hydrophobic fluorine-related groups.<sup>[126]</sup> Plsek et al. reported a convenient mean toward the preparation of FG through a laser-ablation-assisted decomposition of gassy SF<sub>6</sub> sources (Figure 5B). Compared with the fluorination of graphene by directly using CF<sub>4</sub> plasma, this method was performed more gently and the consumption of fluorine sources was much smaller.<sup>[128]</sup> Xu et al. utilized SF<sub>6</sub> plasma fluorine source to fluorinate the CVD-grown graphene and directly constructed the FG/Si heterojunction for photodetection (Figure 5C).<sup>[100]</sup> Yang et al. investigated the fluorination process of graphene under the SF<sub>6</sub> plasma exposure with a layer-dependent characteristic. For the unilaminar graphene, D, D', and D+G bands in the Raman spectra were distinctly observed, while the peaks were lacking in few-layer graphene under same conditions, which was ascribed to the corrugation effect of the monolayer

graphene. Owing to the existence of wrinkles, the carbon atoms protruded on the graphene surface had a much higher activity, so these areas were apt to first interact with fluorine sources.<sup>[127]</sup> Subsequently, Deng et al. took advantage of the multiscale corrugations to achieve the spatially selective fluorination for graphene by using CF<sub>4</sub> plasma (Figure 5D).<sup>[92]</sup>

As mentioned above, the plasma fluorination method is relatively controllable and green, and it is feasible to prepare the FG nanosheets with a special phase structure or heterostructure. Furthermore, carrying out fundamental exploration about the physical properties of individual FG nanosheets prepared through the plasma fluorination will clarify quantitative structure–activity relationship and pave the way for the development of application-oriented advanced FG materials.

#### 2.2.4. Mechanochemical Fluorination

In recent years, the mechanochemical synthesis has gradually shown its unique glamour in organic synthesis. The reaction only needs to be carried out under solid condition without various solvents, and the subsequent tedious purification procedures could be dramatically reduced. During the reaction, local high pressure and high temperature would be generated instantaneously by the input of mechanical energy and some unusual reactions could be realized.<sup>[133–135]</sup>

The mechanochemical fluorination is operated without the assistance of any solvent and needs almost no subsequent purification operation, which is beneficial to realize the industrial production. Meanwhile, the huge mechanical force has the ability of preparing the FGs with small size and even the fluorinated graphene quantum dot.<sup>[69,133]</sup> Posudievsky et al. prepared the nitrogen/fluorine co-doped graphene through mechanochemical synthesis using solid ammonium fluoride (NH<sub>4</sub>F) at low temperature. The selection of NH<sub>4</sub>F as a delamination agent was not only root in its possibility of decomposing into NH<sub>3</sub> and HF during mechanochemical process, but also resulting from their interaction with the defects of unpaired electronic states formed at the edges of mechanically cracked graphite granules. By controlling the amount of NH<sub>4</sub>F and input power, the proportion of doped elements in nitrogen-doped fluorinated graphene (NFG) could be adjusted.<sup>[133]</sup> Moreover, the edge fluorinated graphene could also be prepared by ball milling method (Figure 5E). Due to the high-speed shear action on the graphene sheets in the ball milling system, the lamellae would break and then expose the edge of fractured graphene with high activity and unpaired electronic defects. Under this condition, fluorine sources would preferentially react with these active sites to form edge-functionalized graphene.<sup>[69]</sup>

The mechanochemical fluorination is a green method without the assistance of any solvent, and it needs almost no subsequent purification operation, which is beneficial to achieve industrial production. Meanwhile, the huge mechanical force has the ability of preparing the FGs with small size and even the fluorinated graphene quantum dot. However, this reaction is difficult to trace and investigate, which causes that the corresponding mechanism of mechanochemistry is indistinct. Meanwhile, though the size of FG sheet gets smaller because of huge mechanical force, on the other hand, the corresponding

defect density on FG sheet would increase vastly. Moreover, the fluorine content of FG is always relatively low under the huge mechanical force. Notably, whether the high defect density on FG sheet could make it promising candidate as advanced energy and catalysis material?

To sum up, the top-down strategy avoids the participation of poisonous fluorine sources (fluorine gas, xenon difluoride, etc.) and could be operated in the laboratory without special equipment. Commercially available FGs as raw materials can guarantee a good repeatability for different batches of FG products. However, it is unbecoming for large-scale production as the corresponding efficiency and yield are relatively low. Moreover, how to accurately regulate the nature of C–F bonds through the selection of solvent is an intractable problem. Therefore, the exfoliation approach lacks a fine control of the structure during preparation, making it still a challenge to obtain FG with specific structures and properties. In contrast, the bottom-up method has many technologies and approaches to control the structure of FG nanosheets, and even “customize” the performances of FG products to some extent. Among which, the direct gas fluorination has been considered as a great promise method for the industrial production of FG while the homogeneity of fluorination needs to be further improved. In addition, this method generally requires special equipment and stringent safety procedures, which makes it more hazardous than the top-down method, and the quality of graphene raw materials greatly influences the properties of FG products, which causes that the high-quality FG is relatively difficult to be obtained in a high yield. For the follow-up research, we would make some breakthrough in the following aspects: 1) The exploration of new fluorination reagent and novel fluorination methodology, especially for some green and environmentally friendly methods. 2) The study on the intercalation mechanism of fluorination and for developing the methodology of the interlayer-oriented fluorination. 3) Inspired by the fluorination of graphite, the catalytic fluorination should be applied for the preparation of FG materials with a perfect lamellar structure.

### 3. Intrinsic Properties of FG

Compared with graphene, the peculiarities of FG mainly originate from the fluorine atoms attached on the graphene skeleton. The content, the location, and the types of the C–F bonds have a decisive influence on the performance of FG. Meanwhile, the selection of fluorination methods, raw materials, and reaction conditions also significantly affects the structures, the properties, and the corresponding application fields of FG.<sup>[32–39,42,54,63,136–138]</sup> Therefore, an in-depth understanding of the peculiarities and its structure is essential before exploring its intrinsic properties and applications.

The fluorine atom has the highest electronegativity and the C–F bond in carbon fluoride materials always exhibits different bonding nature, such as covalent bond, semi-ionic bond, or ionic bond.<sup>[28,102,108,137,139–143]</sup> Wang et al. proved that the C–F bonds with different locations and ascriptions exhibited different binding energies according to the X-ray photoelectron spectroscopy (XPS) spectra of FG. By simply adjusting the temperature, time, and the amount of HF for this reaction,

the proportion of C–F bonds with different bonding energies would be changed.<sup>[110]</sup> Bettinger et al. theoretically predicted the existence of semi-ionic C–F bonds for the first time.<sup>[140]</sup> Furthermore, Sato et al. proved the presence of semi-ionic C–F bonds experimentally and subsequently conducted related studies on the properties of them.<sup>[145]</sup> For Fourier transform infrared (FTIR) spectra, the vibration peak of the C–F bonds should be located at 1200 cm<sup>-1</sup>. However, in most instances, the corresponding vibration peak contains at least two peaks located at 1050–1220 cm<sup>-1</sup>, indicating the existence of multiple types of C–F bonds.<sup>[102,108,125,137,146–148]</sup> Until now, it has been semiempirically accepted that the bonding energy of covalent C–F bond is around 290–291 eV while that of the semi-ionic C–F bond is around 287–288 eV in the XPS C 1s spectra.<sup>[30,108,125,126,131,138]</sup> However, due to the complexity of the fluorination, all the abovementioned types of C–F bonds may coexist in the FG sheets, which brings tremendous difficulties for exploring the properties of these different types of C–F bonds, respectively.

Some researchers believed that there were no multiple types of C–F bonds on the FG plane, which was only resulted from the hyperconjugation interaction between the different aromatic regions and the fluorinated regions.<sup>[149]</sup> It is pointed out that the authentic experiments have never confirmed the corresponding specific parameters such as the bond length of the semi-ionic and ionic C–F bonds.<sup>[32]</sup> Hagiwara et al. attempted to find the direct evidence for the semi-ionic C–F bonds by neutron diffraction, but no signal peaks were found.<sup>[150]</sup> In addition, the CF<sub>2</sub> and CF<sub>3</sub> groups with higher binding energy (around 291–293 eV in the XPS C 1s spectra) formed at the defects and edges will affect the characterization of C–F bonding nature and also determine the properties of FG.

The intrinsic characters of C–F bonds produce a crucial influence in the performance of FG, and the corresponding F/C ratio is another crucial factor in determining the overall properties of FG. By controlling the reaction time, reaction temperature, the species and the dosage of fluorine-containing sources, etc., the F/C ratio of FG can be easily adjusted.<sup>[30,35,108,110,129,143]</sup> Wang et al. demonstrated a facile way to synthesize FG with different F/C ratios and fluorine-related groups by changing the temperature and time of the solution fluorination process and the content of hydrofluoric acid.<sup>[110]</sup> By regulating the exposure time in CF<sub>4</sub> plasma atmosphere, Yu et al. realized the regulation of F/C ratio from 0.17 to 0.27.<sup>[129]</sup> Wang et al. achieved to prepare FG with an F/C ratio ranging from 0.65 to 1.02 via controlling the dosage of F<sub>2</sub> in the direct fluorination process.<sup>[108]</sup> The F/C ratio can also be regulated by post-processing. FG disposed by some polar aprotic solvents showed a significant reduction behavior with an obvious decrease of F/C ratio, and the F/C ratio was regulated by varying the solvents and disposal time.<sup>[151]</sup> Thermal annealing and ultrasonic treatment are able to regulate the F/C ratios of FG.<sup>[101,102,107,149,152]</sup> Robinson et al. achieved the single-side and the double-side fluorination of graphene through depositing the graphene films on different substrates, and the bandgap of graphene gradually increased with the rising of the F/C ratio (Figure 5B).<sup>[30]</sup> Lai et al. demonstrated that the bandgap, photoluminescence (PL) intensity, and density of spin centers of FG undergone a salutation when the F/C ratio was about 0.4–0.6, which was ascribed to the “phase reversal” phenomenon with the increasing of fluorinated degree (Figure 6C).<sup>[143]</sup>

Moreover, the configuration diversity (chair, stirrup, boat, twist-boat configurations) of FG would also result in different properties including bandgap, reactivity of C–F bonds.<sup>[37,100,144]</sup> Herein, we give a brief introduction to the intrinsic properties of FGs with different fluorinated structure.

### 3.1. Bandgap

Graphene possesses extremely high carrier migration rate, which enables it to be used in the territory of microelectronic device. Nevertheless, the characteristic of zero bandgap makes it difficult to apply in the semiconductor field.<sup>[13]</sup> Therefore, opening the bandgap of graphene would further expand its applications into field effect transistor and photodetector. For FG, the introduced fluorine atoms have changed the hybridization type of graphene from sp<sup>2</sup> carbon to sp<sup>3</sup> carbon accompanied by destroying the conjugated structure, and the formed sp<sup>3</sup> hybridized carbon also shift the charge density and scattering center in the conduction band.<sup>[34–36]</sup> Meanwhile, in comparison with chlorographene, the highest electronegativity of fluorine atom further localizes the electrons (Figure 7A).<sup>[36]</sup> All the above factors contribute to the increase of bandgap. As a result, with the increase of F/C ratio, FG exhibits a gradual transition from conductor to semiconductor and then to insulator (Figure 7B). Moreover, the bandgap of FG shows a great correlation with its F/C ratio, skeleton configuration, and fluorine distribution (Figure 7C), which offers the opportunities to well tune the bandgap of FG by simply adjusting the aforementioned influence factors.

Based on Liu's calculations, FG with a low fluorine content (CF<sub>0.031</sub>, CF<sub>0.056</sub>, CF<sub>0.125</sub>, even CF<sub>0.5</sub>) exhibited a metallic feature. Simultaneously, by precisely adjusting the amount of fluorine content, the bandgap of FG could be changed from 0 to 3.13 eV.<sup>[35]</sup> Density-functional generalized gradient approximation calculations indicated the bandgap of FG was not only controlled by the fluorine content, but also related to the configuration and the arrangement of fluorine attribution on the graphene plane.<sup>[37]</sup> For FG with different configurations, the bandgap showed a small fluctuation (the bandgap values of the chair, stirrup, boat, twist-boat configurations were 3.10, 3.58, 3.28, 3.05 eV, respectively). Among which, the chair configuration was the most stable one due to alternative arrangement of fluorine atoms on the both sides of FG plane that was energy preferred.<sup>[37]</sup>

In addition, some investigators employed many-body GW approximation to calculate the bandgap of FG and the obtained value was usually 7.3–7.5 eV, which was much larger than the experimental result.<sup>[35,37]</sup> There is a big difference between the bandgap values, respectively, obtained from density functional theory (DFT) and GW since the intercoupling between electrons and holes was involved in the calculation process.<sup>[37]</sup> Also, the value discrepancy of the bandgaps between theory calculations and experiments might ascribe to the existence of the wrinkles or defects of FG in the nonideal system. Sahin et al. thought that the experimental value was a weight average of diverse FG with different F/C ratios or configurations even together with ampliative defects in grain boundaries.<sup>[153]</sup> Therefore, to clearly comprehend the relationship and differences



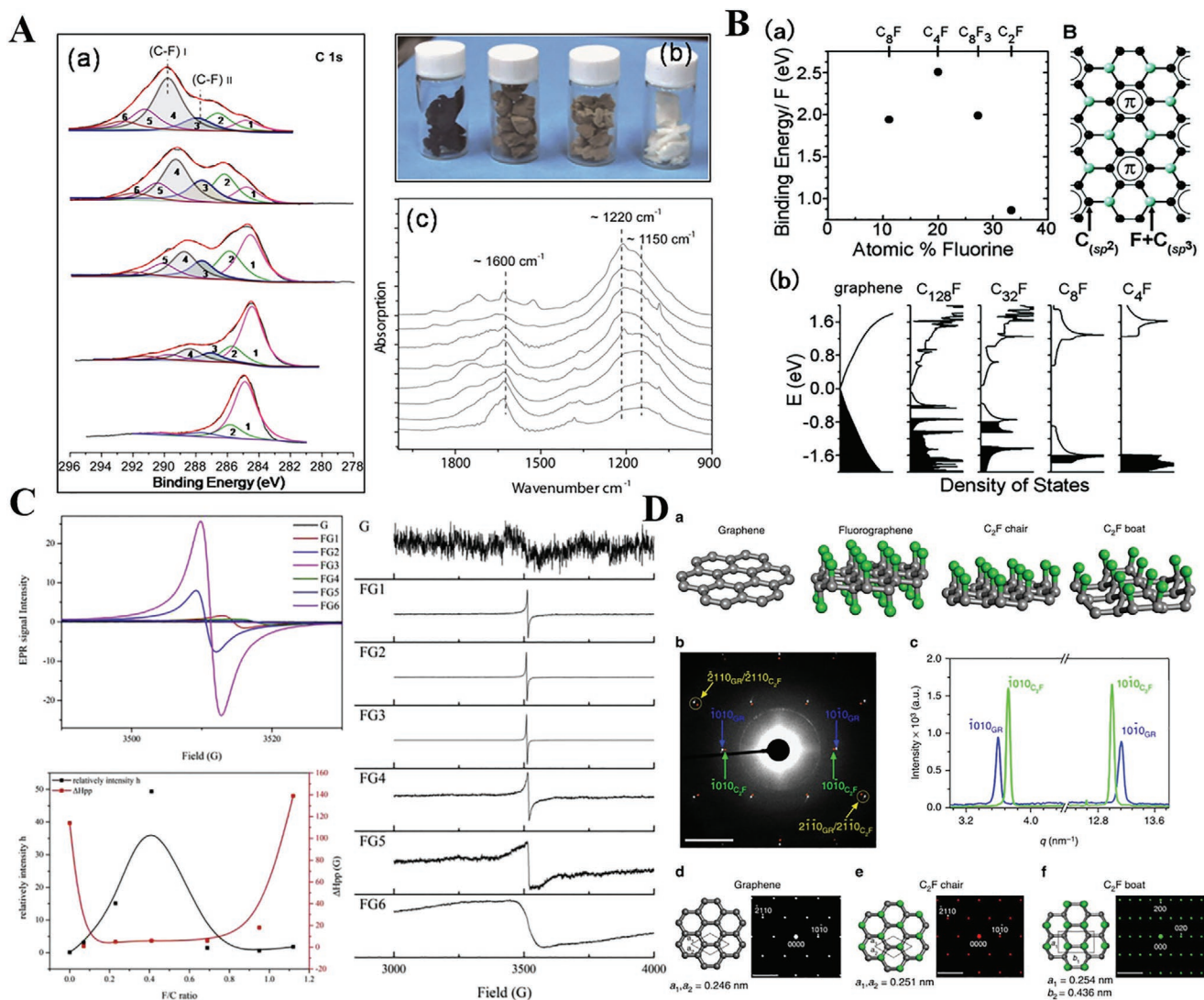


**Figure 6.** A) a) XPS spectra of FG samples with different fluorine content. b) Optical photographs of pristine graphene and FG with different fluorine content. c) The evolution of FTIR spectra of FG samples under different fluorination temperature. A) Reproduced with permission.<sup>[137]</sup> Copyright 2016, American Chemical Society. B) a) Computational bond energy of different contents and the skeleton of the C<sub>4</sub>F configuration with an F/C ratio of 0.25. b) Computational total density of states for single-side fluorination of graphene with different fluorine content. B) Reproduced with permission.<sup>[30]</sup> Copyright 2010, American Chemical Society. C) EPR spectra of FG samples with different fluorine content. Reproduced with permission.<sup>[143]</sup> Copyright 2018, Elsevier. D) Electron diffraction investigation of pristine graphene and the chair/boat configuration of C<sub>2</sub>F. Reproduced with permission.<sup>[144]</sup> Copyright 2014, Springer Nature.

between experimental and theoretical bandgap values, it is necessary to utilize more accurate measurements to characterize single-layer FG nanosheet with a definite structure.

FG exhibits a continuously adjustable bandgap from conductor to semiconductor and then to insulator. The stability of FG is higher than that of other graphene derivatives such as GO, so the fluctuation of its bandgap is limited and the value is relatively steady. Also, some emerging 2D materials such as boron nitride and transition metal sulfide have an inherent bandgap, but the modulation of their bandgap is difficult compared with that of FG. Therefore, the bandgap engineering based on FG materials is awfully fascinating, and it is necessary to clarify the relationship between the band structure of FG and its different fluorine distributions (dispersive or concentrated

with the same F/C ratio), phase structure, and even heterostructure with other 2D materials.

### 3.2. Optical Properties

The introduction of fluorine atoms has caused tremendous changes in the optical property for graphene like transparency, absorption ability, and PL.<sup>[30,37,38,112,154,155]</sup> For pristine graphene with large conjugated structure, it shows a high absorption for visible light range while FG exhibits a decreased absorption of visible light owing to the destruction of conjugated structure.<sup>[38,154,155]</sup> As could be seen from the optical images, the per-fluorinated graphene products are in white color, close to the

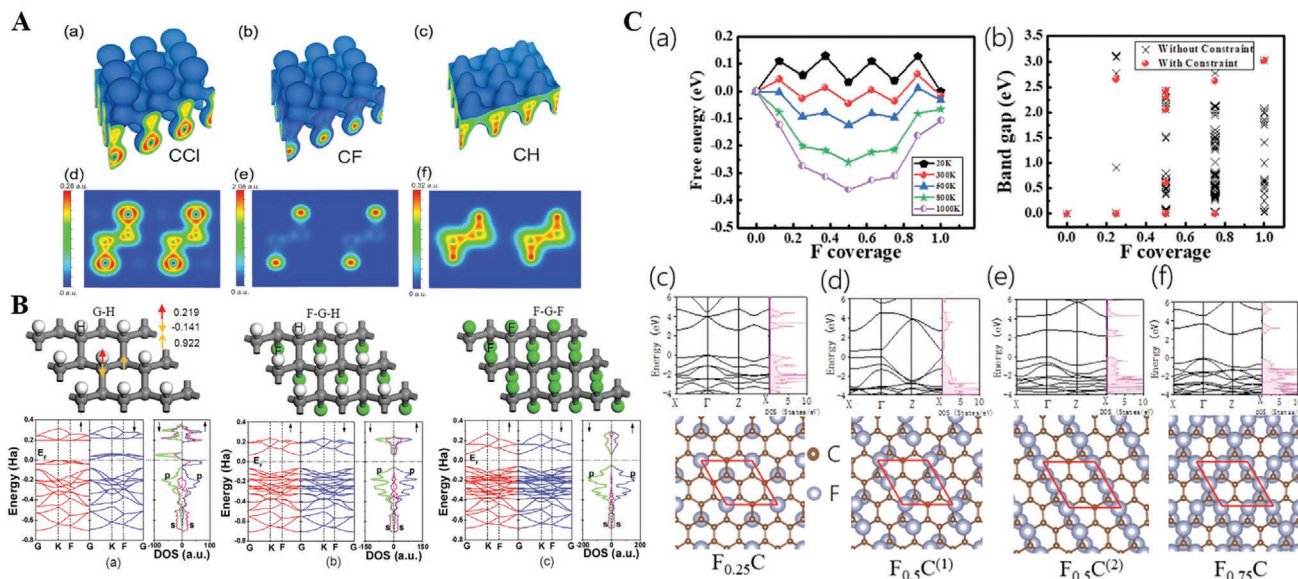


**Figure 7.** A) Total electron densities for chlorographene, fluorographene, and graphane by using HSE06 functional. Reproduced with permission.<sup>[36]</sup> Copyright 2013, American Chemical Society. B) a–c) Calculated geometry structures and electron structures for half-hydrogenated graphene, half-fluorinated and half-hydrogenated graphene, fully fluorinated graphene, respectively. B) Reproduced with permission.<sup>[34]</sup> Copyright 2009, American Institute of Physics. C) a) Calculated free energies of fluorine doping with changed concentrations. b) Calculated bandgaps for FG samples with different F/C ratios. c–f) Energy and DOS of the representative structures:  $F_{0.25}C$ ,  $F_{0.5}C$  (alternating arrangement),  $F_{0.5}C$  (one-sided arrangement), and  $F_{0.75}C$ , respectively. C) Reproduced with permission.<sup>[100]</sup> Copyright 2019, American Chemical Society.

appearance of FGI.<sup>[108]</sup> Zhao et al. prepared FG by employing DAST as fluorine source and studied the optical properties in various solvents. Through UV–vis absorption measurements for different products, FG showed the strong absorption peaks at 220 nm, which was put down to the  $\pi$ – $\pi^*$  transformation of the conjugated polyene-type structures on FG sheet (Figure 8A-a). Moreover, another peak in the absorption spectrum of all FG products occurred in the range of 250–350 nm, indicating the existence of several conjugated aromatic regions with different sizes (Figure 8A-b). The longest absorption peak may be derived from the  $\pi$ – $\pi^*$  transformation of the maximal aromatic region, meanwhile, its initial absorption wavelength might correlate with the narrowest bandgap in the material.<sup>[112]</sup>

The PL phenomenon of FG has also been studied extensively by many researchers in recent years. Jeon et al. found the PL emission of FG was robust when exposing to air and ethanol. As can be seen in Figure 8B-a, the peak at around 3.80 and 3.65 eV was clearly observed in the PL spectra, and the formation mechanism of the two distinct peaks was verified by employing near-edge X-ray absorption spectroscopy (Figure 8B-b).<sup>[38]</sup> Gong et al. reported the preparation of graphene fluoroxide quantum dots (GFOQDs) with adjustable size and F/C ratio which showed highly blue luminescence. The prepared GFOQDs exhibited excellent tolerance to pH variations and displayed steady luminescence in both acid and alkali environments, which was attributed to the changes in band structure and surface energy/surface wettability.<sup>[121]</sup> Fan et al. used a two-step fluorination method to prepare fluorinated graphene oxide (FGO) and the obtained FGO samples had an extremely high photoluminescence quantum yield (PLQY) of 66% compared with pristine GO (<1%), which outdistanced the maximal value for modifying GO (21.2%)

reported up to now (Figure 8C). In the excitation process, a large number of excitons were produced with the aid of new electronic bandgap structure. In the emission process, the larger rigidity and interlayer distance weakened the electron–phonon interactions, thus greatly reducing the nonradiative recombination loss of excitons.<sup>[155]</sup> Subsequently, they further distinguished and summarized the contributions of different C–F bonds for the PL emission. Also, the defect passivation effect brought by fluorination was examined by their further work, and the prepared FPG exhibited giant enhancement of PL emission. The FPG was further applied to achieve the high-efficiency detection of  $Fe^{3+}$  with a high selectivity (Figure 8D).<sup>[154]</sup>

From the results of DFT calculations, the optical property from ground-state FG was usually different from the experimental results, because it did not take the interaction of quasiparticles into consideration.<sup>[156]</sup> Therefore, some researchers utilized the Bethe–Salpeter equation (GW-BSE) to investigate the optical properties of FG and it showed a better accuracy with the experimental results, because the intercoupling between electrons and holes were involved in the calculation process.<sup>[36,37,156]</sup> Although theoretical calculations could not perfectly reproduce the experimental results, the development of theoretical simulations would provide more prospective studies on the optical property of FG in the near future.

The high transparency and the adjustable PL emission of FG guarantee the attractive application prospect of FG in optical field. The oxygen-containing groups in GO sheets are easy to induce the nonradiative recombination of excitons, while the introduced C–F bonds may restrict the phenomenon and the less interlayer interactions between FG sheets also significantly reduce the nonradiative recombination. Interestingly,

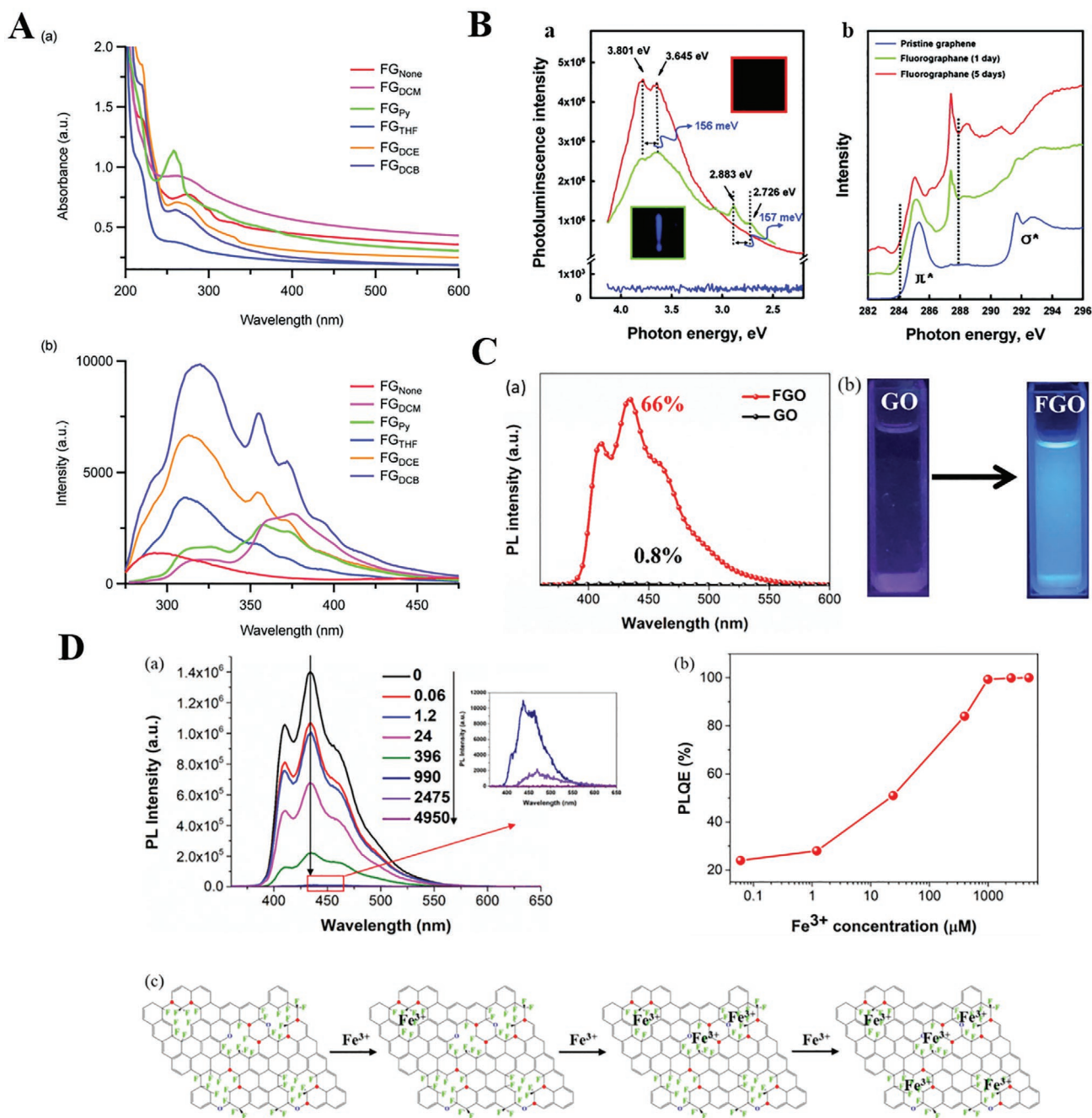


**Figure 8.** A) a,b) UV-vis absorption and PL spectra of FG in acetonitrile solution ( $2.5 \times 10^{-3}$  mg mL<sup>-1</sup>). Reproduced with permission.<sup>[112]</sup> Copyright 2013, The Royal Society of Chemistry. B) a) Typical PL spectra of graphene and FG using acetone as solvent under the excitation of 290 nm. b) Near-edge X-ray absorption fine structure spectra of pristine graphene and FG. B) Reproduced with permission.<sup>[38]</sup> Copyright 2011, American Chemical Society. C) a) PL emission spectra of FPG with changed concentrations after addition of Fe<sup>3+</sup> ions. b) Subplot of PL quenching efficiency for FPG after addition of Fe<sup>3+</sup>. c) Schematic illustration of the FPG sample interacts with Fe<sup>3+</sup> ion. C) Reproduced with permission.<sup>[154]</sup> Copyright 2020, American Chemical Society. D) a) PL emission spectra of GO and FGO ethanol dispersions at ambient temperature. b) PL quenching efficiency of GO and FGO dispersed in ethanol. c) Schematic illustration of the FPG nanosheet with different concentrations of Fe<sup>3+</sup>. D) Reproduced with permission.<sup>[155]</sup> Copyright 2020, Elsevier.

combining with the paramagnetism of FG, the application of its optical properties can be further extended into the biological field for the magnetic resonance imaging (MRI), the fluorescence imaging of cell uptake, and the real-time monitoring of the delivery process of drugs.

### 3.3. Low Surface Energy and Tribological Properties

For FG with a high fluorine content, the skeleton is surrounded by fluorine atoms, so it could be preliminarily regarded as the polytetrafluoroethylene (PTFE) in a 2D state.<sup>[28]</sup> Therefore, the



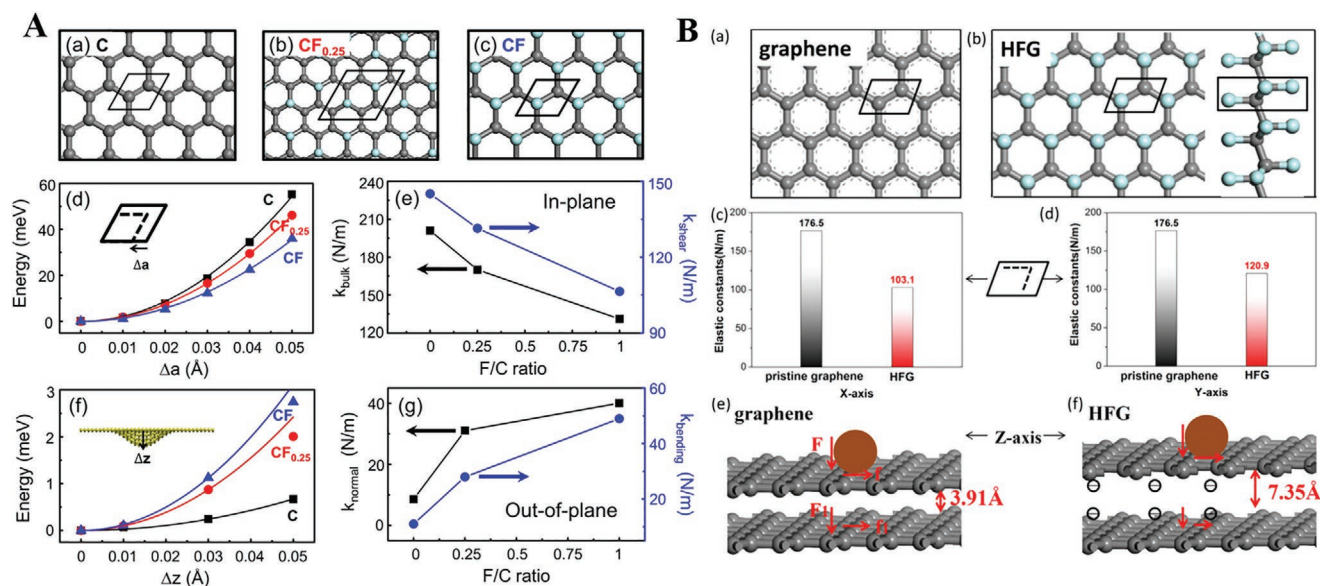


**Figure 9.** A) a–c) Atomic models of graphene, FG ( $C_xF$ ), and perfluorinated graphene (CF). d, f) Calculated total energy versus in-plane biaxial strain/out-of-plane strain. e, g) Calculated in-plane bulk and shear stiffnesses and out-of-plane normal and bending stiffnesses. A) Reproduced with permission.<sup>[45]</sup> Copyright 2012, American Chemical Society. B) a, b) Atomic models of graphene and FG sample. c, d) Calculated in-plane elastic constant on the X/Y-axis of graphene and FG, respectively. e, f) Evolution of stress and friction forces on the Z-axis of multilayer graphene and FG products. B) Reproduced with permission.<sup>[47]</sup> Copyright 2018, American Chemical Society.

property of FG could be inferred from that of PTFE.<sup>[39]</sup> From the experimental point of view, it was also directly proved that FG had extremely low surface energy and the excellent interlayer lubrication characteristic.<sup>[39,44,46–48,99,157]</sup> Fan et al. calculated the surface energy of FG based on contact angle measurement and the obtained value was about  $3.92 \text{ mJ m}^{-2}$ .<sup>[48]</sup> Mathkar et al. prepared FGO with the adjustable hydrophilicity and hydrophobicity by oxidative exfoliation, and they added FGO into NMP solvent as a “paint” to spray on different objects so as to build various surfaces with hydrophilic/hydrophobic performances.<sup>[99]</sup> Akhtar et al. applied FG as a coating and carried out related research on its anti-icing performance. The corresponding results showed that, due to the existence of the superhydrophobic FG layer, the low wettability of the prepared FG surface made it difficult to form a water molecule film, which thus hindered the formation of ice nucleus and the following growth in its 3D space.<sup>[44]</sup> It is worth mentioning that the hydrophobicity causes FG has huge difficulty of dispersing or solubilizing in water, which restricts the applications of FG in water-soluble materials and solution-based fabrication like graphene oxide.

The tribological behavior of FG have also been widely studied in recent years.<sup>[44–50,156,157]</sup> Generally, with the increased F/C ratio on FG, the increased interlayer spacing and the decreased interlayer interactions significantly enhanced its tribological performances as lubricants, namely, its self-lubricating ability.<sup>[119]</sup> Nevertheless, for single-layer FG in nanoscale, it behaved totally different tribological feature since the out-of-plane bending stiffness of graphene remarkably increased by fluorination (Figure 9A,B), and the in-plane stiffness had a corresponding decrease (Figure 9A-d,e,B-c,d).<sup>[45,49]</sup> When atomic force microscopy (AFM) probe slipped on the surface

of single-layer FG, the increased out-of-plane bending stiffness resulted in the enhanced friction coefficient (Figure 9A-f,g). In this circumstance, the friction coefficient depended on the out-of-plane bending stiffness, and degree of defects of FG may also bring about the influences.<sup>[45]</sup> For the multilayer FG in macroscale, the less interlayer adhesion ( $0.056 \text{ mJ m}^{-2}$ , calculated by Fan et al.<sup>[48]</sup>) decreased the layer friction force so as to obtain a low friction coefficient (Figure 9B-e,f). Meanwhile, FG nanosheets were easy to form stable and tough tribofilm on the interface of friction pairs because of the chemical and physical interactions, which thus enabled FG to exhibit fantastic tribological behaviors.<sup>[47,48]</sup> Their experiment using multilayer FG nanosheets as lubricant additive greatly decreased the friction coefficient and wear rate by 51.4% and 90.9%, respectively.<sup>[46]</sup>

Overall, the high density of fluorine atoms covering on the graphene skeleton endows the corresponding FG sheets with an extremely low surface energy similar to PTFE. Weak interlayer interactions and high thermostability present a great potential for long-term lubrication performance. As for GO, the strong interactions between GO lamellas limit the slip of individual nanosheets and the relatively low thermostability results in failure under harsh operating conditions. Also, further research of FG aiming at the improvement of the tribological performance could focus on the regulation of the fluorine-containing species, especially for preparing effective FG’s structure with C–F bonds perpendicular to graphene plane. Here, the fluorination of graphene with perfect lamellar structure would be a good preparation strategy. In addition, exploring the tribological performance of 2D nanomaterials at high torques is also one key issue in lubrication field, because the formed tribofilm on friction pairs is relatively unstable under harsh conditions.

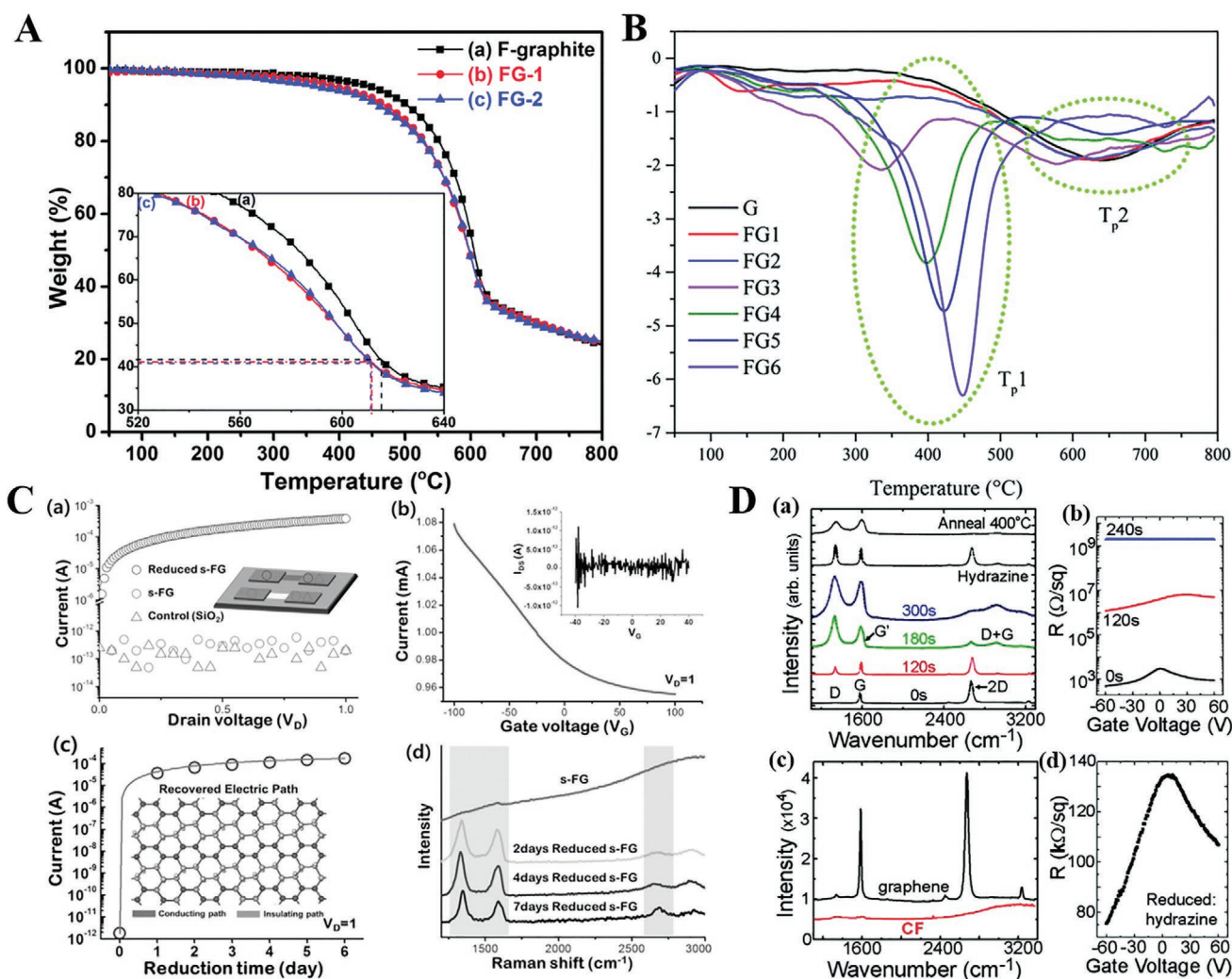


**Figure 10.** A) Thermogravimetric analysis (TGA) curves of FGi and different FG samples. Reproduced with permission.<sup>[102]</sup> Copyright 2014, The Royal Society of Chemistry. B) The derivative TG curves for the FG samples prepared by direct fluorination. Reproduced with permission.<sup>[152]</sup> Copyright 2017, The Royal Society of Chemistry. C) a)  $I$ - $V$  curves of the obtained multilayered semi-ionically fluorinated graphene (s-FG) and the corresponding reduced films. b)  $I$ - $V_g$  curves of multilayered s-FG FET before (inset) and after reduction treatment. c) The measured current in the s-FG films with different reduction time. d) Raman spectra of samples treated with different reduction times. C) Reproduced with permission.<sup>[138]</sup> Copyright 2013, Wiley-VCH. D) a, c) Raman spectra of pristine graphene, single-sided fluorinated samples, perfluorographane, and defluorinated samples. b, d) Graphs of the resistance versus gate voltage for the fabricated graphene-based device treated by  $\text{XeF}_2$  at changed times and the obtained reduced samples. D) Reproduced with permission.<sup>[30]</sup> Copyright 2010, American Chemical Society.

### 3.4. Stability

Based on the conventional cognitions of perfluorinated organic compounds, it seems to be a consensus that FG has the good thermal stability and chemical stability.<sup>[28–30,158,159]</sup> However, the stability of FG is different from PTFE owing to the special 2D structure, and the equivalent perfluorographane (F/C ratio of 1) with perfect structure is still unavailable.<sup>[131]</sup> Simultaneously, the existence of defects also leads to structure diversity that may affect the comprehensive stability of FG.<sup>[48,143,152]</sup> In the initial research, FG prepared by the exfoliation method had extremely high thermal stability ( $>450$  °C, **Figure 10A**),<sup>[28,102]</sup> but FG with relatively low fluorine content obtained by bottom-up synthesis would undergo a significant defluorination phenomenon after a short treatment at 400 °C (or under 400 °C,

**Figure 10B**).<sup>[149,152,160]</sup> The thermal stability of different FG products has a great relationship with their structures, and is closely connected to the properties of the C–F bonds. Although FG prepared from different methods may have the same F/C ratio, its configuration, C–F bond properties, degree of defects, and different fluorine-containing groups would bring about the diverse thermal stability.<sup>[37,137,152]</sup>

Wang et al. thought the thermal stability of C–F bonds with sparse fluorine distribution was relatively lower, which was attributed to that the unstable coplanar structure at sparse fluorine area spontaneously transformed into planar aromatic ring structure in the heating process, thereby inevitably breaking the C–F bonds.<sup>[137]</sup> Additionally, the thermostability and thermal oxygen stability of FG and FPG were studied in detail by Lai et al. The results demonstrated the thermostability of FG

and FPG improved with the increased F/C ratio owing to the improvement of bond energy for the covalent C–F bonds.<sup>[152]</sup> Surprisingly, FPG presented much better in thermal oxygen stability while FG appeared to decompose at lower temperature because of the defects introduced during fluorination. By DFT calculations, the higher proportion of CF<sub>n</sub> groups (*n* = 2,3) in FG would result in relatively worse thermal stability.<sup>[152]</sup> Costa et al. reported that, through the in situ Raman spectra analysis during the heating/cooling process for FG, the desorption energy of some fluorine atoms was extremely low. They attributed this experimental phenomenon to the hyperconjugation effect of fluorine atoms and the adjacent C=C bonds.<sup>[149]</sup> Furthermore, the dissociation energy of C–F bonds in partially fluorinated graphene was about 49.6 kcal mol<sup>-1</sup> while 112.3 kcal mol<sup>-1</sup> for C–F bonds in fully fluorinated graphene, which indirectly proved that the FG framework with higher fluorine content had a better stability.<sup>[141]</sup>

Besides thermal stability, the chemical stability of FG has also attracted much attentions.<sup>[29,102,138,139,151]</sup> FG exhibits fine chemical stability in some solvents like water, ethanol, propanol, etc., while it shows reduction phenomenon after treating by strong nucleophilic agents. Also, the selective reduction of FG was completed after disposing by acetone (Figure 10C).<sup>[138]</sup> Meanwhile, FG would form metastable graphene iodide intermediate and rapidly converted to graphene and iodine at only 150 °C.<sup>[29]</sup> By utilizing zinc nanoparticles, FG could also be reduced into graphene.<sup>[139]</sup> In addition, when FG was exposed to hydrazine vapors at low temperature (Figure 10D), defluorination was also achieved, accompanied by the recovery of conductivity.<sup>[30]</sup> Wang et al. found specific solvents were easy to activate the C–F bonds of FG. FG disposed by polar aprotic solvents showed a significant reduction. However, the C–F bonds were stable in apolar solvents or polar protic solvents (alcohol, methyl alcohol) and the nature of C–F bonds and fluorine content remained almost the same.<sup>[151]</sup>

Ren et al. reported FG was partially reduced under UV irradiation, and the characteristic of C–F bonds transformed from covalent to semi-ionic bonds. The reduction degree of FG could be controlled by irradiation time.<sup>[161]</sup> Particularly, compared with nonaromatic solvents, aromatic solvents presented a “synergistic effect” in the defluorination process.<sup>[161]</sup> Moreover, the double-sided fluorinated graphene and single-sided fluorinated graphene behaved completely different stability with the same treatment. By DFT calculation, the configuration of double-sided fluorinated graphene had the negative and lower formation energy compared to the positive formation energy of the single-sided fluorinated graphene, manifesting that the double-sided configuration had the more stable structure.<sup>[162]</sup>

In general, the good stability of materials is the prerequisite for most applications. In comparison with other graphene derivatives, FG exhibited the highest thermostability owing to the high bonding energy of C–F bonds and its high functionalization density. Here, it should be noted that FGs prepared by the bottom-up and top-down approaches present different thermostability even under the same fluorine content. The thermal decomposition temperature of FG obtained by fluorination method is relatively lower and shows a wide range of decomposition temperature. In addition, the characterization of the fluorine content in the inner layer of FG is still vacant in the

field, while these C–F bonds may determine the comprehensive thermostability of FG. The direct fluorination of graphene may produce less C–F bonds in the inner layer of FG, because the inner fluorination is more difficult owing to the diffusion resistance.

### 3.5. Other Properties

In addition to the above related peculiarities, other potential peculiarities of FG have also been reported in succession. Graphene is a nonmagnetic material, but the introduced C–F bonds on graphene surface has been demonstrated to drastically change its magnetic properties.<sup>[42,76,163]</sup> Moreover, Huang et al. described the special U-shaped variation curve of the thermal conductivity of FG with increased F/C ratio by non-equilibrium molecular dynamics (NEMD) simulations. This pattern of change originated from the variation of phonon scattering, caused by the transition from in-plane sp<sup>2</sup> hybridization carbon atoms to out-of-plane sp<sup>3</sup> hybridization of carbon bonds.<sup>[54]</sup> Fan et al. found that the dormant free radicals on FG plane could be activated by increasing the temperature. The activated radicals achieve to initiate radical polymerization and the formed polymer was further grafted onto FG surface for targeted modifications.<sup>[91]</sup> Notably, FG also possesses the excellent dielectric properties, such as low dielectric constant because of the huge difficulty for polarization of C–F bonds, so FG presents great potentials in the application of electric devices.<sup>[164–167]</sup> Interestingly, the introduced C–F bonds of FG could also provide much active sites for further effective doping owing to the increased electrophilicity, and the prepared nitrogen-doped graphene with a high nitrogen content displayed remarkable catalytic behaviors for oxygen reduction reaction (ORR).<sup>[168–171]</sup>

## 4. Applications of FG

### 4.1. Battery and Electrochemistry

With the continuous improvement of the energy density of lithium-ion batteries over years, the market demand for high-energy density primary battery has gradually decreased. However, in some special fields, such as aerospace, national defense, and military industry, primary batteries still play an irreplaceable role.<sup>[63,172,173]</sup> For primary battery, Li/CF<sub>x</sub> battery was widely applied by virtue of its ultrahigh energy density (with about 2162 Wh kg<sup>-1</sup> in theory),<sup>[32,174]</sup> high operating voltage (at around 2.4 V vs Li<sup>+</sup>/Li),<sup>[63]</sup> long shelf life (more than 10 years under room temperature),<sup>[63]</sup> and wide operating temperature window (–40 to 170 °C) and so on.<sup>[63]</sup> Notably, the performance of Li/CF<sub>x</sub> battery mainly depends on CF<sub>x</sub> electrode materials, and different preparation methods would have a different influence for its electrochemical performances.<sup>[174–179]</sup>

For Li/CF<sub>x</sub> primary batteries, the working principle and charge/discharge mechanism are not complicated. Specifically, the C–F bonds with high chemical potential obtain electrons and reduce to F<sup>-</sup>, whereafter F<sup>-</sup> combines with Li<sup>+</sup> to form LiF and deposited on the cathode.<sup>[63,174,180,182,183]</sup> The corresponding reaction mechanism and the relationship between the fluorine



content and the theoretical specific discharge capacity are shown as follows<sup>[180]</sup>



$$Q_{th}(x) = xF / (3.6(12 + 19x)) \quad (2)$$

With the increase of the F/C ratio, the corresponding capacity also increases gradually. However, the process is irreversible since the F atoms on  $CF_x$  are gradually removed from the skeleton during the discharge process.<sup>[63,180]</sup> Meanwhile, due to the poor conductivity of the  $CF_x$  materials themselves, Li/ $CF_x$  batteries are usually only able to work at a very small currents.<sup>[65,68,70,71]</sup> In recent years, for  $CF_x$  materials (mainly FG) as the electrode materials, the F/C ratios and the C–F bonding character as well as fluorine distribution have been adjusted to improve the electrochemical performances. Meduri et al. synthesized FG with different F/C ratio (0.47, 0.66, and 0.89) and found the  $CF_{0.47}$  had the best electrochemical properties. The  $CF_{0.89}$  with a high fluorine content was composed of insulating groups such as  $CF_2$  and  $CF_3$  rather than the semi-ionic C–F bonds, thus leading to the significant increase of overall resistance. In contrast, the low fluorine content and the large unfluorinated graphene domains in  $CF_{0.47}$  conducted to improve its integrated performance of  $CF_{0.47}$ .<sup>[124]</sup> The study by Feng et al. indicated that FG with a larger proportion of semi-ionic bonds as the primary lithium battery cathode material exhibited a better  $Li^+$  diffusion and charge mobility through the individual nanosheet of FG, which thus possessed a prominent discharge rate.<sup>[102]</sup> It is shown in **Figure 11A–c** that for the original FG or the FG samples with a little of semi-ionic C–F bonds, the voltage platform and specific capacity were significantly lower under the same discharge rate. The obtained FG exfoliated by chloroform showed a high specific capacity of  $520 \text{ mA h}^{-1}$ , and the voltage platform of 2.18 V with the current density of 1 C (**Figure 11A–c**), and it also showed the maximal power density of  $4038 \text{ W kg}^{-1}$  at 3 C (**Figure 11A–d**).<sup>[102]</sup> Moreover, from the results of Feng et al., there was a certain correlation between energy density and power density (**Figure 11A–d**), and it is still challenging to obtain Li/ $CF_x$  battery with high energy density and power density simultaneously.<sup>[102]</sup> Zhong et al. conducted studies on the poor rate capability of Li/FG primary battery and found that the semi-ionic C–F bonds among all C–F bonds presented the most conclusive influence on the rate performance. The relatively poor rate capability of FG-based battery is associated with its poor electrical conductivity derived from the destruction of the conjugated structure. Here through taking advantage of the high electrical conductivity of the semi-ionic C–F bonds in FG, the high energy density could be achieved without compromising the charge transport ability. By optimizing the proportion of semi-ionic C–F bonds in FG, the as-prepared FG with an F/C ratio of 0.8 exhibited a very high energy density of  $1073 \text{ Wh kg}^{-1}$  and a prominent power density of  $21460 \text{ W kg}^{-1}$  ( $10 \text{ A g}^{-1}$  current density).<sup>[66]</sup> In addition, Damien et al. had also performed relevant research in this aspect. By regulating the fluorine content, they found the optimal point for balancing the energy density and the power density. Thus, an enhancement in all the three parameters,

including energy density, power density, and faradic yield was achieved in a feasible way.<sup>[183]</sup> Rangasamy et al. demonstrated the Li/ $CF_x$  battery with a  $Li_3PS_4$  (LPS) solid electrolyte delivered a capacity ( $1095 \text{ mA h g}^{-1}$ ), even exceeding the theory prediction ( $865 \text{ mA h g}^{-1}$ ). During the discharge process, the LPS electrolyte showed dual functions that behaved as the inactive electrolyte at the anode and the active constituent at the cathode. The cooperative discharge process is through the discharge products LiF, which activates the electrochemical discharge of LPS at an approximate electrochemical potential of FG.<sup>[184]</sup>

Recently, Mar et al. had successfully prepared graphite oxifluorides with three-phase structure by adjusting the Hummer's oxidation process and the fluorination process, where fluorinated part guaranteed high potential and oxygenated part allowed durability as well as the carbonaceous region provided conductivity. When graphite oxifluorides were employed as cathode material in primary lithium battery, the maximum of energy density about  $2400 \text{ Wh kg}^{-1}$  was reached finally. Moreover, this method was also widely applied in the preparation of specific graphene oxifluorides.<sup>[71]</sup> Besides adjusting the fluorine content, the use of multiple doping methods for increasing the specific capacity of lithium-ion batteries present promising prospects, as well. Peng et al. prepared an original FG/S hybrid electrode material to improve both of the energy density and the power density of Li/FG battery, which showed a higher electrochemical activity, lower overpotential, and faster ion transfer during discharge. With the presence of S atoms, the battery exhibited extremely high energy density of  $2341 \text{ Wh kg}^{-1}$  and a power density about  $13621 \text{ W kg}^{-1}$  at  $8.0 \text{ A g}^{-1}$ .<sup>[70]</sup> Particularly, Cheng et al. reported the FG-modified Li cathode for excellent lithium–oxygen cells. Compared with bare Li electrode, the introduction of FG led to a remarkable improvement on rate capability and cycling life when only 3 wt% FG was added. They attributed this result to the fact that the LiF layer was formed by the reaction between Li and FG and prevented the formation of lithium dendrite (**Figure 11B**).<sup>[67]</sup> Moreover, through the in situ observation by using optical microscopy, the obvious inhibition effect of FG for lithium dendrite growth was vividly observed. Also, the conversion from FG to LiF was confirmed by their further DFT calculations.<sup>[67]</sup>

Notably, some investigators also used  $CF_x$  as electrode materials for preparing the lithium-ion secondary battery during recent years, though the related research progress is relatively slow. Feng et al. synthesized fluorine-doped reduced graphene oxide (FrGO) with predominant  $CF_2$  groups by a one-step solvothermal fluorination, which showed excellent cycling stability as the anode materials. The  $CF_2$  group had higher dissociation energy and better lithium-ion storage capacity, which obviously increased the cycle stability and specific capacity of the battery.<sup>[65]</sup> Also, they prepared fluorine and nitrogen co-doped graphene (NFG), which showed excellent reversible specific discharge capacity ( $1075 \text{ mA h g}^{-1}$  at  $100 \text{ mA g}^{-1}$ ) and superb cycle stability (capacity retention of 95% at  $5 \text{ A g}^{-1}$  after 2000 cycles, **Figure 11C**).<sup>[181]</sup> Later, they also synthesized NFG sheet by solvothermal method to apply as advanced anodes toward flexible sodium-ion battery (SIB). Fluorine atoms and nitrogen atoms embedded into the graphene skeleton synergistically increased the structure defects, providing highly active sites and enlarged the interlayer spacing of graphene that were beneficial to

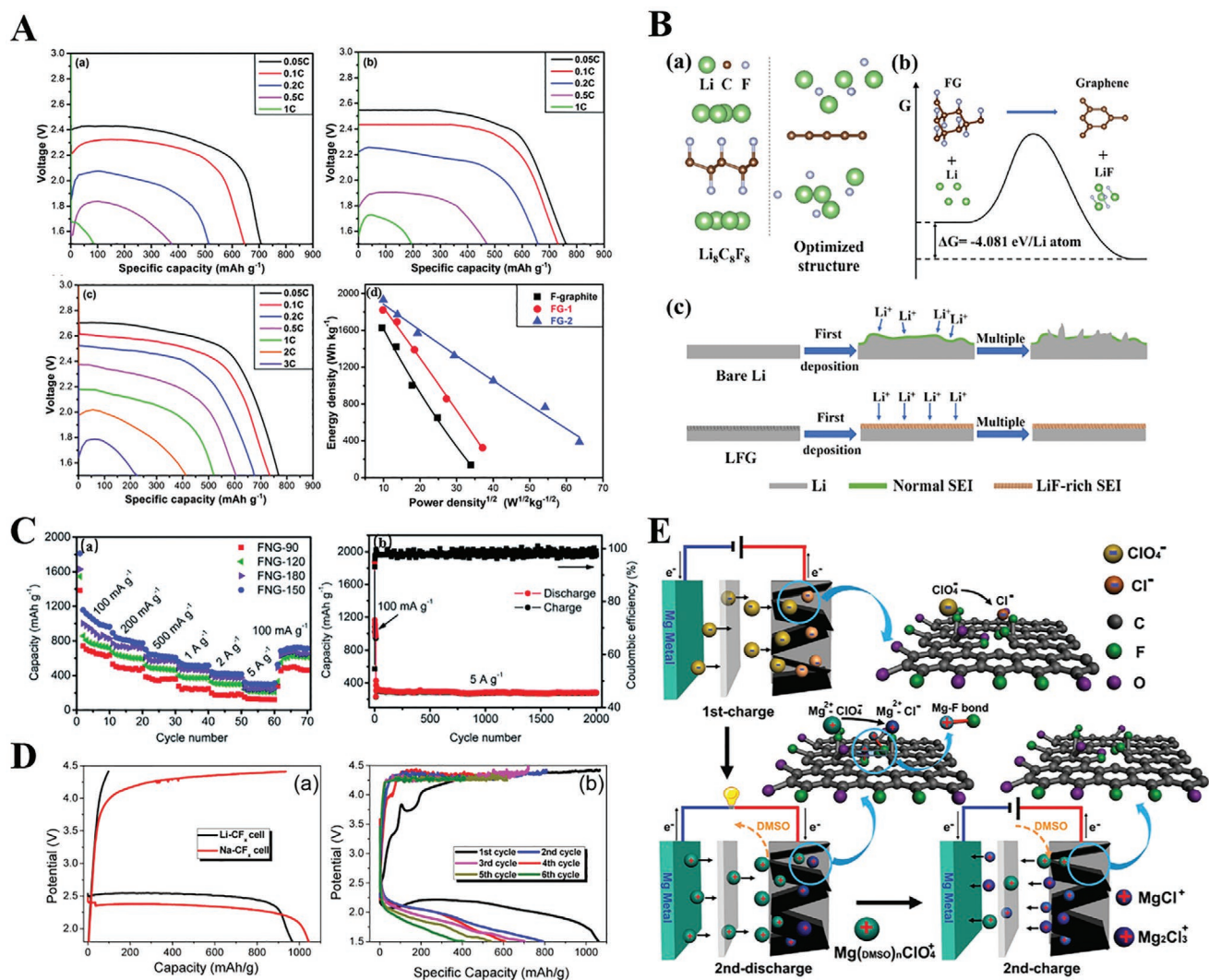


**Figure 11.** A) a–c) The galvanostatic discharge curves at changed discharge rates for FG-i (a), FG-1(chloroform as the exfoliation reagent) (b), and FG-2 (acetonitrile as the exfoliation reagent) (c), and d) Ragone plot of the abovementioned samples. A) Reproduced with permission.<sup>[102]</sup> Copyright 2014, The Royal Society of Chemistry. B) Schematic diagram of morphological changes of the different electrodes and the corresponding simulation of the intercalation process. Reproduced with permission.<sup>[67]</sup> Copyright 2019, American Chemical Society. C) a) Rate capabilities of NFG-based batteries at different current densities. b) Cycling stability of NFG-150 as the anode materials at a current density of 100 mA g<sup>-1</sup> and 5 A g<sup>-1</sup> for 2000 cycles. C) Reproduced with permission.<sup>[181]</sup> Copyright 2015, The Royal Society of Chemistry. D) a) The initial discharge–charge graphs of Na–CF<sub>x</sub> battery and Li–CF<sub>x</sub> battery. b) Potential profiles and specific capacities of Na–CF<sub>x</sub> battery during discharge/charge process. D) Reproduced with permission.<sup>[182]</sup> Copyright 2014, American Chemical Society. E) Schematic illustration of the electrochemical reaction mechanism/steps of Mg/FG battery. Reproduced with permission.<sup>[97]</sup> Copyright 2015, Wiley-VCH.

improve the Na<sup>+</sup> storage capability. Finally, the obtained battery presented a reversible capability of 203 mA h g<sup>-1</sup> at 50 mA g<sup>-1</sup> after 100 cycles (even 56.3 mA h<sup>-1</sup> at 1 A g<sup>-1</sup> after 5000 cycles).<sup>[64]</sup> Liu et al. demonstrated that CF<sub>x</sub> cathodes exhibited rechargeable capability for SIB with the initial discharge capacity of 1061 mA h g<sup>-1</sup> and a reversible discharge capacity of 786 mA h g<sup>-1</sup>.<sup>[182]</sup> For the Li/CF<sub>x</sub> system, the LiF generated by the reaction between CF<sub>x</sub> and Li<sup>+</sup> in the discharge process had a high bond energy and large grain size, which hindered the decomposition of LiF and resulted in that the fluorine atoms could not come back to embed in the CF<sub>x</sub> skeleton again. But for the Na/CF<sub>x</sub> battery, owing to the lower bond energy and dissociation energy of NaF, this system could achieve reversible

charge/discharge process and was further made into rechargeable battery (Figure 11D).<sup>[182]</sup> Additionally, Xie et al. prepared the transition-metal-free Mg-based battery activated by anionic insertion into FG interlayers, which exhibited a capacity of 110 mAh g<sup>-1</sup> at 10 mA g<sup>-1</sup> (90 mAh g<sup>-1</sup> at 50 mA g<sup>-1</sup>). Compared with conventional Mg/FGi batteries, its advantage was located on the ignorable voltage polarization between discharge and charge, and the pseudocapacitance-like reversible electrochemistry appeared under a higher voltage (Figure 11E).<sup>[97]</sup>

Moreover, FG also presented great potentials in the field of supercapacitors. Jiang et al. presented a novel and high-efficiency method to prepare NFG through thermal annealing of FGO using ammonia (Figure 12A). The nitrogen content

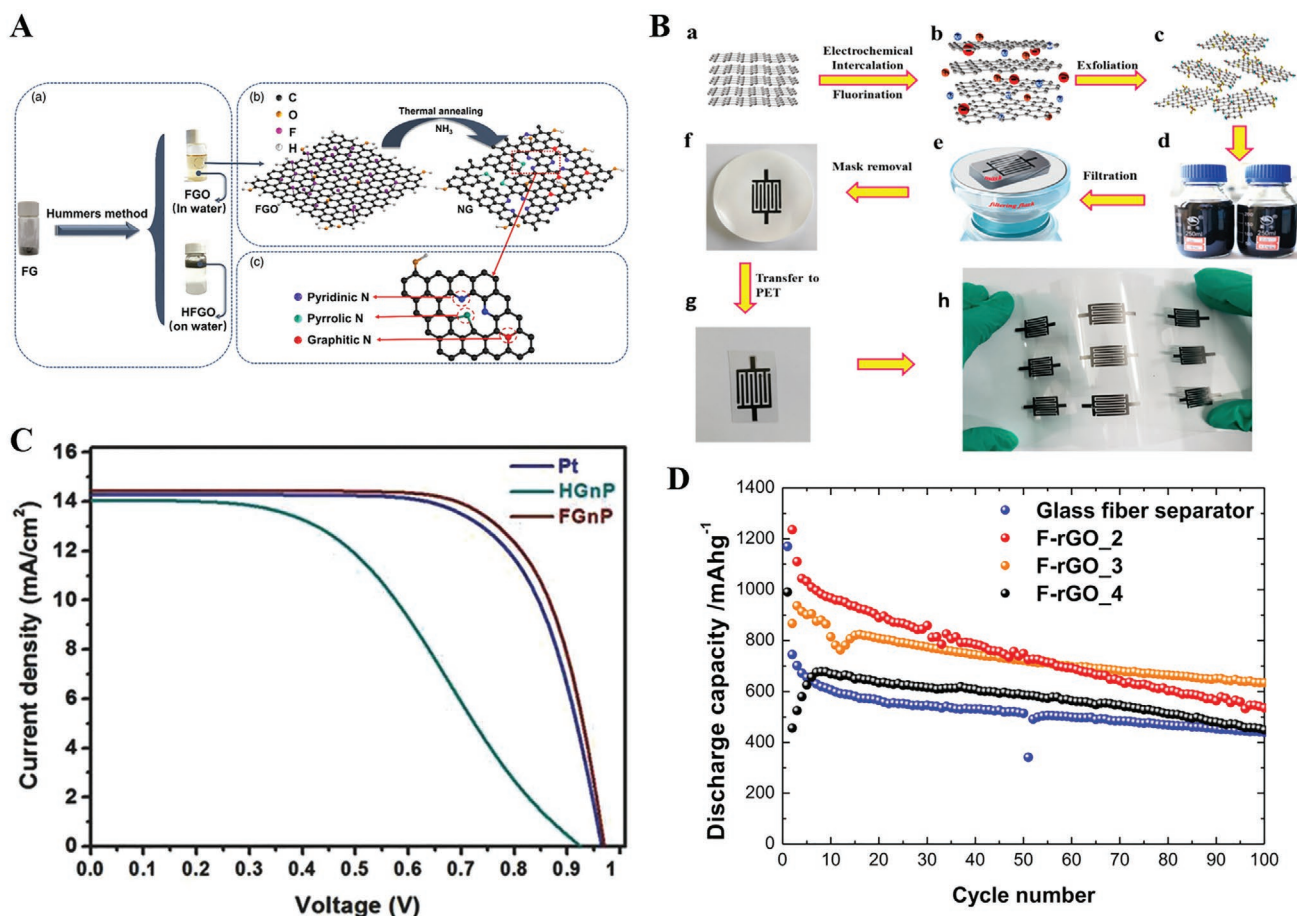


**Figure 12.** A) a) Schematic diagram of the synthesis of FGO and HFGO. b,c) Illustrative photographs of the doping process and the lattice structure of FGO and NG. A) Reproduced with permission.<sup>[185]</sup> Copyright 2019, Society of Chemical Industry. B) Schematic of the fabrication procedure of the FG-based microsupercapacitors. Reproduced with permission.<sup>[120]</sup> Copyright 2018, American Chemical Society. C) *I*–*V* curves of the dye-sensitized solar cells. Reproduced with permission.<sup>[69]</sup> Copyright 2015, Wiley-VCH. D) Cycling stability of four kinds of Li–S batteries. Reproduced with permission.<sup>[186]</sup> Copyright 2015, American Chemical Society.

of NFG was up to 12.45%, which guaranteed the excellent capacitance of the supercapacitors when NFG was applied as electrode material. Therefore, due to the high nitrogen doping and large number of active sites, the highest specific capacitance attained 225.2 F g<sup>-1</sup> at a current density of 1 A g<sup>-1</sup> in the three-electrode configuration.<sup>[185]</sup> Zhou et al. developed a scalable, one-step electrochemical exfoliation of FGi to prepare the highly solution-processable FG toward preparation of flexible and high energy density ionogel-based microsupercapacitors (Figure 12B), which delivered an energy density of 56 mWh cm<sup>-3</sup>. Furthermore, the all-solid-state microdevices offered the exceptional cyclability with about 93% reservation after 5000 cycles, due to the introduction of electrochemical active fluorine atoms and a larger interlayer spacing.<sup>[120]</sup>

Jeon et al. synthesized the edge-fluorinated graphene nanosheets as the high-performance electrodes for dye-sensitized solar cells by ball-milling method.<sup>[69]</sup> Because of the large discrepancy in electronegativity between the fluorine and carbon atoms, the edge-fluorinated graphene nanosheets offered the maximal charge polarization, higher electrochemical activities, and better in-plane charge transfer properties. Therefore, the

solar cells exhibited prominent electrochemical performance and excellent cycle life (fill factor: 71.5%;  $J_{sc}$ : 14.44 mA cm<sup>-2</sup>;  $V_{oc}$ : 970 mV; power conversion efficiency: 10.01%, Figure 12C).<sup>[69]</sup> Moreover, Vizintin et al. utilized FrGO as the interlayer additive supported by a glass fiber separator in lithium–sulfur batteries (Figure 12D), which successfully hindered the diffusion of polysulfides from the porous cathode to the lithium anode and thus prevented the redox shuttle effect.<sup>[186]</sup>

For FG-based lithium batteries, the property of the FG cathode materials directly determines the overall discharge performance of the battery, but there is a contradiction between the fluorine content and the discharge platform. Nearly all relevant works are devoted to reconcile the contradictions between the aforementioned two parameters, such as the regulation of the C–F bonding nature, the structure of fluorination-phase, and the co-doping of other atoms. Indeed, the average discharge potential of FG is significantly lower than the theoretical electrochemical potential from the purely ionic C–F bond (4.5–5 V vs Li<sup>+</sup>/Li). Later works should pay close attention to develop new fluorination methods or post-treatment methods to prepare special FG materials with the dominated ionic or semi-ionic



C–F bonds and a high fluorine content, which has the potential to bring about a brand-new height. In addition, it has been a challenge to make FG into a rechargeable battery by building a new system equipped with the charge/discharge reversibility. Also, the formed semi-ionic bonds on graphene surface and the enhanced interlayer distance as well as the introduced active sites are helpful to the increase of specific capacitance when FGs are employed as the electrode materials. Further research of FG-based supercapacitors could focus on the exploration of co-doping effect and the incorporation of fluorine atoms into other 2D materials, such as transition metal oxide.

#### 4.2. Lubrication, Self-Cleaning, and Oil–Water Separation

The specific C–F bonds bring about great changes for surface character of FG like low surface energy, which thus expands the applications of FG in relevant fields including lubrication, self-cleaning, and oil–water separation.<sup>[46–48,50,157,187–197]</sup> FG with a high fluorine content has been considered as an excellent lubricant, including its noumenal film coating and additive in lubricating oil and composites materials. Lei et al. prepared high-quality FG nanosheets via the intercalation of raw FGi by *N,N*-dimethylformamide (DMF) through microwave treatment. The obtained high-quality nanosheets exhibited distinguished lubrication behavior in oil only with 1 wt% FG nanosheets, which was attributed to the uniform dispersion of FG in the oil.<sup>[197]</sup> Fan et al. constructed a lubricating system with an ultralow friction coefficient of 0.08 by using FG as the lubricating-oil additive. Meanwhile, the as-prepared FG showed excellent dispersibility in oil as well as prominent thermal stability (over 400 °C). Compared with the pristine lubricating oil, the addition of highly fluorinated graphene with an F/C ratio of 1.0 achieved a 90.9% and 51.4% decrease in the wear rate and friction coefficient, respectively (Figure 13A).<sup>[47]</sup> In addition, they also used GO as the raw material to prepare FGO with good water dispersity, thus extending the excellent tribological performance of FG into the water environment.<sup>[46]</sup> On the strength of previous work, they further developed a facile and moderate way to complete nondestructive covalent functionalization for FG by activation of its dormant radicals that were stabilized by the surrounding aromatic regions and typical 2D skeleton. The active radicals at certain temperature initiated acrylic acid (AA) to be grafted onto the FG surface, which was totally different from sacrificing C–F bonds through nucleophilic substitution reaction. The obtained FG-AA product showed improved water dispersity and also maintained inherent lubricating ability because of reserved abundant fluorine-related groups.<sup>[91]</sup>

FG was also applied as the self-cleaning and anti-corrosion coating owing to its low surface energy and high hydrophobicity. Yang et al. prepared a superhydrophobic epoxy coating modified by FG on the Cu substrate. The FG sheets with low surface energy were stacked on the surface of the adhesive epoxy resin coating, which endowed the organic coating with superb water repellency and mechanical abrasion resistance. Furthermore, the fabricated epoxy coating exhibited excellent protection performance in the sodium chloride solution

(3.5 wt%) owing to the air trapped in the interface of electrolyte/coating.<sup>[157]</sup> Bharathidasan et al. compounded FGO with poly(dimethylsiloxane) (PDMS) to prepare the transparent polymeric films with superhydrophobic and oleophobic properties over aluminium alloys and transparent glass substrates by a simple spray painting technique. When the fluorine content of FG was 60 wt%, it showed the water contact angle of 173.7° and oil contact angle of 94.9°, indicating FG had great potential as the self-cleaning and corrosion resistive coatings.<sup>[199]</sup> By electrophoretic deposition method, FG nanosheets were deposited on a copper substrate. Owing to the existence of ionic–covalently bonded F–Cu–F and Cu–F–C on the interface between FG sheets and the copper foil, the deposited film exhibited ultrastrong adhesion. Also, the increase of water contact angle from 83.43° to about 122.44° and good thermal stability up to 300 °C was realized under the ambient atmosphere for the modified surface of copper.<sup>[200]</sup>

In addition, Jayaramulu et al. prepared the (HFGO)@ZIF-8 composite by using HFGO and the zeolite imidazole framework (ZIF-8, Figure 13B).<sup>[188]</sup> Compared with pure HFGO and ZIF-8 (Figure 13C-a,b), the composite exhibited a ultrahigh water contact angle of 162° (Figure 13C-c) and an ultralow oil contact angle of 0° (Figure 13C-d). When it was utilized for oil–water separation, the synergistic properties of C–F groups, the alkyl-substituted imidazole groups, nanoscale roughness, and micro–mesoporous nanoarchitecture made the composites exhibit an ultrahigh sorption selectivity, fast kinetics, and fine absorbencies for the selective absorption of polar/non-polar organic solvents from water (Figure 13C-e,f). Moreover, immobilizing metal–organic framework nanoparticles on FG surface was achieved for the first time by their work.<sup>[188]</sup> Along the same lines, Yogapriya and Kasibhatta prepared the hydrophobic/superoleophilic nanoporous composites through FG nanosheets supporting copper-based metal organic framework (HKUST-1) based on the “solution-assisted self-assembly route.”<sup>[187]</sup> The hydrophobic composites exhibited an high oil uptake in the range of 220–726 wt%, which ensured its excellent ability of separating oil from water. Surprisingly, when the prepared composites were employed to coat commercial polyurethane sponge, the obtained FG-HKUST-1 composites sponges presented a distinguished separation ability for oil and organics (ranging from 3966 to 7423 wt%) and they also showed the commendable tolerance to extreme pH conditions and mechanical disruption.<sup>[187]</sup>

On account of the self-lubricating and enhanced out-of-plane bending stiffness for FG, the recent work had further combined the two effects faultlessly.<sup>[198]</sup> It was demonstrated that the straightforward dry compression could be employed to fleetly manufacture highly close-knit FG monoliths under room temperature without any solvent assist (Figure 13D). The increased bending stiffness of FG ensured relatively smooth sheet and the remarkable lubricating property actuated flat sheets to voluntarily glide, thereby achieving the organized and close-knit stacking with an interlocking network. Moreover, the FG monolith annealed by high temperature displayed a good electrical conductivity of  $5.5 \times 10^4 \text{ S m}^{-1}$  and a mechanical strength of 77 MPa.<sup>[198]</sup> Importantly, for the first time, this work realized to prepare the macroassembly of FG and pushed the application of FG from “filler” to “block.”

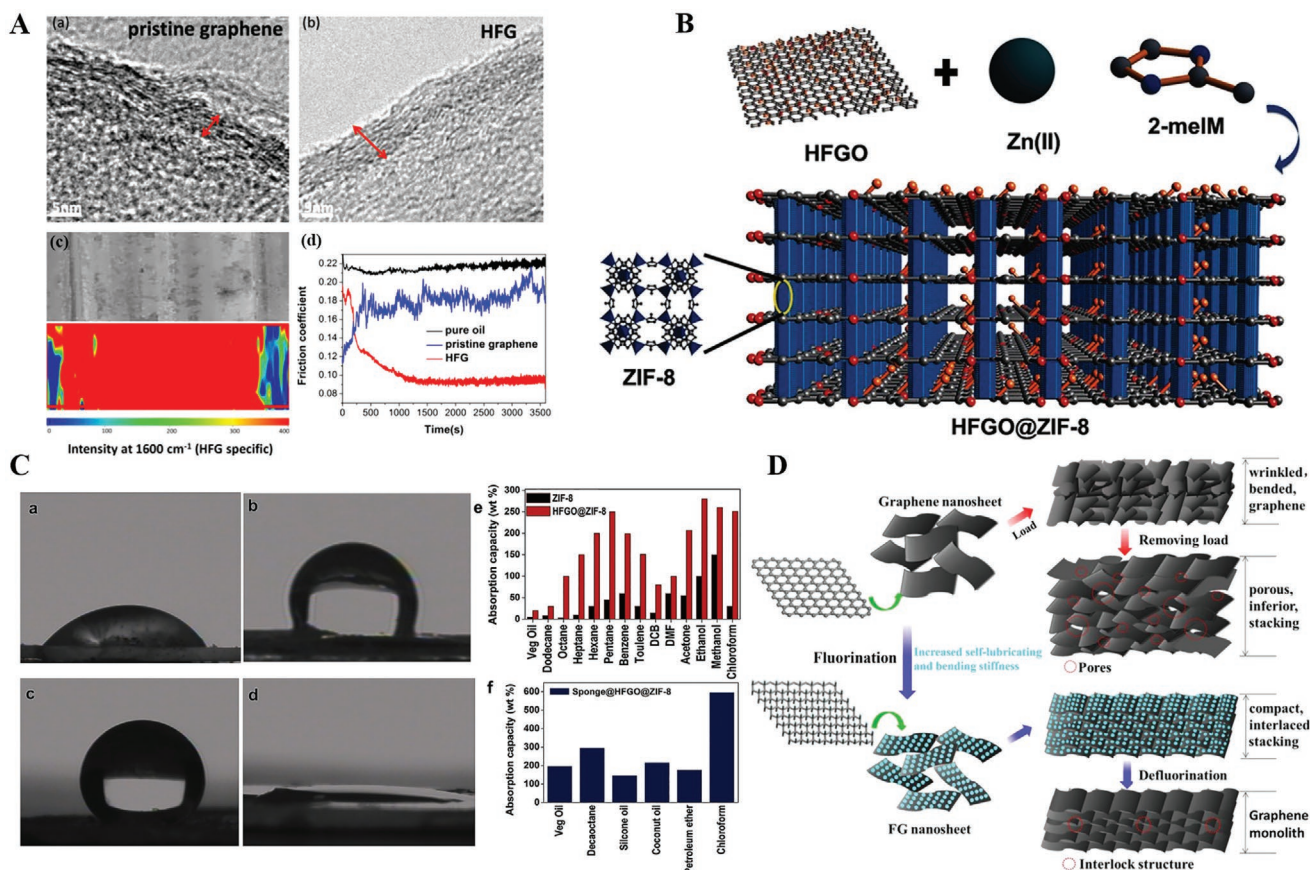


**Figure 13.** A) a,b) TEM photograph of the interlayer structure of pristine graphene and HFG. c) Optical images and the corresponding Raman mapping of the wear surface of HFG. d) Curves of friction coefficient of lubricating oil with different additives. A) Reproduced with permission.<sup>[47]</sup> Copyright 2018, American Chemical Society. B) Schematic illustration of the fabrication and structure of HFGO@ZIF-8. C) a,b) Optical images of the water contact angles of ZIF-8 and HFGO. c,d) Photographs of the water contact angles of HFGO@ZIF-8 and the prepared HFGO@ZIF-8. e,f) Absorption of oil and specific organic solvents with ZIF-8 and the prepared HFGO@ZIF-8 composite and oil absorption with Sponge@HFGO@ZIF-8. B,C) Reproduced with permission.<sup>[188]</sup> Copyright 2016, Wiley-VCH. D) Schematic diagram of dry-compression molding procedure for pristine graphene and the fluorinated samples at ambient temperature. Reproduced with permission.<sup>[198]</sup> Copyright 2020, Wiley-VCH.

The low surface energy and self-lubricating properties of FG with a relatively high F/C ratio are the unique advantages compared with other halogenated graphene and graphene oxide, which expands the application of graphene-based materials into more extensive fields. Meanwhile, the low surface energy and high thermostability also makes FG exhibit a better durability in rigorous environments. For the lubrication of FG, FG has presented the excellent tribological performances in some fields such as mechanical engineering, and it is expected to apply in biological lubrication systems in future. However, the tribological performances under high load are still troublesome question for the 2D materials, because the formed tribofilm is always unstable due to the strong adsorption force on the surface of friction pairs. Notably, based on the unique functional reactivity of FG, polymers with abundant adsorption sites or N/P-containing organic lubrication molecules can be grafted onto FG surface to enhance the stability of its tribofilm. FG-based nanofluids are also expected to be prepared for the practical applications, which also presents great potential of improving the tribological performance and leading to some novel properties simultaneously. In addition, later research is

necessary to pay attention to improve the quality of FG such as guaranteeing a less defect density, which is the important material foundation.

### 4.3. Thermally Conductive Yet Electrically Insulating Material

The fast development of wearable electronic equipment like cell phone, tablet, wearable device requires the miniaturization and the fine integration, which brings about the severe heat dissipation issues that are fatal for the service life and the dependability of the electronic equipment. Therefore, heat dissipation materials are crucial for the practical application of electronic equipment, and this market demand is also increasing.<sup>[201,202]</sup> Graphene-based heat dissipation films have caught the public's eye due to the ultrahigh thermal conductivity and preponderant flexibility. Nevertheless, the high electrical conductivity of these films restricts their applications in aforementioned field, because the good conductivity usually causes short circuit, thereby severely affecting the daily use of electronic devices.<sup>[203]</sup> In the related investigations reported in the literatures, boron

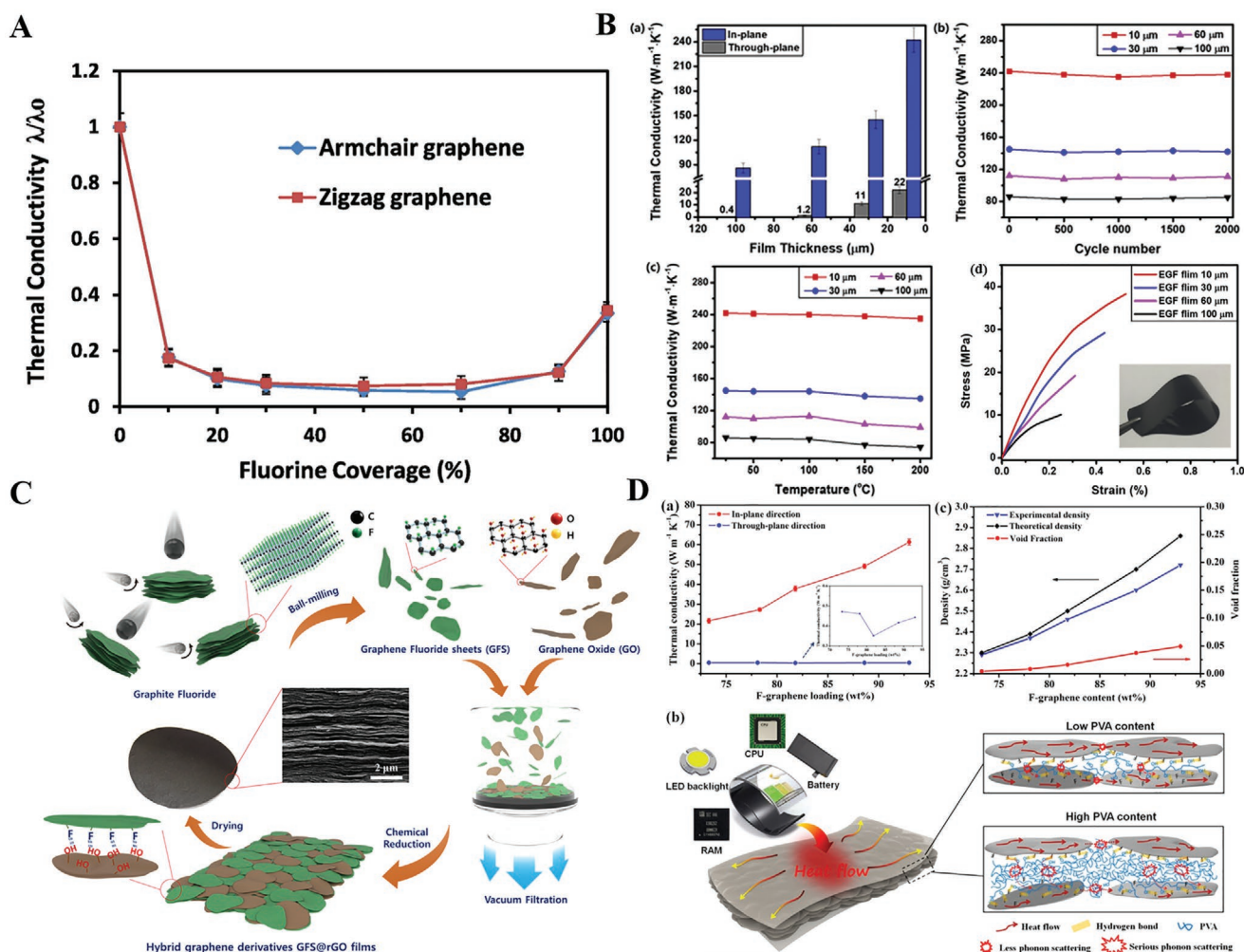


**Figure 14.** A) Simulation results of thermal conductivity versus fluorine content for FG with different configurations. Reproduced with permission.<sup>[54]</sup> Copyright 2012, Elsevier. B) a) Thermal conductivity of the fabricated FG films with different thicknesses. b,c) In-plane thermal conductivity of the prepared FG films upon bending cycle and temperature, respectively. d) Mechanical property of FG films with different thicknesses. B) Reproduced with permission.<sup>[53]</sup> Copyright 2019, Elsevier. C) Illustrative image of the preparation process of the FG@rGO composite films. Reproduced with permission.<sup>[52]</sup> Copyright 2020, American Chemical Society. D) a) In-plane and through-plane thermal conductivity of the prepared FG hybrid films with different fluorine contents. b) Schematic diagram of the heat dissipation mechanism for FG hybrid films with different PVA contents. c) Theoretical density, experimental density as well as void fraction of FG hybrid films. D) Reproduced with permission.<sup>[55]</sup> Copyright 2019, American Chemical Society.

nitride (BN) with good thermally conductive and electrically insulating property has always been regarded as a hotspot in heat dissipating field. Nevertheless, due to its shortcomings such as difficulty of exfoliation and relatively low thermal conductivity, BN-based materials still need further investigation and optimization so as to authentically apply in commercialized heat dissipating films that have a high requirement for in-plane thermal conductivity in higher power electronics.<sup>[204–206]</sup>

FG, as an emerging graphene derivative material, preserves the 2D structure of graphene, and the introduced fluorine atoms with extremely high electronegativity enable it to complete the transformation from conductor to insulator. Interestingly, Huang et al. performed the in-depth research on the thermal conductivity of FG by applying NEMD simulations for the first time.<sup>[54]</sup> The simulation results indicated that the thermal conductivity of FG first reduced and then enhanced with the increase of the fluorine content, showing an

unexpected U-shaped change (Figure 14A). Notably, when the F/C ratio of FG finally reached 1.0, the corresponding thermal conductivity was restored up to 35% of the original graphene. This phenomenon was further explained by phonon theory, i.e., the initial decrease in thermal conductivity came from the scattering of phonons by the hybrid lattice of  $\text{sp}^2$  and  $\text{sp}^3$  hybridized carbon atoms on graphene plane, and the final thermal conductivity recovery came from the formation of the unitary and regular  $\text{sp}^3$  hybridized carbon atoms.<sup>[54]</sup> Therefore, FG presents great potentials as a novel and advanced thermally conductive yet electrically insulating material for heat dissipating of electronic devices.

Therefore, a series of studies have been performed in succession. Vu et al. exfoliated FG in NMP by ball milling into single- or few-layer FG sheets and then prepared the FG films through vacuum-assisted infiltration.<sup>[53]</sup> By adjusting the thickness, the optimized 10  $\mu\text{m}$  FG film showed a high in-plane thermal



conductivity of  $242 \text{ W m}^{-1} \text{ K}^{-1}$  (Figure 14B-a) and through-plane thermal conductivity of  $21.8 \text{ W m}^{-1} \text{ K}^{-1}$  accompanied by a high electrical insulation ( $10^{-9} \text{ S m}^{-1}$ ). Mechanical tests showed that the FG film possessed a high tensile strength of 38.3 MPa and Young's modulus of 11.8 GPa (Figure 14B-d). Additionally, the thermal conductivity of the fabricated FG film exhibited good temperature tolerance and cyclic stability (Figure 14B-b,c). It is worth noting that the in-plane thermal conductivity of FG film presents the maximal value reported in thermally conductive and electrically insulating film up to now, which makes FG film show promising prospects in practical applications.<sup>[53]</sup> To improve the comprehensive property of the thermal conductive FG film, further experimental explorations were carried out by them. They prepared FG@GO hybrid films using FG and GO nanosheets via vacuum-assisted infiltration (Figure 14C). Subsequently, the film had gone through reduction with treatment of hydrogen iodide under a low temperature so as to obtain the FG@rGO film, which still showed an extremely high in-plane thermal conductivity ( $212 \text{ W m}^{-1} \text{ K}^{-1}$ ) and distinguished electrical insulating performance (volume resistivity of  $1.1 \times 10^{11} \Omega \text{ cm}$ ). The tensile strength and the Young's modulus of the film improved with increased content of rGO and finally attained 69.3 MPa and 10.2 GPa at 20 wt% of rGO, respectively. The significant enhancement of mechanical strength was attributed to the well-connected network between rGO and FG. Moreover, the thermally conductive film also presented a good tolerance to high temperature, which effectively prevented potential hazards such as burning caused by short circuits during operating.<sup>[52]</sup> Meanwhile, Wang and Wu prepared FG/polyvinyl acetate (PVA) free-standing composite film through vacuum filtration, which also showed the ultrahigh in-plane thermal conductivity of  $61.3 \text{ W m}^{-1} \text{ K}^{-1}$  at 93% of FG content (Figure 14D). Although the filler content was extremely high, the film still possessed an outstanding electrical insulation property (volume resistivity over  $10^{11} \Omega \text{ cm}$ ). When the PVA content reached 26.7 wt%, the composite film exhibited a high tensile strength of 84.4 MPa and an elongation at break of 5.7%.<sup>[55]</sup>

Much lately, fluorinated graphene aerogel (FGA) was prepared by freeze drying means. The self-assembly macroscopic materials were composed of designed interlaced graphene networks accompanied by the adjustable F/C ratio. Mechanical measurements showed that the FGA had the high elasticity and fatigue resistance, even at a low density of  $10.6 \text{ mg cm}^{-3}$ . Furthermore, the aerogel exhibited a superb insulating property of  $4 \times 10^{-7} \text{ S cm}^{-1}$  and prominent heat dissipation ability during the cycle of heating and cooling. Therefore, the FGA exhibited great potential to prepare thermoconductive polymer composite materials toward electronic packaging.<sup>[51]</sup>

It is known that boron nitride is the traditional material with thermally conductive yet electrically insulating peculiarity, and here FG also presents great potentials as a novel and advanced material in this field. In fact, FG has showed the higher heat conductivity while maintaining the electrical insulating property. In addition, the low-*k* dielectric always shows the low thermal conductivity simultaneously, which results in the difficulty of the heat dissipation in the high-power-density electron devices. The unique thermally conductive and electrically insulating peculiarity accompanied by the low dielectric constant and dielectric loss make FG exhibit a promising application

potent ion in the abovementioned pivotal area. In addition, the direct fluorination may cause the interlayer crosslink and further enhance the vertical heat conductivity which would bring about the multidimensional heat dissipation effect. To achieve the great potential of FG in this field, the future works should aim to improve the quality of FG, such as largening the sheet size, reducing the defect density, and realizing the fully fluorinated FG sheet, which will effectively enhance its heat conductivity. Of course, once FG sheets are integrated into macroscopic materials (film or monolith), the optimization of the molding technology is required to develop for reducing the interface thermal resistance.

#### 4.4. Gas Detection, Storage, and Separation

FG has been demonstrated to easily interact with gas molecules thanks to the introduced polar C–F bonds. The existence of fluorine atoms has also changed the charge distribution of graphene plane, which further increases the interaction between FG and gas molecules. Moreover, the effective gas-sensitive groups could be introduced onto the graphene plane through derivative reactions of FG. As a result, FG is regarded as a potential candidate in gas detection, storage, and separation.<sup>[98,207–212]</sup> Liu et al. displayed that FG showed a distinct color variation from white to dark yellow under the atmosphere of ammonia, which could be observed with naked eyes directly. The corresponding sensitivity reached a high value of 4.05% by PL measurement. The succedent DFT calculations demonstrated that the fluorine atoms on FG plane changed the charge-transfer properties between graphene and ammonia, so FG exhibited enhanced adsorption ability for ammonia.<sup>[98]</sup> Kim et al. prepared FGO by a facile solution fluorination using hydrofluoric acid, which adapted to room temperature ammonia sensing with a high selectivity, good recyclability, and fast response feature, accompanied by a detection limit of 6.12 ppb. Compared with pristine rGO, the sensitivity was about 20 times higher. DFT calculations revealed that F atoms effectively improved the ammonia detection ability by changing the charge distribution of oxygen-related groups, resulting in the reduction of the gas adsorption energy.<sup>[209]</sup> Also, Zhang et al. synthesized the large-area monolayer FG by  $\text{SF}_6$  plasma treatment and then applied it as the gas-sensing material, which possessed the excellent performance for ammonia detection. DFT simulation results indicated the fast response/recovery behavior for ammonia detection came from the enhanced physical adsorption of ammonia molecules owing to the introduced C–F bonds.<sup>[212]</sup>

Besides the detection of  $\text{NH}_3$ , FG is also applied to achieve the adsorption and separation of  $\text{CO}_2$ . Li et al. prepared FG with porous structure using diamine as crosslinking point, based on the nucleophilic substitution reaction between the reactive C–F bonds and various amine-terminated molecules. By controlling the type and amount of diamine, FG with different pore structures were further obtained. They showed a good adsorption capacity for  $\text{CO}_2$  (18  $\text{CO}_2$  molecules per  $\text{nm}^2$  at  $0^\circ \text{C}$  and 1.1 bars), and had a  $46.1 \text{ kJ mol}^{-1}$  adsorption heat at zero coverage, which was attributed to the high specific surface area, pore structure of different scales, and abundant active

adsorption sites.<sup>[148]</sup> Wu et al. demonstrated that FG film had the distinguished selectivity for CO<sub>2</sub>/N<sub>2</sub> separation through molecular dynamic simulations. They chose the pore-22 (with 22 carbon atoms drilled out) with dangling bonds as the graphene model and carried out an in-depth study by calculating the diffusion energy barriers for CO<sub>2</sub> and N<sub>2</sub>. Without fluorination, the pore-22 had a low selectivity because of the small distinction for the diffusion resistance for CO<sub>2</sub>/N<sub>2</sub>. After fluorination, the diffusion barrier for CO<sub>2</sub> reduced down to 0.029 eV but that for N<sub>2</sub> significantly improved to 0.116 eV, thus giving a high selectivity. The proposed mechanism suggested that CO<sub>2</sub> molecules with larger quadrupole produced strong interactions with C–F bonds, thereby easily adsorbing into the porous FG film. Also, the simulation results well matched with the experimental results.<sup>[213]</sup>

Some researchers have also utilized fluorinated carbon materials for hydrogen storage. Cheng et al. carried out experimental verification and simulation calculations on this peculiarity.<sup>[207]</sup> They found that the quasi-hydrogen bonds between the semi-ionic C–F bonds and the antibonds orbit of H<sub>2</sub> increased the adsorption enthalpy, thus showing a good hydrogen storage capacity.<sup>[207]</sup> Zhang et al. synthesized FG with porous structure through hydrothermal fluorination and further prepared FG-LiBH<sub>4</sub> composite material by ball milling. The obtained LiBH<sub>4</sub>-20 wt% FG showed excellent hydrogen storage capacity and enhanced cycling stability. Notably, the initial dehydrogenation temperature of the LiBH<sub>4</sub>-20 wt% FG reduced about 120 °C compared with that of pure LiBH<sub>4</sub>. It was attributed to that the activation energy of hydrogen desorption of LiBH<sub>4</sub> was reduced from 181.80 to 130.87 kJ mol<sup>-1</sup>, displaying the preeminent hydrogen desorption kinetics.<sup>[210]</sup>

Fluorine atoms significantly increase the gas sensing/storage abilities through changing the charge distributions in the graphene skeleton, which leads to the variation in the gas adsorption energies. In addition, based on the functional reactivity of FG, the functional molecules with a high gas sensitivity can be further grafted onto FG plane, which would improve the gas detection/storage capabilities. Notably, the stability and circulation ability of gas sensing/storage for the FG-based materials deserve to further demonstrate. The future works should confirm the contributions of the different fluorine-containing groups and fluorine distributions to the sensitivity of different gas molecules. Especially, the difference of fluorine distributions in FG sheets could produce the different bandgap and electronic effect, which would bring about the variable responding path for the gas sensing/storage.

#### 4.5. Biomedicine

It has been demonstrated that the C–F bonds of FG exhibits good biological responses and paramagnetic behavior, so it has attracted the attentions of many researchers in the biomedical field.<sup>[61,146,43]</sup> Loh et al. applied FG sheets as a scaffold to support the growth of mesenchymal stem cell (MSCs; **Figure 15A-a,b**), and the result demonstrated that FG induced better propagation and enhanced polarization of MSCs (**Figure 15A-c-e**). The observed differences in cell shape were attributed to the polarization effect of the C–F bonds, which promoted the cell

alignment and the nucleus elongation through the electrostatic induction at the interface between cell and FG.<sup>[146]</sup> Moreover, the fluorine content of FG showed crucial influence on cell morphology and nuclear elongation of MSCs (**Figure 15A-f,g**).<sup>[146]</sup> In addition, the introduced fluorine atoms on GO sheets could conspicuously change its magnetic properties.<sup>[214–217]</sup> Ajayan et al. demonstrated that FGO acted as a multimodal material (magnetic resonance imaging contrast agent, ultrasound and photoacoustic imaging, **Figure 15B-a-e**) for biological applications without any addition of magnetic nanoparticles.<sup>[43]</sup> Their subsequent work also indicated the synthesized fluorinated graphene quantum dots showed a temperature-dependent magnetic behavior followed Curie's law. By further DFT calculations, the paramagnetism arose from fluorine atoms and other functional groups was confirmed.<sup>[61]</sup>

Wang et al. compared the antibacterial properties from GO to FG as well as guanidine-modified graphene (PHGH-G).<sup>[56]</sup> It was found that PHGH-G with 2% grafting ratio had extremely high antibacterial activity when employed to the culture medium with the concentration of 20 µg mL<sup>-1</sup>. It achieved to reduce about 99.9% survivability for *Escherichia coli*, accompanied by the collapse of bacterial cell membranes through the affinity between PHGH-G with positive charge and the negatively charged cell membranes.<sup>[56]</sup> Gong et al. developed a straightforward strategy to synthesize water-soluble FGO sheets through the drastic oxidation of FG sheets (**Figure 15C**).<sup>[60]</sup> By changing the reaction conditions, FG sheets were successfully transformed into ultrasmall-sized FGO granules with improved photothermal performance, which achieved the easy uptake of cells by endocytosis. The introduced oxygen-containing groups endowed FGO with high reactivity and hydrophilicity, and then targeted folic acid or chitosan could be grafted on FGO surface, accompanied by excellent water dispersibility.<sup>[57,60]</sup> Also, the FGO nanoparticles exhibited relucant PL with on/off switchable peculiarity depending on the loading and release of doxorubicin triggered by pH stimulation, which was further applied to monitor the whole drug load and release process in real-time. Furthermore, the FGO with ultrasmall sheet size had excellent near-infrared absorption and achieved the synergistic cancer chemo-photothermal therapy under the irradiation of near-infrared light.<sup>[57,60,62]</sup> Additionally, their further DFT results proved the noncovalent interactions like hydrogen bonds and van der Waals force governed the drug loading and releasing process, thus providing an in-depth study into the exploration of drug delivery systems.<sup>[58]</sup>

Up to now, only several works reported the application of FG in biomedicine, but it has presented obvious potentials in this field on account of the unique fluorine effect. In fact, many organic fluorine-containing small molecules have played a leading role in this field, which gives us an explicit direction. For example, the introduced fluorine endows FG with a strong paramagnetism, which is crucial for its application in MRI. Meanwhile, FGs have the tunable bandgap and their PL emission can be designed to achieve the target detection in biological systems. Moreover, the chemical activity of C–F bonds in FG sheets enables the specific molecules to be grafted into FG surface, which shows the great advantages for functional integration. Meanwhile, in view of this biological systems, the water dispersibility of FG is still crucial problem. Through

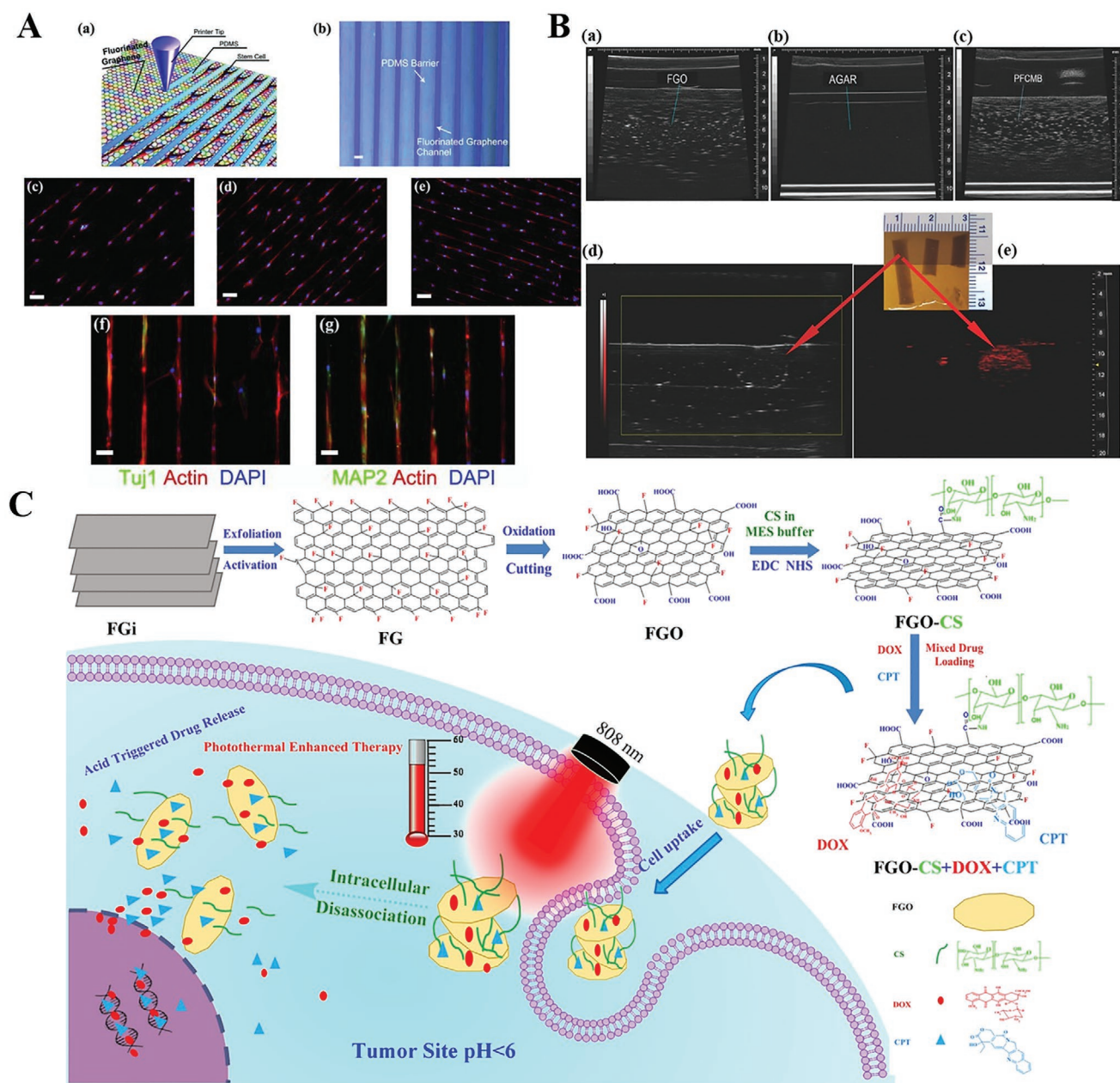


**Figure 15.** A) a) Schematic illustration of the fabrication process of the scaffold for stem cell growth by using FG as the substrate. b) Optical image of the fabricated scaffold. c–e) The orientated growth of stem cell on different substrates. f, g) MSCs tend to attached on the FG arrays. A) Reproduced with permission.<sup>[146]</sup> Copyright 2012, Wiley-VCH. B) a–c) Ultrasound and d, e) photoacoustic behavior of FGO. B) Reproduced with permission.<sup>[43]</sup> Copyright 2013, Wiley-VCH. C) Schematic diagram of the synthesis of FGO nanoparticles and the subsequent drug loading process, drug release process, and photothermal enhancing therapy behavior. Reproduced with permission.<sup>[60]</sup> Copyright 2017, Wiley-VCH.

decreasing the fluorine content and increasing the oxygen content, the water dispersibility will be definitely improved. However, we always expect to achieve the high fluorine content and the water dispersibility simultaneously. So, it may be a perfect solution to utilize the free radicals in FG sheets to initiate the polymerization of monomer and realized the in situ grafting of the obtained polymer, which would not sacrifice the C–F bonds in FG sheets. In addition, it should be noted that the biological toxicity and biocompatibility of FG must be further confirmed and investigated.

#### 4.6. Other Applications

In addition to the aforementioned application fields, the application of FG in other aspects have also been preliminarily reported by investigators.<sup>[170,218–230]</sup> Zhao et al.'s study indicated that FG with single-sided fluorination could be used as the metal-free electrocatalyst in ORR reactions. Through simulations, single-sided fluorinated graphene had a high spin density, which enhanced the adsorption of  $O_2$  and promoted the  $4e^-$  reaction process with an excellent electrocatalytic activity.<sup>[170]</sup>



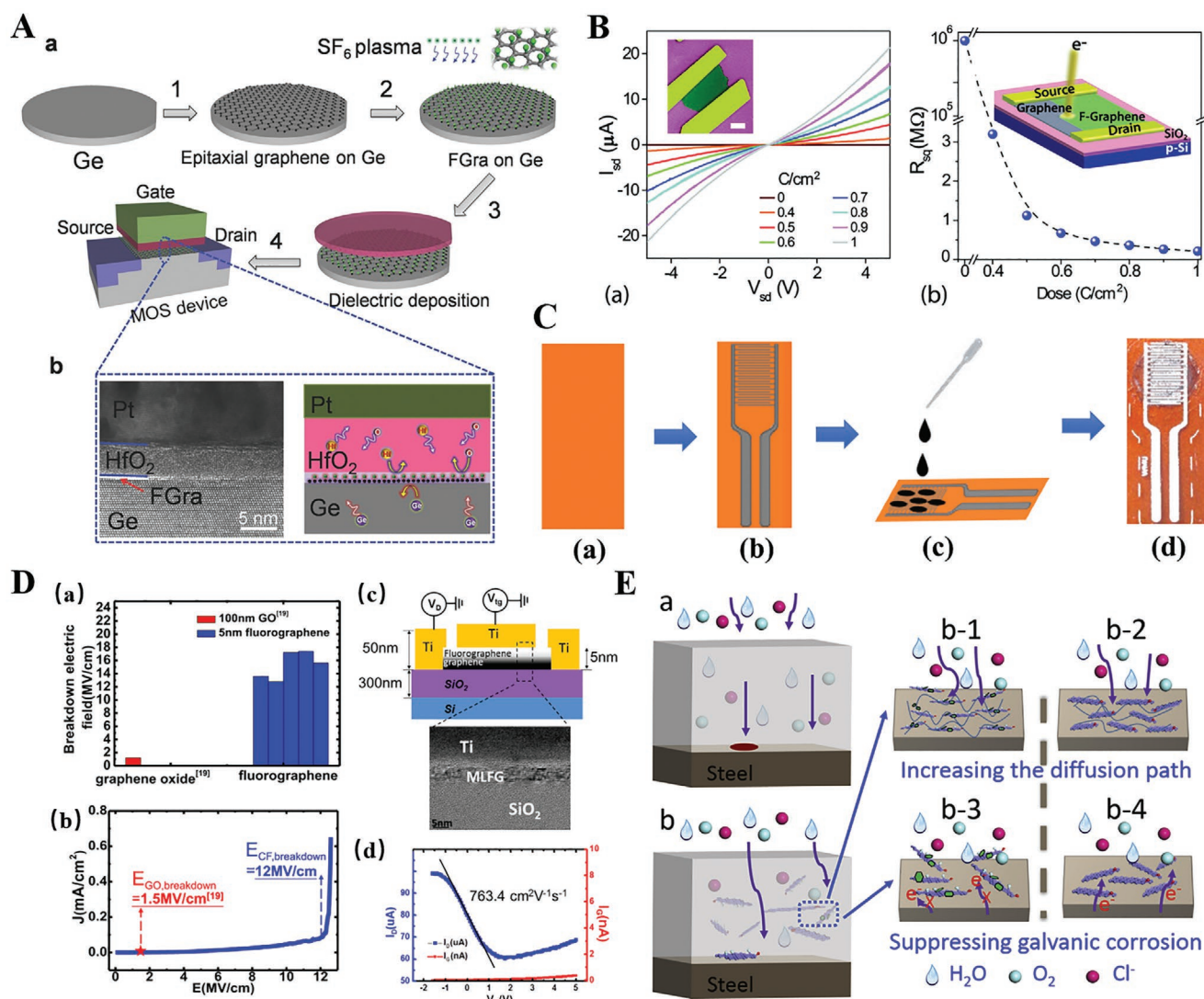


**Figure 16.** A) Schematic illustration of the fabrication process of diffusion barrier layer in the Ge-based MOS device. Reproduced with permission.<sup>[164]</sup> Copyright 2015, Wiley-VCH. B) a)  $I$ - $V$  characteristics for the fabricated FG-based device. b) The obtained resistance per square plotted versus electron irradiation dose. B) Reproduced with permission.<sup>[220]</sup> Copyright 2011, American Chemical Society. C) Schematic images of the fabrication process of the humidity sensor on polyimide substrate. Reproduced with permission.<sup>[221]</sup> Copyright 2020, IEEE. D) a) Breakdown electric field of GO and 10-layered FG. b) The current density of FG-based capacitor in (a). c) Schematic illustration of the prepared FET device consisted of FG gate dielectric. The inset shows the TEM cross-sectional microscopy image. d) The transfer characteristics and the gate current of the graphene-based transistor. D) Reproduced with permission.<sup>[167]</sup> Copyright 2014, The Authors, published by Springer Nature. E) Schematic illustration of anticorrosion mechanism for epoxy coating and composite coatings. Reproduced with permission.<sup>[115]</sup> Copyright 2019, Elsevier.

The research of Antonova et al. showed that FG could be used as an insulating layer for flexible electrodes, which showed excellent transparency and mechanical strength, and the prepared flexible electrodes had low leakage current and high breakdown strength.<sup>[218]</sup> According to Wang et al.'s work, the prepared FG/polyimide hybrid membrane (F/C ratio of 1.0, with only 1.0 wt% FG) presented prominent dielectric property with drastically reduced dielectric constant from 3.1 to 2.1 (1 MHz), while the dielectric loss still maintained the same level in the whole frequency.<sup>[219]</sup> Feng et al. provided a simple and efficient strategy to prepare fluorinated polyimide (f-PI)/modified FG composite film with a low dielectric constant (2.09, 1 MHz) and high tensile strength (300.1 MPa). The dispersibility

of FG in the f-PI matrix was promoted by the grafting of 2,2''-bis(trifluoromethyl)-[1,1''-biphenyl]-4,4'-diamine on the skeleton of FG.<sup>[229]</sup> Also, they utilized this composite film as the dielectric layer to fabricate the organic thin-film transistor, and it exhibited good transistor mobility and ON/OFF ratio.<sup>[229]</sup> Meanwhile, the thermal and mechanical properties of PI was improved via employing FG sheets as the nanofillers. Compared with pure PI matrix, the addition of 0.5 wt% FG sheets in PI could increase the tensile stress by 30.4% and elongation at break by 115.2%.<sup>[223]</sup> Zheng et al. employed FG as the diffusion barrier between the channel and dielectric layer in Ge-based semiconductor devices (Figure 16A). The obtained semiconductor device showed extremely low leakage and negligible

capacitance versus voltage hysteresis.<sup>[164]</sup> Withers et al. performed selective reduction on FG surface by laser irradiation, and the conductivity of the reduced area was several orders of magnitude higher than that of original FG (Figure 16B). On this basis, the conductivity or semiconductor performance was controlled in the range of several micrometers or tens of nanometers, and this pattern-based reduction was further developed to prepare advanced resistive memory and multibyte data storage.<sup>[220]</sup>

Hajian et al. developed a methodology to prepare highly sensitive FG-based humidity sensor by dropping the FG suspension on the interdigitated silver electrodes (Figure 16C), which possessed a high sensitivity even under 0.24%/relative humidity. By DFT calculations, the formation of hydrogen bonds between C–F bonds and water molecules guaranteed the high sensitivity as a humidity sensor.<sup>[221]</sup> The result of Krstić et al. demonstrated that FG could be a promising candidate for nanoelectronic applications like chemical sensor or thermoelectric layer by engineering the electrical charge transport peculiarity through individual flakes and films.<sup>[222]</sup> Ho et al. prepared the new graphene-based transistor by employing FG as the dielectric material (Figure 16D-c).<sup>[167]</sup> As shown in Figure 16D-a,b, the measured breakdown electric field for the 5 nm thickness FG film was more than 10 M V<sup>-1</sup>. In addition, the fabricated top-gated transistor based on the FG/graphene heterostructure, exhibited an average mobility of above 760 cm<sup>2</sup> V<sup>-1</sup> s<sup>-1</sup> (Figure 16D-d), which was higher than that of SiO<sub>2</sub> or GO as the gate dielectric materials.<sup>[167]</sup> Recently, Wu et al. adopted acridinium ionic liquid (IL) [MAC]Br to well disperse fluorinated reduced graphene oxide (FrGO) by noncovalent interaction, and then the stabilized FrGO mixture was added into the waterborne epoxy matrix for underwater corrosion protection of steel artifacts. As shown from Figure 16E, the labyrinth effect brought by the well-dispersed FrGO in the matrix resin could significantly increase the diffusion path of the corrosion-related molecules, namely, the shielding effect. Moreover, compared with unmodified rGO, FrGO had extremely low conductivity, which effectively reduced micro-galvanic corrosion in the composite coating.<sup>[115]</sup>

## 5. Derivative Chemistry of FG and Its Applications

### 5.1. Mechanism of FG's Derivative Chemistry

For graphene, owing to the existence of its stable 2D conjugated structure, the energy barriers for various grafting reactions on graphene surface are relatively high, so it is difficult for pristine graphene to obtain derivative products that meet the expected requirements. But for FG, it exhibits much higher chemical reactivity, since the introduced C–F bonds destroy the original stable conjugated structure.<sup>[28–30,137,138,141]</sup> However, the classical organic chemistry generally believes that the C–F bonds have a high bond energy, so the chemical reactions associated with the C–F bond transition are difficult to occur.<sup>[158,159]</sup> For example, many fluorine-containing organic substances such as PTFE have extremely high chemical and thermal stability.<sup>[231–234]</sup> But from previous research, FG would undergo partial reduction of C–F bonds under suitable conditions, along with noteworthy

changes in the electrical properties, bandgap, and thermal stability.<sup>[138,139,141,151,161,220]</sup> Additionally, FG could also go through various derivative reactions for grafting different functional groups, such as nucleophilic substitution reactions and free radicals initiating polymerization, which is extremely arduous to complete on pristine graphene.<sup>[75,83–85]</sup> From the perspective of most researchers, those marvelous cleavage of fluorine atoms may be attributed to the presence of semi-ionic C–F bonds and ionic C–F bonds on the FG plane with lower bond energy, and the 2D structure also causes the unsteadiness of C–F bonds.<sup>[137,138,140,149]</sup>

It is worth mentioning that the reaction mechanism is very complicated and some controversies about the specific classification of the C–F bond types still exist. Meanwhile, the elaborated process and mechanism of chemical reactions on FG surface also lack sufficient and direct evidences, though many researchers have tried to certify them.<sup>[84,141,143]</sup> According to Dubecký's DFT calculations, the C–F bond dissociation energies for homo- and heterolytic cleavage were above 100 kcal mol<sup>-1</sup>, thus the nucleophilic substitution reaction could hardly be attributed to the S<sub>N</sub>1 mechanism. Through their experiments, it was found that the activation energy barrier was only 14 ± 5 kcal mol<sup>-1</sup> for the S<sub>N</sub>2 substitution when FG reacted with NaOH in acetone (at ambient temperature), so they classified the nucleophilic reaction of FG as the S<sub>N</sub>2 process, which was kinetically preferred.<sup>[141]</sup> However, during the S<sub>N</sub>2 reaction, nucleophilic reagents must attack from the opposite direction of the C–F bonds, thereby inevitably causing the inversion of configuration for the carbon skeleton, which seems impossible in the large 2D structure of FG.<sup>[84]</sup> From Lai et al.'s work, by employing electron paramagnetic resonance (EPR) spectroscopy, both defluorination and grafting reactions of FG occurred in a radical mechanism, as supported by radical capture method coupled with simulation calculations.<sup>[80,84,143]</sup> The defluorination was initiated by the single electron transfer reaction between C–F bonds and nucleophilic agents. By the removing of fluorine atom and the subsequent formation of graphene radicals, nucleophile reagents attack the active radicals so as to be grafted onto FG surface. Further DFT calculations demonstrated traditional S<sub>N</sub>1 or S<sub>N</sub>2 mechanism was unbecoming for the nucleophilic substitution reaction of FG.<sup>[84]</sup> Nevertheless, the further Friedel–Crafts reaction of FG reported by Lai et al. seemed contradictory with the abovementioned radical mechanism for the nucleophilic substitution reaction, because Friedel–Crafts reaction is commonly regarded as S<sub>N</sub>1 reaction process.<sup>[77]</sup> Therefore, the process and mechanism of nucleophilic substitution reactions on FG surface still need in-depth and detailed study to indicate its rationality. In a word, through the study of its derivative reaction mechanism, the existing problems and application bottlenecks of FG can be well clarified and solved.

### 5.2. Derivative Reactions and Applications

Based on the high reactivity of C–F bonds in FG, researchers took advantage of this peculiarity to carry out large quantities of derivative reactions and extended it to different reaction systems, as shown in **Figure 17**. Stine et al. developed

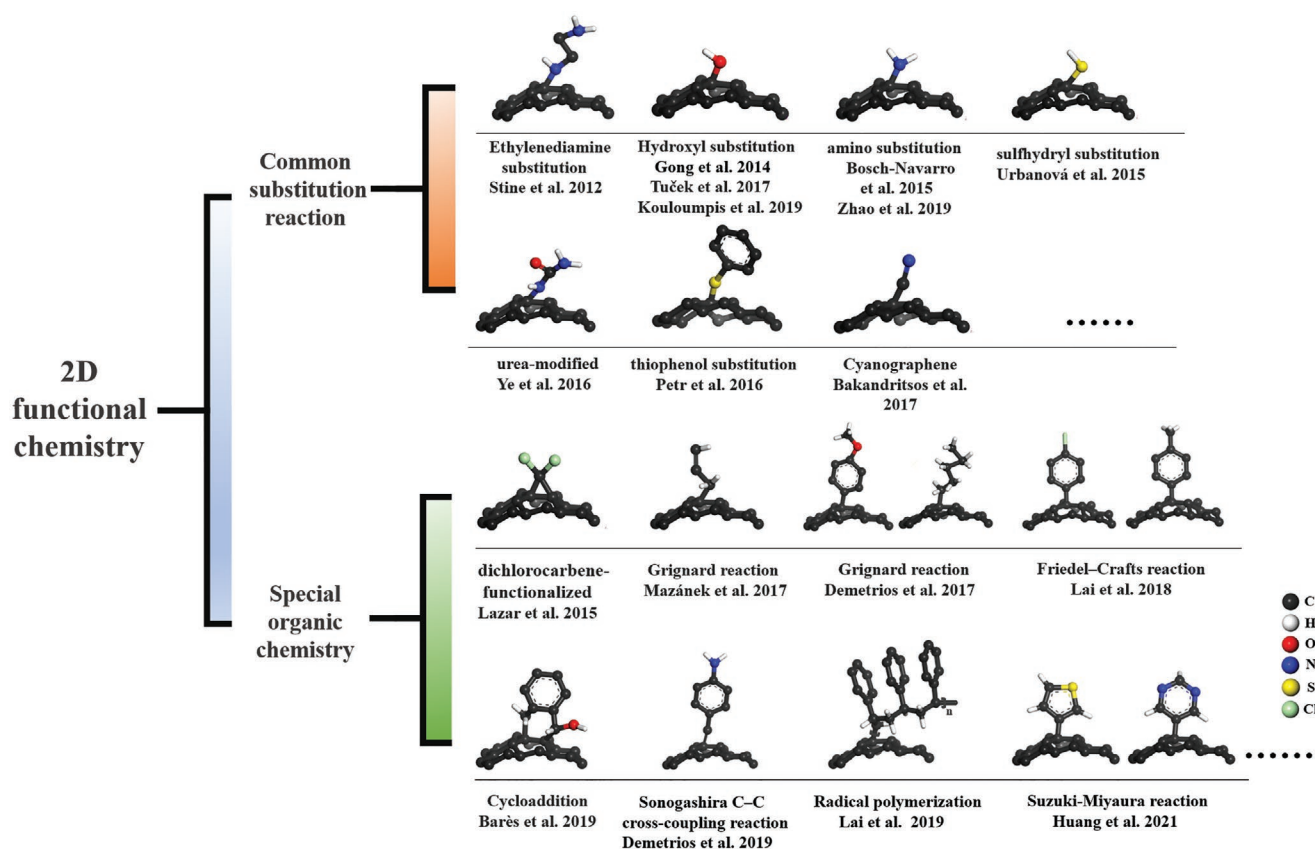


Figure 17. Broad derivative chemistry of fluorinated graphene, arranged in chronological order.

a method for the covalent functionalization of FG with ethylenediamine to obtain the amino-functionalized graphene. The layer packing density was calculated to be  $23.7 \text{ \AA}^2$  per molecule, indicating a tightly packed monolayer. Also, the product appeared to be stable under heating or solvent immersion and the unreacted amine group on the other side was capable of further chemical reactions.<sup>[86]</sup> Bosch-Navarro et al. prepared water-soluble FG by covalent modification with amino groups, and gold nanoparticles were successfully loaded on the 2D surface for detecting the grafting sites.<sup>[88]</sup> Lazar et al. introduced dichlorocarbene (DCC) onto FG plane, and they confirmed the DCC-FG existed with a stable state when F atoms adsorbed on graphene plane, as demonstrated by DFT calculations.<sup>[235]</sup> Ye et al. used urea as a nucleophile to react with FG so as to obtain urea-functionalized FG. The dispersibility in water was greatly increased and the excellent water-based lubrication performance has been demonstrated, thereby paving a pathway for FG to be applied in water environment.<sup>[89]</sup> Kovaříček et al. confirmed the nucleophilic reaction process of gaseous aromatic thiol on the surface of FG, thereby successfully achieving aromatic thiol functionalization of FG. Simultaneously, by employing surface-enhanced Raman spectroscopy, the derivative reactions of FG were visualized. This derivative reaction of FG provides a universal route for customizing specific graphene derivatives, and it also paves the way for fine-tuning the bandgap of graphene materials, which is vital for graphene-based transistors.<sup>[72]</sup>

According to the work of Bakandritsos et al. work, cyanographene was also successfully prepared by employing NaCN as the nucleophile to react with FG in DMF for the first time, and the consequent hydrolysis of cyanographene under acidic medium condition resulted in the formation of graphene acid (Gr-COOH), namely, a 2D carboxylic acid with a low and explicit pKa of 5.2, which could form a stable colloidal dispersion in the aqueous solution with pH = 8 (Figure 18A-b). At different pH values, the carboxyl group showed different degrees of deprotonation, thus exhibiting completely different self-assembly behaviors (Figure 18A-c).<sup>[73]</sup> Furthermore, the carboxyl groups enabled straightforward, customized, and broadly accessible 2D chemistry onto graphene, which was proved through the reaction with other amino reagents. Also, as the highly conductive solid 2D carboxylic acid, Gr-COOH was expected to be a potential candidate in sensor, battery, and proton-conducting films.<sup>[73]</sup> Zhao et al. took advantage of FG as a precursor to react with  $\text{NaNH}_2$  to synthesize N-doped graphene, which exhibited excellent electrochemical activity in the ORR reaction. They found  $\text{NH}_2/\text{F}$  ratio had a decisive influence on the electrochemical performance of the N-doped graphene. By controlling the fluorination process,  $(\text{NH}_2)_{70}\text{-C}_{100}\text{-F}_{2.8}$  even delivered better electrocatalytic activity than a Pt/C catalyst.<sup>[81]</sup>

Chronopoulos et al. developed Grignard reaction on FG surface to achieve targeted functionalization under mild condition, and a series of alkyl, alkenyl, and aryl moieties were grafted onto the FG surface successfully, which yielded the



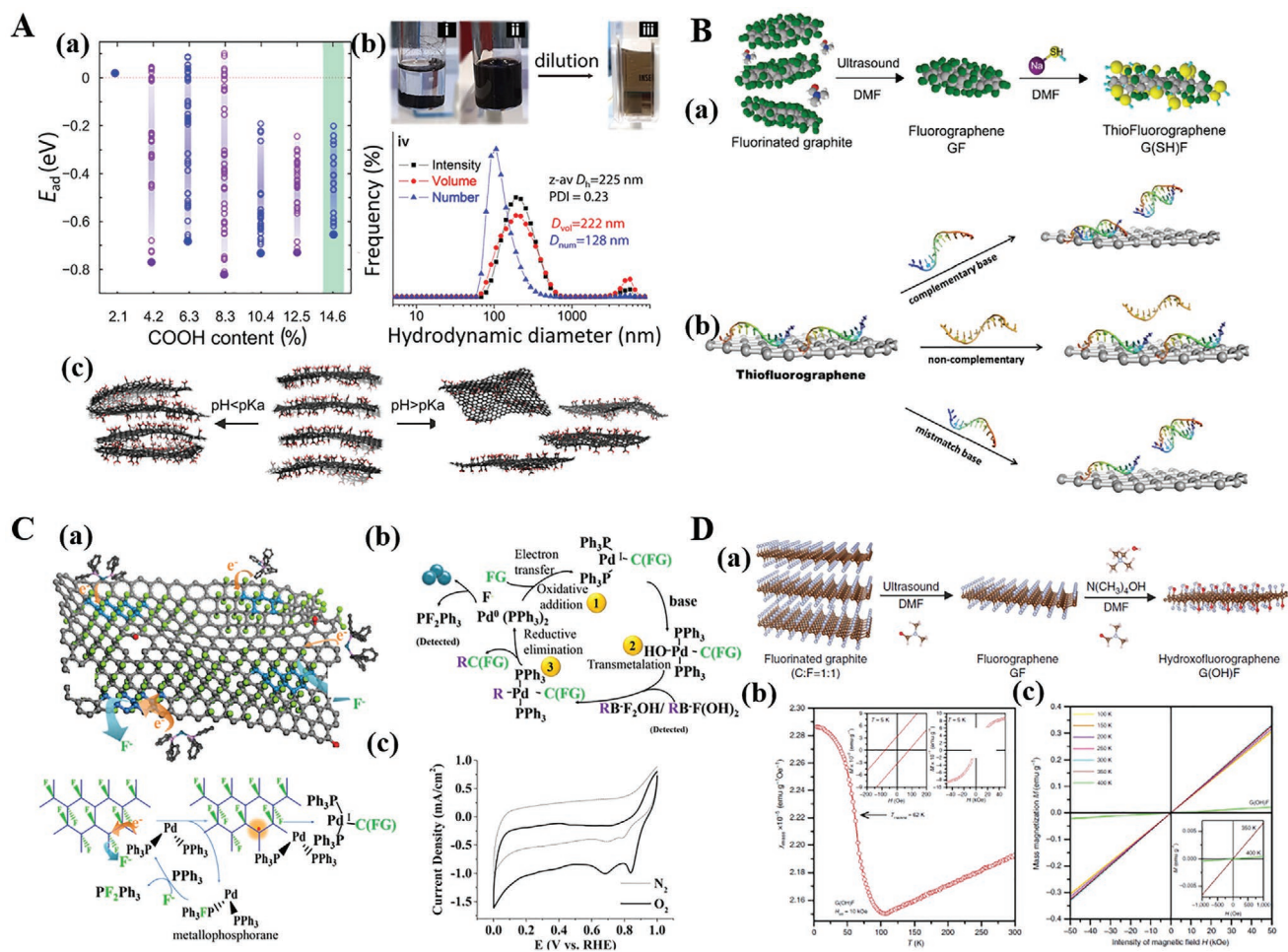


**Figure 18.** A) a) The adsorption energy of carboxyl to graphene. b) i–iii) photographs of the FG aqueous solution, the formed steady colloid dispersion of the Gr-COOH in H<sub>2</sub>O (pH = 8) and the transparent dispersion formed through dilution of the colloid solution, respectively. iv) Hydrodynamic diameter distribution of Gr-COOH in H<sub>2</sub>O (pH = 8). c) Structures of protonated and partially (50%) deprotonated Gr-COOH in water at low/high pH values obtained by molecular dynamics simulations, showing their spontaneous self-assembly behavior. A) Reproduced with permission.<sup>[73]</sup> Copyright 2017, American Chemical Society. B) a) Illustrative image of the preparation process of thiofluorographene. b) Schematic illustration of the working principle of the DNA biosensor. B) Reproduced with permission.<sup>[90]</sup> Copyright 2015, Wiley-VCH. C) a) Schematic illustration of single electron transfer (SET) between FG and Pd(PPh<sub>3</sub>)<sub>4</sub>. b) Possible mechanism of the Suzuki reaction for FG. c) Cyclic voltammograms of FG-TBA in oxygen- and nitrogen-saturated 0.1 M KOH at a scan rate of 10 mV s<sup>-1</sup>. C) Reproduced with permission.<sup>[83]</sup> Copyright 2021, The Royal Society of Chemistry. D) a) The fabrication procedure of the G(OH)F. b) Temperature evolution of the mass magnetic susceptibility ( $\chi_{mass}$ ) of G(OH)F. The insets display the hysteresis loops of G(OH)F at 5 K. c) Isothermal magnetization curves of G(OH)F, recorded from 100 to 400 K. The inset shows the isothermal magnetization curves at 350 and 400 K. D) Reproduced under the terms of the CC-BY Creative Commons Attribution 4.0 International License (<https://creativecommons.org/licenses/by/4.0/>).<sup>[76]</sup> Copyright 2017, The Authors, published by Springer Nature.

homogenous, double-sided, and high-density (5.5–11.2%) functionalization, as well. Through their theoretical calculations, it was found that the nucleophilicity determined the nucleophilic substitution reaction for FG.<sup>[75]</sup> Additionally, their further exploration demonstrated that alkynyl could be successfully grafted onto graphene surface through Sonogashira C–C cross-coupling between FG and terminal alkynes.<sup>[78]</sup> Almost at the same time, ethyl, vinyl, ethynyl, and propargyl were further grafted onto FG surface by the Grignard reaction. Meanwhile, the terminal C≡C bonds on propargyl were utilized for click reactions toward miscellaneous azides, thereby resulting in the formation of triazole rings on graphene plane.<sup>[74]</sup> Thiofluorographene was successfully prepared by Urbanová based on the nucleophilic reaction between FG and sodium hydrosulfide in DMF

(Figure 18B-a), which showed promising application prospects in impedimetric of DNA hybridization (Figure 18B-b).<sup>[90]</sup> Barès et al. proved that the C=C bonds around the polar C–F bonds of FG have larger activity, so the photo-induced radical-free Diels–Alder cycloaddition between FG and diene could occur. Meanwhile, the nucleophilic substitution reaction using amine was subsequently realized, which enabled the preparation of dual-functional graphene derivative.<sup>[79]</sup> Lately, various types of organoboron reagents such as 3-thiopheneboronic acid (TBA) were grafted onto graphene plane via Suzuki–Miyaura reaction (Figure 18C-a,b), and the prepared FG-TBA with Pd nanoparticles fixed on the graphene plane showed a better activity than commercial Pt in ORR reaction under optimal conditions (Figure 18C-c).<sup>[83]</sup>

Lai et al. developed the Friedel–Crafts reaction between FG and aryl agents based on the good chemical reactivity of C–F bonds. Under the catalysis of Lewis acid, FG could react with aryl component such as toluene, chlorobenzene, and polystyrene, thus leading to the formation of C–C bonds that are perpendicular to the graphene plane. Notably, the grafting density of arylation functionalization using FG reached about 20%.<sup>[83]</sup> In addition, through introducing EPR detection in the defluorination and nucleophilic substitution processes, an unexpected strong paramagnetic/radical signal was detected.<sup>[84]</sup> Inspired by this phenomenon, the polymerization of vinyl monomer could be successfully triggered by FG, which almost possessed comparative initiation efficiency compared with the traditional azodiisobutyrodinitrile initiation systems. Additionally, by further investigations, the polymerization triggered by FG behaved some extraordinary characteristics, e.g., the insusceptibility to oxygen molecules and long lifetime of radical centers.<sup>[80]</sup>

Gong et al. reported a facile and convenient means to prepare hydroxylated graphene (HOG). Through analyzing element constituent, it was found that the hydroxy was uniformly grafted onto graphene surface. Additionally, the obtained HOG showed a split peak in the PL emission spectrum when excited by UV radiation and the highly adjustable PL emission ranging from greenish white (0.343, 0.392) to deep blue (0.156, 0.094) was achieved, as well. Their work provided an easy way for preparing graphene derivatives with adjustable PL performance.<sup>[87]</sup> Hydroxyl functionalized graphene was also reported by Tuček via the reaction between FG and appropriate hydroxy-containing organic reagents at room temperature (Figure 18D-a). Hinging on the chemical composition and  $sp^3$  coverage, these novel graphene derivatives exhibited antiferromagnetic ordering under room temperature, which is never reported for the  $sp$ -based materials (Figure 18D-b,c). Also, the further theoretical calculation indicated the origin of the room temperature magnetism in terms of  $sp^2$ -conjugated diradical motifs embedded in the  $sp^3$  matrix and superexchange interactions via hydroxy functionalization.<sup>[76]</sup> Based on this peculiarity, the hydroxyl functionalized FG could be applied in spintronics and magnetically separable nanocarriers.<sup>[76]</sup> Recently, Kouloumpis et al. reported the one-step means to prepare Janus-type hydroxylated graphene at a water/toluene interface via nucleophilic substitution reaction. During the reaction, the water phase with pH of about 11 enabled the hydroxyl to replace C–F bonds in a mild condition while the toluene phase protected C–F bonds. The obtained bifunctional product exhibited entirely different self-assembly behaviors in various solvents.<sup>[82]</sup>

In conclusion, by taking advantage of the unique functional chemistry of FG, specific functional groups are designed to be grafted onto the graphene surface, which opens a universal route for the functionalization and even multifunctionalization of graphene, which further expands its application fields. In addition, the generality of its derivative chemistry for some other classical organic reactions has been verified. However, the utilization efficiency of C–F bond has been not very high ( $\leq 30\%$ ), especially in the presence of some strong nucleophiles. FGs always complete the defluorination reaction rapidly rather than the successful grafting reaction. Some recent experimental results show that the defluorination process was controlled by

adjusting kinetics, which present the potential for achieving the effective utilization of C–F bonds.

Notably, the C–F bonds are crucial for the application of FG in many situations such as in the field of lubrication, while the further function is also needed. Therefore, it is expected to achieve the nondestructive modification of FG without sacrificing C–F bonds. This is an obvious Gordian knot in the area. Interestingly, some works have employed free radicals of FG to initiate polymerization and realize the in situ grafting, so this method presents a great potential for achieving the nondestructive modification of FG.

## 6. Structure Engineering

Due to the multitudinous and distinctive properties, FG are endowed with a promising prospect in many application fields.<sup>[32,33,40,41]</sup> In order to adequately achieve great potentials of FG, the well controlling of its fine structure is crucially needed. The specific structures/properties of FG are always necessary for meeting the requirements of some particular applications. However, the lacking of the structure engineering would limit the exploitative peculiarity and application of FG.<sup>[54,65,71,93–95,141,149,184,220]</sup> Therefore, the elaborate structure engineering for customizing the structure and performances of FG is the most important research point in the past several years, which is also the urgent and significant avenue in its future development. The fluorine content is the simplest and fundamental character of FG, which has been introduced in the above intrinsic properties section.<sup>[94,104,122,123,128,130,236]</sup> Herein, we mainly aim at the recent processes about the engineering of other structural characters such as fluorine distribution, fluorine type, radicals, interlayer structure, and present how do the corresponding performances and applications be regulated and optimized.

### 6.1. Microscale Structure Engineering

Since graphene and other 2D nanomaterials were reported, a series of related nanotechnologies have also acquired a significant progress.<sup>[1,2,5,9,26]</sup> It should be emphasized that the particular functional partitioning has been one of important nanotechnologies for the surficial function of the 2D materials and expand their functionality and applications, such as promoting to develop the graphene-based electron devices.<sup>[19,95]</sup> In face of the structure engineering of FG, microscale regulation could always design the fine structure on FG nanosheets directly based on the advanced nanotechnology and equipment. For example, pristine graphene was first deposited onto the  $SiO_2$  substrate, and then the polymer (PDMS) as a shielding layer was applied to paint on the graphene sheet. Subsequently,  $XeF_2$  or fluorine plasma were employed and the fluorination was easy to proceed on the uncovered graphene surface while the covered regions with polymer still maintained the pristine state (Figure 19A).<sup>[95]</sup> Thus, the targeted fluorination on the specified region on graphene sheet was realized, which effectively regulated the characters of the specified regions, such as surface energy, friction characteristic, electrical conductivity.<sup>[93–96]</sup> As another approach, one fluoropolymer was

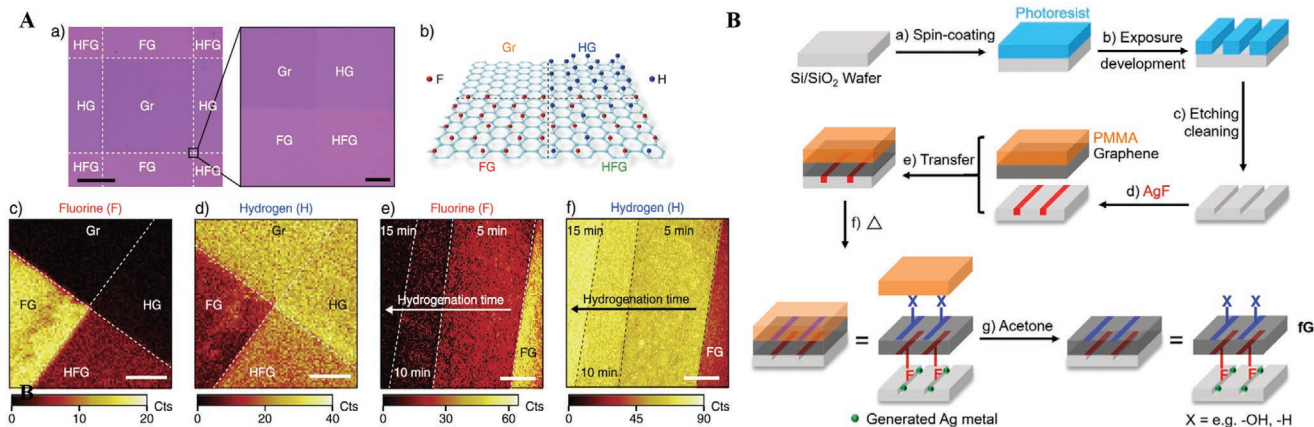


**Figure 19.** A) a,b) Optical images and illustrative images of patterned graphene regions composed of pristine graphene, FG, hydrogenated graphene, and hydro-fluorinated graphene. c–f) Time-of-flight secondary ion mass spectrometry (TOF-SIMS) plots of the fluorine and hydrogen contents on the surface of the patterned graphene. A) Reproduced with permission.<sup>[95]</sup> Copyright 2019, Wiley-VCH. B) Illustrative image of the structured fluorination on graphene by 2D substrate patterning. Reproduced with permission.<sup>[93]</sup> Copyright 2020, The Authors, published by Wiley-VCH.

selected as a shielding layer to cover the surface of graphene. Subsequently, the laser was utilized and controlled to accomplish the selective radiation of the fluoropolymer. Under the radiation of laser, the fluoropolymer decomposed and release the active fluorine radicals, which operated the in situ selective fluorination of graphene.<sup>[96]</sup> Notably, graphene was always closely deposited on the surface of substrate, so it was difficult for fluorine sources to contact and react with the other bottom surface of the graphene, which leads to the single-sided fluorination of its top surface.<sup>[30]</sup> Bao et al. imitated the photoresist pattern to selectively etched the substrate and obtain grooves on its surface, and then the grooves were filled by the AgF solution (Figure 19B). Afterward, graphene was transferred onto the surface of the substrate, and its bottom surface was selectively fluorinated by the decomposed AgF under a raised temperature.<sup>[93]</sup>

The abovementioned selective fluorinations of graphene sheets were mainly realized by defining the contact regions between graphene and the fluorine sources. In contrast, Deng et al. operated the selective fluorination through regulating the reactivity of the specific graphene regions. In detail, the graphene sheets were adhered on the surface of a stretched polymer substrate, where thickness, strain direction, and deformation extent were defined, and thus the graphene achieved the wrinkle-structure after the recovery of polymer substrate from being stretched.<sup>[92]</sup> The wrinkled region presented a high chemical reactivity during fluorination in comparison with the smooth region, which makes it possible to selectively fluorinate the wrinkled graphene sheet.<sup>[92]</sup> Meanwhile, investigators achieved the single and double-sided fluorination on the graphene sheet by changing the polymer substrate, and the graphene-based heterojunction with an unsymmetrical location of chemical bonds was also prepared (Figure 20A).<sup>[94]</sup> Apart from selective fluorination, the inter-layer structure between two fluorinated graphene sheets can also be regulated during fluorination. Yang et al. reported the efficiency of fluorination and the fluorinated structure was closely related to the layer numbers of graphene. For example, the fluorination of the Bernal (AB)-stacked bilayer graphene,

obtained the carbon–carbon cross-bonding which linked the top and bottom graphene sheets and achieved the fluorinated double-layer graphene with a diamond-like structure (Figure 20B).<sup>[237]</sup>

Different from the abovementioned bottom-up fluorination strategy, the top-down defluorination provides a reverse route to realize the structure engineering of FG. For example, FG sheet was first deposited onto a rigid substrate, and then a heated AFM probe or an electron beam was employed to implement the defluorination at the appointed regions, which thus directly controlled the fluorine distribution of FG.<sup>[238]</sup> The conductivity of defluorination regions increased several orders of magnitudes compared with that of pristine fluorinated regions. Therefore, the conductivity or semiconductive properties of FG can be regulated in this way even in a small scale of several microns and even tens of nanometers, which makes it feasible to prepare the graphene-based transparent and flexible electronic devices.<sup>[220]</sup>

## 6.2. Macroscale Structure Engineering

The microscale structure engineering of FG sheet may be able to satisfy the demands of the micro-electronics territory. However, taking a large-scale application into account, the macroscale structure engineering of FG is the challenge which we have to face. It should be noted that the macroscale structure engineering is not aimed at the individual FG nanosheet, while it requires to deal with a mass of FG nanosheets at the same time.

### 6.2.1. Fluorine Distribution

In spite of the simpleness of the top-down exfoliation method for preparing FG, it is difficult to finely regulate the fine structure.<sup>[122]</sup> The bottom-up fluorination method has presented the advantage of regulating the structure of FG, which thus achieves to customize the particular FG toward the specific



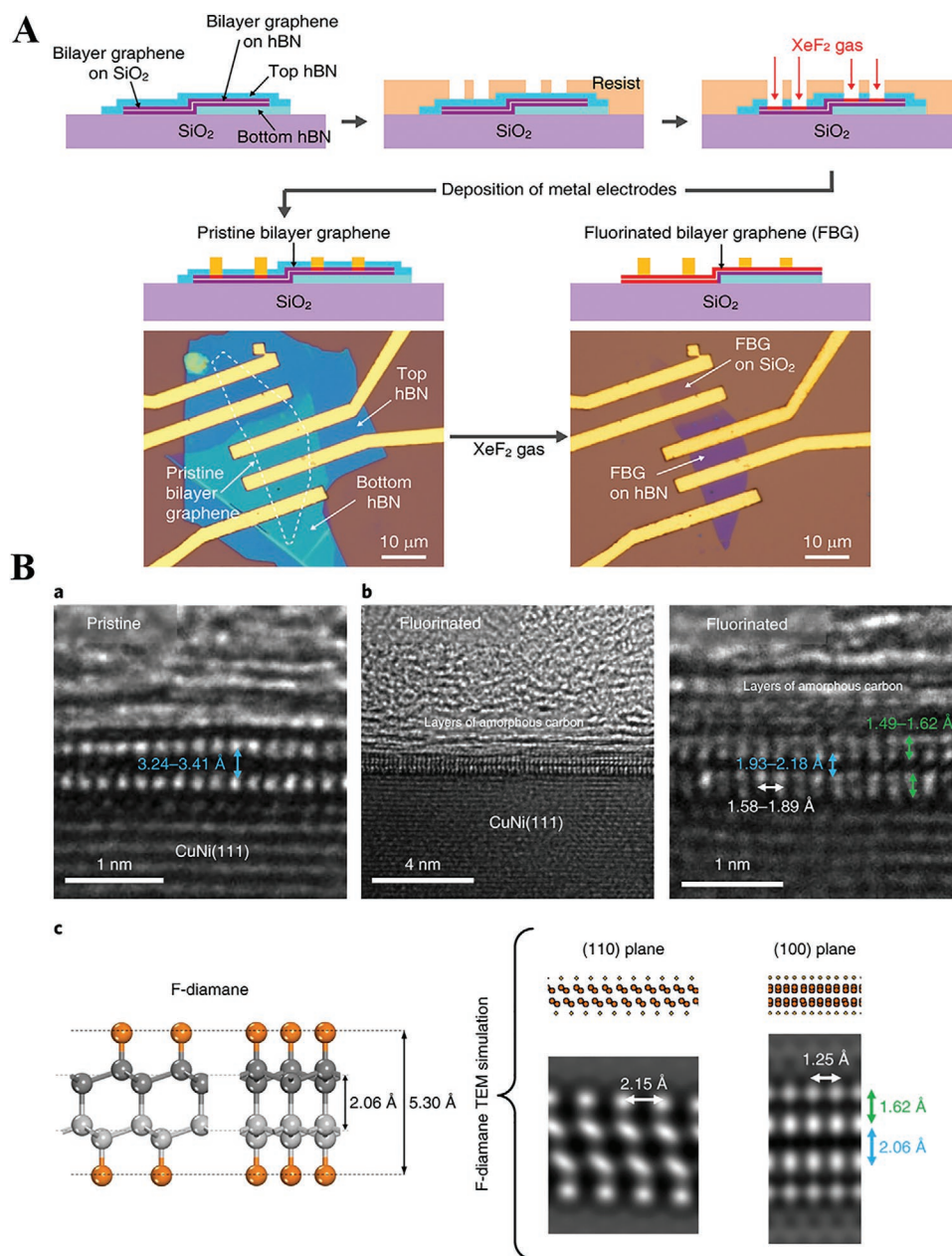


**Figure 20.** A) Schematic illustration of the fabrication procedure of the bilayer graphene device and the optical microscopic images of the bilayer graphene device before and after  $\text{XeF}_2$  gas treatment. Reproduced with permission.<sup>[94]</sup> Copyright 2020, American Chemical Society. B) a,b) High-resolution cross-sectional TEM images of original bilayer graphene (a) and the fluorinated sample (>12 h fluorination) (b). c) Simulated HR-TEM photograph of DFT-optimized F-diamane. B) Reproduced with permission.<sup>[237]</sup> Copyright 2019, The Authors, published by Springer Nature.

application.<sup>[92,93]</sup> Notably, the structure engineering is always closely dependent on the progress of fluorination chemistry and corresponding fluorination methods of FG.<sup>[33,84,239,240]</sup>

Liu et al. proved that the defect on graphene sheet possessed a higher fluorination reactivity through experiments and DFT calculations. Meanwhile, fluorination preferentially initiated at the defects of graphene by producing the active radicals, and then further proceeded into other regions of graphene through a chain radical diffusion mode (Figure 21A).<sup>[143]</sup> Based on this mechanism, they initiated the fluorination at defect sites of porous graphene and achieved the FPG with

aggregation C–F bonds at defects. These aggregated C–F bonds also endowed FPG with an excellent thermostability compared with other FGs. More interestingly, the fluorine aggregation at defects of FPG restricted the motions of defects and impaired the interlayer interactions which reduced the nonradiative recombination loss as excitons at excited state back to ground state and thus endowed the FPG with a high PL emission.<sup>[48,152,154]</sup> In addition, the high-energy ball-milling can effectively damage and exfoliate graphite to the graphene sheets with abundant defects and edges. According to the high fluorination-reactivity of defects and edges, the FG with

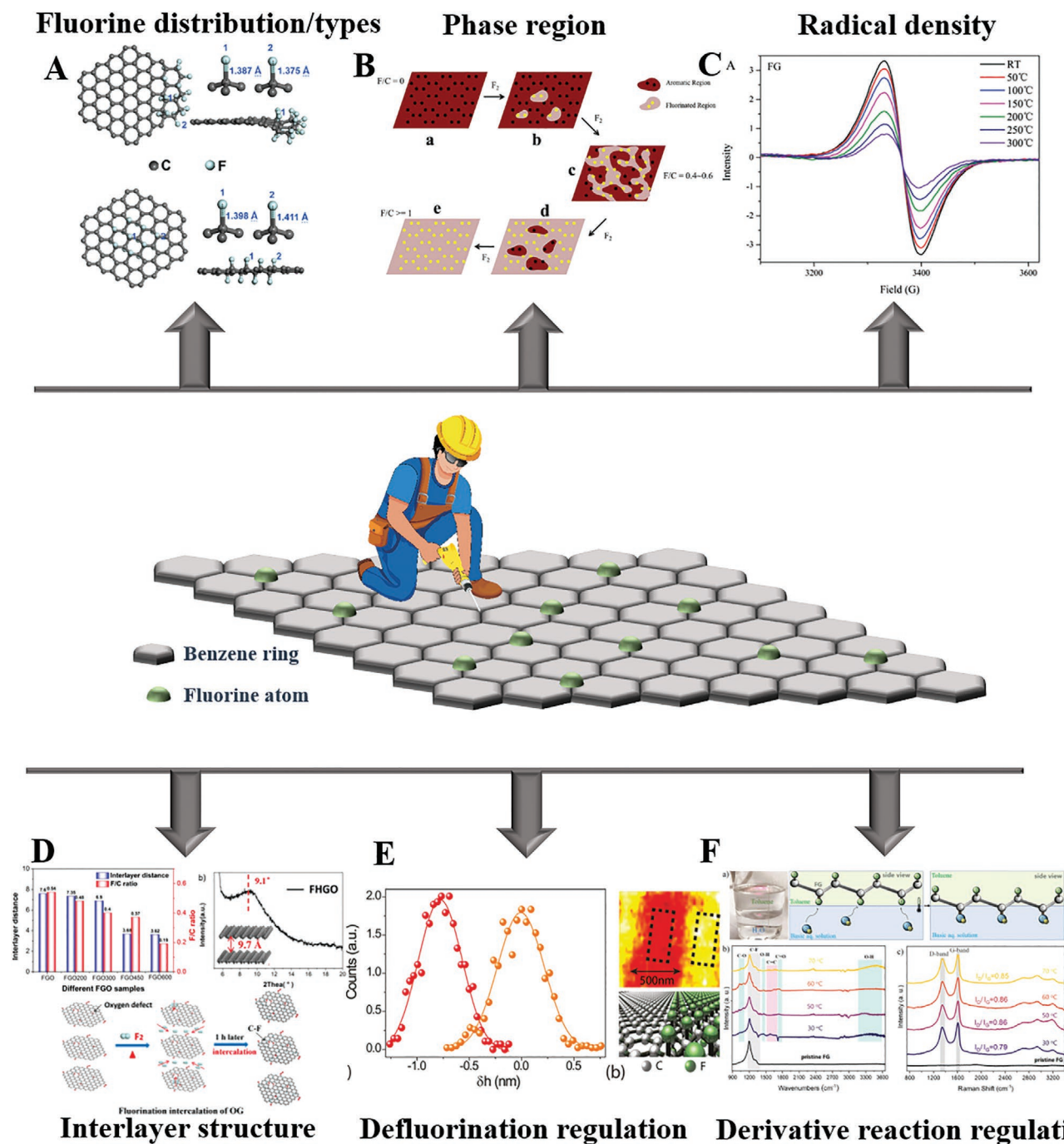


**Figure 21.** A–F) Illustrative images of the macroscale structure engineering of FG. Image for “Fluorine distribution/types” in (A): Reproduced with permission.<sup>[125]</sup> Copyright 2017, Elsevier. Image for “Phase region” in (B): Reproduced with permission.<sup>[143]</sup> Copyright, 2018, Elsevier. Image for “Radical density” in (C): Reproduced with permission.<sup>[152]</sup> Copyright 2018, Elsevier. Image for “Interlayer structure” in (D): Reproduced with permission.<sup>[48]</sup> Copyright 2019, The Royal Society of Chemistry. Image for “Defluorination regulation” in (E): Reproduced with permission.<sup>[220]</sup> Copyright 2011, American Chemical Society. Image for “Derivative reaction regulation” in (F): Reproduced with permission.<sup>[82]</sup> Copyright 2020, Wiley-VCH.

most C–F bonds at defect edge was easy to prepare by the direct fluorination, which always exhibits the enhanced chemical stability and cycle life during electrochemical measurement.<sup>[69,241]</sup> Fan et al. selected two kinds of graphene materials with different defects density (high and low), and successfully achieve the different distribution of C–F bonds at defects and

on plane of graphene sheets. Furthermore, the C–F bonds on graphene plane greatly increased the out-plane bending stiffness of graphene, and guaranteed the flat state of FG sheet which facilitates the direct solid molding of FG through the layer-by-layer compact stacking.<sup>[198]</sup> However, the C–F bonds at defects have little ability of increasing the out-plane

bending stiffness of graphene, which results in the failure of direct solid molding of the corresponding FG sheets.

Wang et al. found that some chemical defects, such as the oxygen groups of GO, can also effectively facilitate the fluorination reaction on graphene, so the FG with a high F/C ratio was easily prepared by the fluorination of GO.<sup>[108,125]</sup> On the basis of this finding, Fan et al. further confirmed that the hydroxy of GO can promote the fluorination of its surrounding aromatic regions. Therefore, under a low temperature and low fluorine gas concentration, fluorination only proceeded on the aromatic regions of GO and the original oxygen groups were reserved, which thus prepared the fluorine and oxygen double functionalized graphene (FGO) with a high functionalization density. This FGO also presented a fine dispersibility in water on account of reserved abundant oxygen groups, so it exhibits a great potential as the excellent water-based lubricant additive.<sup>[46]</sup> In addition, by introducing nitrogen atoms into the skeleton of graphene, Liu et al. achieved to prepare the FG with an aggregation of C–F bonds around the doped N-atoms due to the active-effect of N-atoms on the surrounding carbon atoms.<sup>[242]</sup>

### 6.2.2. Fluorine Types

The nature of C–F bonds and the corresponding fluorine types have a decisive influence on the integrated performances of FG. By simply adjusting the preparation conditions, FG with entirely different C–F bonding nature could be obtained. In the typical fluorination and the exfoliation process, the bonding nature is closely related to the corresponding reaction conditions.<sup>[65,150]</sup>

Lee et al. prepared the FG with dominated semi-ionic C–F bonds via one-step liquid ClF<sub>3</sub> treatment. Surprisingly, the C–F bonds were partially reduced accompanied by the recovery of conjugated aromatic structure when the FG was disposed by acetone, which further confirmed the existence of C–F bonds with a low bonding energy.<sup>[138]</sup> Feng et al. reported that there was a large proportion of semi-ionic C–F bonds in the FG sheet which was exfoliated by using chloroform, and they attributed this phenomenon to the formed hydrogen bonds between the C–F bonds and chloroform molecules. Taking advantage of this feature, they prepared the FG-based primary lithium battery with a superior electrochemical performance.<sup>[102]</sup> By employing polarized attenuated total reflection (ATR)-FTIR, Wang et al. confirmed that there were at least two kinds of C–F bonds on FG plane: (C–F)<sub>I</sub> and (C–F)<sub>II</sub>. The (C–F)<sub>II</sub> bonds were located at the coplanar carbon atoms on the sparse fluorine region while the (C–F)<sub>I</sub> bonds aggregated on the highly distorted graphene skeleton, and these two types of C–F bonds behaved a huge difference in thermostability.<sup>[137]</sup> Also, FG can be activated by some polar aprotic solvent and a noteworthy transition from the covalent C–F bond to the semi-ionic bond was distinctly observed according to the FTIR spectra.<sup>[151]</sup> Besides, after heat treatment, one part of the semi-ionic C–F bonds occurred thermal cracking with the leaving of fluorine atoms while another part of the semi-ionic C–F bonds transformed into the covalent C–F bonds.<sup>[149,151]</sup> In addition, the results of many studies have demonstrated that there are not only the covalent bond and semi-ionic C–F bond, but also some other

fluorine-contained groups in the graphene plane, such as CF<sub>2</sub> or CF<sub>3</sub> groups, which were normally found in the XPS spectrum with a higher binding energy. Especially, just by regulating the reaction temperature and the amount of fluorine gas during the direct fluorination, the specific FG product can be obtained with an expected content of CF<sub>n</sub> related groups.<sup>[104,108,122,125,137]</sup> This method offers a straightforward route to tailor the properties of FG and it can be utilized in many fields, such as batteries and super-hydrophobic layers.

Heteroatom doping can also be deemed as a powerful tool to control the properties of C–F bonds.<sup>[70,181,185,243]</sup> The doped nitrogen atoms in graphene skeleton can significantly improve the fluorination reactivity and promote the local aggregation of C–F bonds, which definitely enhanced the covalent bonding nature of C–F bond even at a low F/C ratio. Therefore, a fluorination-doping-fluorination technology was further developed for synthesizing the bifunctional graphene derivative with the high N/C and F/C ratio which holds the potential application prospect in electrocatalysis field.<sup>[243]</sup>

### 6.2.3. Phase Region

The concept of phase region distribution appears frequently in the field of composite materials, the introduction of this concept into the 2D materials will help to deepen the research on the modification of 2D materials.<sup>[240,244]</sup> Lai et al. investigated the elaborate structure evolution of FG during fluorination and introduced the concept of “phase region” (Figure 21B).<sup>[143]</sup> An interesting phase region evolution was described: in initial stage of fluorination, fluorine region with a small proportion was the island phase while predominant aromatic region was continuous phase; when the F/C ratio of FG reached 0.4–0.6, the reversal behavior of phase region appeared on the surface of FG. That is, the fluorine region transferred into continuous phase and the aromatic region changed into island phase. Such phase reversal behavior on the surface of FG would bring about the mutation of many properties, such as bandgap, conductivity, fluorescence.<sup>[143]</sup> Based on the evolution of phase region, Fan et al. designed two-step fluorination to controllably modify GO and prepared FG with a continuous fluorinated phase and an aromatic island phase. Under a low temperature, the fluorination removed hydroxy of plane that easily induced non-radiative recombination; under high temperature, fluorination proceeded at defects so as to further restrict the nonradiative recombination loss of defects.<sup>[155]</sup>

### 6.2.4. Radical Density

The intrinsic free radical properties of 2D materials have gradually become a research hotspot in recent years.<sup>[242,245,246]</sup> Meanwhile, the straightforward gas–solid reaction between F<sub>2</sub> and graphene is always involved in a radical process.<sup>[78,80,84,143,247,248]</sup> Especially, the fluorination of polymer would introduce a good deal of free radicals, as demonstrated in most literatures, and many investigators have utilized these radicals to produce crosslinking and initiate radical polymerization for surface modification.<sup>[249–252]</sup> Therefore, the fluorination of



graphene also introduces abundant radicals into the surface of FG, which may adopt a chain radical fluorination mechanism similar to the fluorination of polymer. The radicals of FG are relatively stable and even possess a long-term stability in the air atmosphere, which is attributed to that the existed fluorine atoms, aromatic regions, and particular 2D skeleton of FG stabilize the corresponding radicals (Figure 21C).<sup>[80,143]</sup> The radical density of FG can also be regulated by the fluorination degree. The half-fluorinated graphene with a middle fluorine content had the largest radical density, while the radical density of FGs with a high or low fluorine content was relatively small.<sup>[143]</sup> Based on this mechanism, Fan et al. prepared FGs with many stable radicals by direct fluorination and the stable radicals can be activated under a certain temperature. The activated radicals were able to initiate the radical polymerization of acrylic acid and realized the in situ modification by grafting the polymer macromolecule. Compared with the traditional nucleophilic modification reaction of FG by sacrificing the C–F bonds, the abovementioned modification method successfully preserved the original C–F bonds, which thus achieved the targeted functionalization and maintained the intrinsic self-lubricating performance.<sup>[91]</sup>

#### 6.2.5. Interlayer Structure

As a typical 2D material, FG has the supramaximal aspect ratio (the ratio of the transverse size to the longitudinal thickness), so the super-wide (horizontal direction) and narrow (perpendicular direction) interlayer naturally generates in the multilaminar structure and via the self-assembling by van der Waals interactions, which is also the significant and unique character of 2D materials. Recent processes in 2D materials manifest that it is vital to many applications to make use of the interlayers and regulate their structure, such as in the area of lubrication, separation, electrochemistry, catalysis, and even exfoliation. Therefore, subtly regulating the interlayer structure of FG is desired to have a significant harvest.<sup>[253–256]</sup> Fan et al. investigated the reaction mechanism of the intercalation during the fluorination of graphene. They demonstrated that the physical defect (point defect) on graphene nanosheet had little ability to promote the progression of the intercalation, despite there are many diffusion paths for fluorine gas. The oxygen groups of graphene can effectively facilitate the intercalation during fluorination. That is, the hydroxy and epoxy groups on graphene plane produced the active radicals during decomposition and promoted the fluorination intercalation, and the carbonyl and carboxyl promoted the fluorination intercalation by activating their surrounding aromatic regions.<sup>[48]</sup> On the basis of this mechanism, the FG with an ultrahigh interlayer distance was prepared and effectively exfoliated into a single-layer FG (Figure 21D).<sup>[48]</sup> In addition, the distribution of C–F bonds in the graphene sheets has an obvious influence on the interlayer distance. The C–F bonds at defects had little ability to increase the interlayer distance of FG, which resulted in an inferior tribological property. In contrast, the C–F bonds located in the plane of graphene sheet played a leading role in increasing the interlayer spacing of FG, which greatly

enhanced the tribological performance of FGs and make it possible to be an advanced lubricant additive.<sup>[47,48]</sup>

#### 6.2.6. Defluorination Regulation

Apart from the bottom-up fluorination, the defluorination as a contrary process is also worthy of more attentions to realize the structure engineering of FG.<sup>[151,161,220,247]</sup> Notably, the fluorine atoms with the maximal electronegativity greatly attract the electrons of carbon skeleton, so the nucleophilic reagent is easy to attack the carbon atom of the C–F bond and lead to the defluorination of FG.<sup>[141,151]</sup> Here, FG has the 2D structure of carbon skeleton, which facilitates that the C–F bonds on the skeleton of graphene are easier to be reduced with the recovery of the conjugated aromatic structure. Therefore, after the defluorination process, only the C–F bonds located at the defects and edges were survived in the FG sheet, which achieves to regulate the fluorine distribution (Figure 21E).<sup>[137,151,220]</sup>

Relative to the chemical reduction of FG, the thermal defluorination is mainly related to the bond energy of C–F bonds on different regions of FG nanosheet. The C–F bonds at defects are relatively unstable because of the broken carbon skeleton. Therefore, by regulating the temperature of thermal treatment, the C–F bonds at defects are preferentially removed and the C–F bonds on graphene plane are reserved, which can alter the fluorine distribution as well. Furthermore, the C–F bonds on graphene plane can be removed by changing temperature, the large fluorine cluster splits into the small fluorine cluster which possesses an enhanced edge effect and increases the local spin magnetic moment and induces ferromagnetic curie.<sup>[42,61,101,107,149,152,257]</sup> In addition, the introduced heteroatom can assist to regulate the structure of FG by thermal treatment. For example, doped nitrogen atom in FG nanosheets has a strong adsorption capacity, which causes that the accumulative fluorine atoms gradually separated during the thermal treatment and thus achieve the independent fluorine distribution.<sup>[243]</sup> Moreover, the UV light can also regulate the structure of FG by promoting the defluorination, i.e., under the work of UV light, the nature of C–F bonds will transform from the covalent to the semi-ionic.<sup>[161]</sup>

#### 6.2.7. Derivative Reaction Regulation

Different from the chemical inertness of graphene, the introduced fluorine endows FG with a good chemical reactivity. On the basis of derivative reactions of FG, it is toiless to directly prepare multifunctional graphene-based materials and expand the applications of FG.<sup>[77–79,82,83,258–260]</sup> Similar to the structure engineering of C–F bonds in FG sheets, the structure engineering based on the derivative reaction of FG is also one of the important strategy to optimize the structure and the corresponding performance, such as controlling the modified region of the FG derivatives. Otyepka et al. found that the C–F bonds of FG increase the polarity of surrounding aromatic regions and facilitated the photo-induced cyclization reaction. Therefore, the 2-formyl-3-(methylphenoxy-methyl)-benzoate was easy to achieve the selectively photo-induced cycloaddition

into the aromatic regions close to the C–F bonds, and obtained a high-density and homogenous grafting on FG. In addition, they further found that thienyl only reacted with the aromatic regions close to the C–F bonds, which also facilitated the selective modification on the surface of FG.<sup>[79]</sup> Also, partial substitution/reduction of FG leads to the formation of regional functionalization.<sup>[259,260]</sup> By optimizing the reaction process, the electron-donating groups such as methoxythiophenol, dimethylaminothiophenol, and diethylamide can be grafted onto the skeleton of FG, where C–F groups act as strong electron acceptor, the  $sp^2$  domains act as the  $\pi$ -conjugated bridges, thus formed a donor– $\pi$  bridge–acceptor nonlinear optical chromophore scheme.<sup>[259,260]</sup> The abovementioned regulations of the derivative reaction of FGs mainly take the advantage of the different chemical reactivity in FG sheets, however, the spatial structure can also be utilized to regulate its derivative reaction. For example, when FG is directly dispersed into two-phase interface between water–oil system, the surface of FG close to water phase takes the nucleophilic substitution reactions with water and the hydroxy is grafted onto its surface, while the other surface of FG close to oil phase does not have any reactions. Thus, “Janus” FG derivative is successfully prepared in this way (Figure 21F).<sup>[82]</sup> Hence, the derivative reactions of FG provide various feasible methods to precisely manage its structure in a large scale.

#### 6.2.8. Other Structure Engineering

FG is a typical 2D material, so the above review mainly displays the structure engineering about the surface and interlayer of this 2D FG sheet. Notably, the spatial size and structure of FG somehow have important influence on its performances as well. For example, Gong et al. found the sheet size of FG significantly affects its photothermal performance. The synthesized FG sheets with an optimized size exhibited a commendable near-infrared light absorption ability.<sup>[57,62]</sup> Choi et al. demonstrated that the double-layer FG as a solid lubricating film can obviously reduce friction coefficient, while the single-layer FG contrarily increased the friction coefficient, which guides the design of layer number of FG.<sup>[49]</sup>

In addition, FG sheets have been further integrated into foam or aerogel state with spatial 3D network in some research work, which is supposed to produce some advanced materials with the distinct characters on magnetoresistive effect and supercapacitor.<sup>[49]</sup> However, although the independent FG sheet encompasses many excellent intrinsic performances, these macromaterials based on FG sheets would not completely inherit or develop their advanced properties. Therefore, it is one of the important directions in future work to optimize the performance of FG-based macromaterial through its structure engineering.

## 7. Conclusions and Outlooks

We have reviewed the synthesis methods, intrinsic properties, applications, functional chemistry, and structure engineering of FG. Since the discovery and preparation of FG, the unique

properties of FG have been gradually developed and reported, and FG has shown great application prospects in many fields, such as battery and electrochemistry, oil–water separation and lubrication, thermally conductive yet electrically insulating material, gas detection, storage and separation, biomedicine. In addition, on the basis of the chemical reactivity of C–F bond and its subsequent derivative reactions, a variety of functional groups can be grafted onto the graphene surface, which opens a universal route to prepare various graphene derivatives. Facing the established properties and applications of FG and its derivatives, the engineering of their fine structures is the key factor to further optimize the abovementioned properties and applications, and is also an up-to-date research hotspot in this field. By adjusting the fluorine distribution, fluorine types, phase region, free radicals, interlayer structures, etc., of FG, we could tailor the structure and property to match different application requirements.

It should be noted that a series of graphene derivatives has been explored to further enrich the properties and applications of graphene-based materials, such as GO, FG, brominated graphene, hydrogenated graphene. Among which, FG and GO are two of the most important graphene derivatives, and they obtain more attentions and applications compared to other graphene materials. Therefore, we presented the specific advantages and weaknesses between representative FG and GO, as shown in Figure 22. As follows, reported work up to now, FG presents these advantages, such as high functionalization density, high grafting/doping density, high thermal stability, distinct magnetic property, thermally conductive yet electrically insulating material, abundant derivative chemistry; meanwhile, it contains some weaknesses, such as single functional group, no liquid crystal state, general processing property. Although FG and GO possess some different and even opposite characters, both of them exhibit the obvious advantages in different applications. For example, the high hydrophobicity and low surface energy endow FG with excellent lubrication performances, strong corrosion resistance, good ice resistance, and so on; in contrast, the high hydrophilicity and high surface energy endow GO with strong adsorption capacity, good water dispersibility for preparing aerogels and fibers, excellent sea water desalination of GO film, and so on.

Here, although remarkable progress has been made from the preparation to the application and to the structure engineering of FG, there are still some intractable problems to solve in certain fields as follows: high-quality preparation, high thermal stability, controllable defluorination, elaborate structure design, distinctive 2D chemistry, in situ characterization techniques, high energy/power density and secondary battery, high-performance composite materials, and so on.

#### 1) High-Quality, Large-Scale, and Low-Cost Preparation of FG

Although many preparation methods have been developed during the past 10 years, these methods are basically limited to the laboratory level due to their some shortcomings. For example, the top-down exfoliation method requires the solvent assistance and the subsequent purification procedures, which is time-consuming and environmentally hazardous. The ball-milling method always severely destroys the lamellar structure of FG. For the bottom-up fluorination, the direct gas–solid fluorination of graphene-based materials does not require the solvent assistance

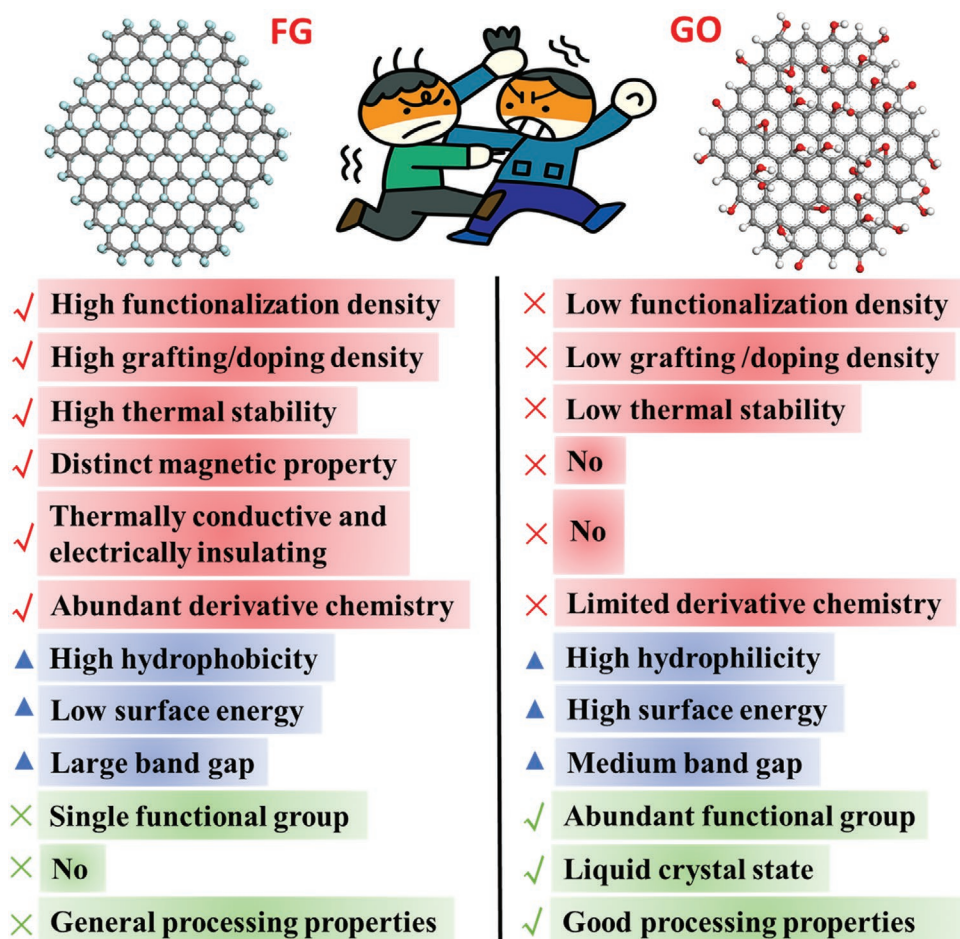


**Figure 22.** The specific advantages and weaknesses between FG and GO.

and the subsequent separation and exhibits the prospect of large-scale production, but the product homogeneity of the gas–solid reaction is relatively poor. Therefore, it is still a big challenge to develop the high-quality, large-scale, low-cost synthesis strategy of FG. Nevertheless, in face of this issue, we should thoroughly study the reaction chemistry involved in the fluorination process and optimize the fluorination technology and even design the equipment to achieve the preparation of homogenous FG products with uniform structure and property.

### 2) Structure Engineering of FG-Based Materials

For the further development, FG will certainly be supposed to meet the needs of multifunctional applications by realizing the multiscale structural designs. For example, it is expected to pattern the fluorinated region on the FG sheets and controllably stack them layer by layer in order to construct the FG-based microcircuits. Meanwhile, the structure engineering of FG is required not only to face the specific demands for application, but also simultaneously achieve the optimal performance and the high efficiency for production.

### 3) 2D Chemistry of FG

The original graphene is chemically inert due to the large conjugated structure which makes it difficult to undergo derivative

reactions to achieve specific functions. In contrast, FG exhibits a good chemical reactivity due to the introduction of C–F bonds, which opens up a facile way to prepare multifunctional graphene derivatives. However, most research has focused on the application of derivative modifications and has ignored the front-end reaction mechanism, while the modifications and fine structure engineering of FG invariably rely on the thorough study of reaction mechanism. Compared with small molecules, the large 2D continuous structure and the large steric effect in FG sheets would endow it with a unique chemical mechanism for its derivation reactions. The study on 2D derivative chemistry of FG will support us to regulate the nucleophilic substitution process and even discover the bran-new reaction mechanism which breaks up the traditional theory. This should be a crucial research direction of 2D material chemistry in future.

### 4) Further Exploring the Intrinsic Physical Characters of FGs

In this review, the emphasis is mainly put on the chemistry of FG, such as the synthesis of FG and its fine structure and derivative reactions. However, the physical characters of FGs could not be taken lightly, which is the main reason for its rise and almost determines the upper limit of its development. On the basis of the progress of FG chemistry, the exploration of FG physics is supported by a good material foundation, and more interesting



physical discovery is expected, such as the unique band structure and the host spin-polarized electronic state, which would render them promising materials in carbon-based nanoelectronics and spintronics. In addition, it is worthy of attention in future research to investigate the effect of the stacking behavior (such as stacking-angle) of one FG sheet with another one or other 2D material sheet on its physical characters.

#### 5) Defluorination

There has already been plenty of research on the fluorination process, including fluorination mechanism, fluorine content, fluorine distribution, and other structure engineering. In contrast to the fluorination process, the defluorination behavior is rarely studied. Actually, as a reverse process of fluorination, the defluorination can be utilized as a supplement to control the structures and properties of FG. However, it is worth noting that the defluorination process is not completely symmetrical with the fluorination process. It is impossible to completely transform the FG into the original graphene just through the defluorination which always leads to some topological defects in the graphene skeleton and makes it exhibit unique properties in catalytic and energy source field. Therefore, it is worthy of attention in future research to manage the defluorination process to control the type and distribution of various groups and the defect structure in the final graphene-based materials.

#### 6) Developing In Situ Characterization Techniques

In situ characterization of the relation between the structure and property of materials plays an increasingly important role in the preparations and applications of materials at present. If we could clarify the different contributions of defect sites and chemical groups on FG to the properties, the formation of the corresponding structure during the preparation of FG is possible to be well controlled, which will save cost and achieve a high efficiency production. In addition, the in situ characterization technique can also facilitate the deep analysis of the reaction mechanism related to FG and the further regulation of the fine structure of FG. In situ transmission electron microscope, XPS, AFM, Raman, and X-ray absorption near-edge structure could be used to detect the preparation of FG, or to probe the reaction kinetics and surface chemical environment in real time. Some special characterization techniques, such as cryo-electron-microscopy, could monitor the reaction process at different temperatures more precisely, as well.

#### 7) Further Optimizing the Overall Performance of FG-Based Batteries

For lithium/FG batteries, the property of the FG cathode materials directly determines the overall discharge performance of the battery, but there is a contradiction between the fluorine content and the discharge platform. FG is an insulating material, and the internal resistance of FG is enhanced with increased F/C ratio, which further hinders the diffusion of lithium ions in the electrode materials and weakens the discharge performance. The conductivity of the FG cathode could be improved by blending or doping, but the effect is very limited. In order to radically enhance the electrochemical performance of the batteries, future research should focus on the further characteristics and optimization of the structure of FG.

This would provide the basis for achieving simultaneously the high energy density and the high power density, and it could also be suitable for the high-current operating conditions.

In addition, it is a pity that the excellent properties of FG itself could only work in the primary batteries at present. Although there are some reports of secondary batteries based on FG cathode materials, the specific capacity of the batteries is really low and the corresponding research remains at a very initial stage. Hence, there is still an infinite space for the research focusing on the development of the secondary batteries based on FG cathode materials.

#### 8) FG-Based Composite Materials

The introduced C–F bonds could effectively overcome the agglomeration effect of graphene in composites via covalent and noncovalent interactions with matrix in the interface. However, it is still an urgent problem to highly effectively extend the intrinsic excellent property of FG to FG-based composites. In facing of this issue, we should pay attention to the following aspects: interaction between FG and matrix (covalent and non-covalent interactions), the orientation and distribution of FG in composites, the conversions in the structure or distribution of FG during the molding process.

#### 9) Thermal Stability of FG

So far, the prominent progress of FG research has been made in its preparations and applications. However, the thermal stability of FG, one of important basic properties, has not been effectively studied yet. The thermal stability of FG is the best one in comparison with other graphene derivatives and far exceeds the thermal stability of GO (the temperature of its main weight loss is around 200 °C). However, it has been demonstrated that the main weight loss of FG happened at around 400 °C while the actual defluorination really started at a low temperature and even at room temperature, which resulted from the inevitable existence of some defects and the inhomogenous distribution of fluorine in the lamellae. This feature would severely limit its practical application. For example, the bandgap of the semiconductor prepared by FG would gradually change during a long-term service due to the slow defluorination behavior, which will inevitably result in the device failure. Hence, it deserves more attention to develop feasible methods and technologies to enhance the thermal stability of FG, such as repairing defects by post-processing, increasing the aggregation degree of C–F bonds.

In a word, the rational structure engineering and the thorough mechanism study as well as broad applications are the essential scientific issues to be urgently discussed for the future development of FG. Meanwhile, such review and outlooks of FG at present from synthesis to applications including functional chemistry and structure engineering would also provide a reference for the precise modification of other 2D materials.

### Acknowledgements

This work was financially supported by the National Natural Science Foundation of China (grant nos. 51803129, 51633004, and 51573105), International Visiting Program for Excellent Young Scholars of SCU and Postdoctoral Interdisciplinary Innovation Startup Fund of Sichuan

University. The authors acknowledge the Analytical & Testing Centre of Sichuan University. The authors thank the laboratory members for their generous help.

## Conflict of Interest

The authors declare no conflict of interest.

## Author Contributions

X.C. and K.F. contributed equally to this work. The manuscript was written through the contributions of all authors. All authors have given approval to the final version of the manuscript.

## Keywords

C–F bonds, fluorinated graphene, functional chemistry, structure engineering, synthesis and applications

Received: March 1, 2021

Revised: May 27, 2021

Published online:

- [1] Y. Kang, Y. Xia, H. Wang, X. Zhang, *Adv. Funct. Mater.* **2019**, *29*, 1902014.
- [2] X. Gong, O. Voznyy, A. Jain, W. Liu, R. Sabatini, Z. Piontkowski, G. Walters, G. Bappi, S. Nokhrin, O. Bushuyev, M. Yuan, R. Comin, D. McCamant, S. O. Kelley, E. H. Sargent, *Nat. Mater.* **2018**, *17*, 550.
- [3] O. Hod, E. Meyer, Q. Zheng, M. Urbakh, *Nature* **2018**, *563*, 485.
- [4] C. Kang, Z. Zhang, V. Wee, A. K. Usadi, D. C. Calabro, L. S. Baugh, S. Wang, Y. Wang, D. Zhao, *J. Am. Chem. Soc.* **2020**, *142*, 12995.
- [5] Z. Wang, Q. Jingjing, X. Wang, Z. Zhang, Y. Chen, X. Huang, W. Huang, *Chem. Soc. Rev.* **2018**, *47*, 6128.
- [6] S. Thurakkal, X. Zhang, *Adv. Sci.* **2019**, *7*, 1902359.
- [7] K. Wu, J. Wang, D. Liu, C. Lei, D. Liu, W. Lei, Q. Fu, *Adv. Mater.* **2020**, *32*, 1906939.
- [8] M. Kühne, F. Börrnert, S. Fecher, M. Ghorbani-Asl, J. Biskupek, D. Samuelis, A. V. Krasheninnikov, U. Kaiser, J. H. Smet, *Nature* **2018**, *564*, 234.
- [9] X. Wang, Y. Jia, X. Mao, L. Zhang, D. Liu, L. Song, X. Yan, J. Chen, D. Yang, J. Zhou, K. Wang, A. Du, X. Yao, *Chem* **2020**, *6*, 2009.
- [10] H. Huang, H. Shi, P. Das, J. Qin, Y. Li, X. Wang, F. Su, P. Wen, S. Li, P. Lu, F. Liu, Y. Li, Y. Zhang, Y. Wang, Z. S. Wu, H. M. Cheng, *Adv. Funct. Mater.* **2020**, *30*, 1909035.
- [11] B. G. Márkus, P. Szirmai, K. F. Edelthammer, P. Eckerlein, A. Hirsch, F. Hauke, N. M. Nemes, J. C. Chacón-Torres, B. Náfrádi, L. Forró, T. Pichler, F. Simon, *ACS Nano* **2020**, *14*, 7492.
- [12] X. Xu, C. Liu, Z. Sun, T. Cao, Z. Zhang, E. Wang, Z. Liu, K. Liu, *Chem. Soc. Rev.* **2018**, *47*, 3059.
- [13] V. Georgakilas, M. Otyepka, A. B. Bourlinos, V. Chandra, N. Kim, K. C. Kemp, P. Hobza, R. Zboril, K. S. Kim, *Chem. Rev.* **2012**, *112*, 6156.
- [14] L. Chen, G. Shi, J. Shen, B. Peng, B. Zhang, Y. Wang, F. Bian, J. Wang, D. Li, Z. Qian, G. Xu, G. Liu, J. Zeng, L. Zhang, Y. Yang, G. Zhou, M. Wu, W. Jin, J. Li, H. Fang, *Nature* **2017**, *550*, 380.
- [15] J. Cai, J. Chen, P. Zeng, Z. Pang, X. Kong, *Chem. Mater.* **2019**, *31*, 3729.
- [16] Y. Yang, X. Yang, L. Liang, Y. Gao, H. Cheng, X. Li, M. Zou, R. Ma, Q. Yuan, X. Duan, *Science* **2019**, *364*, 1057.
- [17] C. Luo, W. Lv, C. Qi, L. Zhong, Z. Pan, J. Li, F. Kang, Q. Yang, *Adv. Mater.* **2019**, *31*, 1805075.
- [18] J. L. Suter, R. C. Sinclair, P. V. Coveney, *Adv. Mater.* **2020**, *32*, 2003213.
- [19] W. Fang, L. Peng, Y. Liu, F. Wang, Z. Xu, C. Gao, *Chin. J. Polym. Sci.* **2021**, *39*, 267.
- [20] W. Xu, T. Lee, *Mater. Horiz.* **2016**, *3*, 186.
- [21] A. Narita, X. Y. Wang, X. Feng, K. Mullen, *Chem. Soc. Rev.* **2015**, *44*, 6616.
- [22] X. Zhou, G. Yu, *Adv. Mater.* **2019**, *32*, 1905957.
- [23] M. Panighel, S. Quiroga, P. Brandimarte, C. Moreno, A. Garcia-Lekue, M. Vilas-Varela, D. Rey, G. Sauthier, G. Ceballos, D. Peña, A. Mugarza, *ACS Nano* **2020**, *14*, 11120.
- [24] X. Wen, H. Chen, T. Wu, Z. Yu, Q. Yang, J. Deng, Z. Liu, X. Guo, J. Guan, X. Zhang, Y. Gong, J. Yuan, Z. Zhang, C. Yi, X. Guo, P. M. Ajayan, W. Zhuang, Z. Liu, J. Lou, J. Zheng, *Nat. Commun.* **2018**, *9*, 1859.
- [25] D. Nutting, J. F. Felix, E. Tillotson, D. Shin, A. De Sanctis, H. Chang, N. Cole, S. Russo, A. Woodgate, I. Leontis, H. A. Fernández, M. F. Craciun, S. J. Haigh, F. Withers, *Nat. Commun.* **2020**, *11*, 3047.
- [26] D. K. Bediako, M. Rezaee, H. Yoo, D. T. Larson, S. Y. F. Zhao, T. Taniguchi, K. Watanabe, T. L. Brower-Thomas, E. Kaxiras, P. Kim, *Nature* **2018**, *558*, 425.
- [27] J. Zhang, T. Zhu, Y. Wang, J. Cui, J. Sun, J. Yan, Y. Qin, X. Shu, Y. Zhang, J. Wu, C. S. Tiwary, P. M. Ajayan, Y. Wu, *Mater. Today* **2020**, *36*, 83.
- [28] R. R. Nair, W. Ren, R. Jalil, I. Riaz, V. G. Kravets, L. Britnell, P. Blake, F. Schedin, A. S. Mayorov, S. Yuan, M. I. Katsnelson, H. Cheng, W. Strupinski, L. G. Bulusheva, A. V. Okotrub, I. V. Grigorieva, A. N. Grigorenko, K. S. Novoselov, A. K. Geim, *Small* **2010**, *6*, 2877.
- [29] R. Zbořil, F. Karlický, A. B. Bourlinos, T. A. Steriotis, A. K. Stubos, V. Georgakilas, K. Šafářová, D. Jančík, C. Trapalis, M. Otyepka, *Small* **2010**, *6*, 2885.
- [30] J. T. Robinson, J. S. Burgess, C. E. Junkermeier, S. C. Badescu, T. L. Reinecke, F. K. Perkins, M. K. Zalalutdniov, J. W. Baldwin, J. C. Culbertson, P. E. Sheehan, E. S. Snow, *Nano Lett.* **2010**, *10*, 3001.
- [31] J. Son, J. Kwon, S. Kim, Y. Lv, J. Yu, J. Lee, H. Ryu, K. Watanabe, T. Taniguchi, R. Garrido-Menacho, N. Mason, E. Ertekin, P. Y. Huang, G. Lee, A. M. Van Der Zande, *Nat. Commun.* **2018**, *9*, 3988.
- [32] W. Feng, P. Long, Y. Feng, Y. Li, *Adv. Sci.* **2016**, *3*, 1500413.
- [33] D. D. Chronopoulos, A. Bakandritsos, M. Pykal, R. Zbořil, M. Otyepka, *Appl. Mater. Today* **2017**, *9*, 60.
- [34] J. Zhou, M. M. Wu, X. Zhou, Q. Sun, *Appl. Phys. Lett.* **2009**, *95*, 103108.
- [35] H. Y. Liu, Z. F. Hou, C. H. Hu, Y. Yang, Z. Z. Zhu, *J. Phys. Chem. C* **2012**, *116*, 18193.
- [36] F. Karlický, M. Otyepka, *J. Chem. Theory Comput.* **2013**, *9*, 4155.
- [37] D. K. Samarakoon, Z. Chen, C. Nicolas, X. Wang, *Small* **2011**, *7*, 965.
- [38] K. Jeon, Z. Lee, E. Pollak, L. Moreschini, A. Bostwick, C. Park, R. Mendelsberg, V. Radmilovic, R. Kostecki, T. J. Richardson, E. Rotenberg, *ACS Nano* **2011**, *5*, 1042.
- [39] P. Lazar, E. Otyepková, F. Karlický, K. Čépe, M. Otyepka, *Carbon* **2015**, *94*, 804.
- [40] T. Wang, X. Zang, X. Wang, X. Gu, Q. Shao, N. Cao, *Energy Storage Mater.* **2020**, *30*, 367.
- [41] Y. Liu, L. Jiang, H. Wang, H. Wang, W. Jiao, G. Chen, P. Zhang, D. Hui, X. Jian, *Nanotechnol. Rev.* **2019**, *8*, 573.
- [42] R. R. Nair, M. Sepioni, I. Tsai, O. Lehtinen, J. Keinonen, A. V. Krasheninnikov, T. Thomson, A. K. Geim, I. V. Grigorieva, *Nat. Phys.* **2012**, *8*, 199.
- [43] R. Romero Aburto, T. N. Narayanan, Y. Nagaoka, T. Hasumura, T. M. Mitcham, T. Fukuda, P. J. Cox, R. R. Bouchard, T. Maekawa,

- D. S. Kumar, S. V. Torti, S. A. Mani, P. M. Ajayan, *Adv. Mater.* **2013**, 25, 5632.
- [44] N. Akhtar, G. Anemone, D. Farias, B. Holst, *Carbon* **2019**, 141, 451.
- [45] S. Kwon, J. Ko, K. Jeon, Y. Kim, J. Y. Park, *Nano Lett.* **2012**, 12, 6043.
- [46] K. Fan, J. Liu, X. Wang, Y. Liu, W. Lai, S. Gao, J. Qin, X. Liu, *J. Colloid Interface Sci.* **2018**, 531, 138.
- [47] K. Fan, X. Chen, X. Wang, X. Liu, Y. Liu, W. Lai, X. Liu, *ACS Appl. Mater. Interfaces* **2018**, 10, 28828.
- [48] K. Fan, J. Fu, X. Liu, Y. Liu, W. Lai, X. Liu, X. Wang, *Chem. Sci.* **2019**, 10, 5546.
- [49] K. Matsumura, S. Chiashi, S. Maruyama, J. Choi, *Appl. Surf. Sci.* **2018**, 432, 190.
- [50] Y. Liu, J. Li, S. Yi, X. Ge, X. Chen, J. Luo, *Carbon* **2020**, 167, 122.
- [51] C. Zhang, R. Huang, P. Wang, Y. Wang, Z. Zhou, H. Zhang, Z. Wu, L. Li, *ACS Appl. Mater. Interfaces* **2020**, 12, 58170.
- [52] M. C. Vu, I. Kim, W. K. Choi, C. Lim, M. A. Islam, S. Kim, *ACS Appl. Mater. Interfaces* **2020**, 12, 26413.
- [53] M. C. Vu, N. A. Thi Thieu, J. Lim, W. Choi, J. Chan Won, M. A. Islam, S. Kim, *Carbon* **2020**, 157, 741.
- [54] W. Huang, Q. Pei, Z. Liu, Y. Zhang, *Chem. Phys. Lett.* **2012**, 552, 97.
- [55] X. Wang, P. Wu, *ACS Appl. Mater. Interfaces* **2019**, 11, 21946.
- [56] X. Wang, P. Lu, Y. Li, H. Xiao, X. Liu, *RSC Adv.* **2016**, 6, 8763.
- [57] P. Gong, S. Ji, J. Wang, D. Dai, F. Wang, M. Tian, L. Zhang, F. Guo, Z. Liu, *Chem. Eng. J.* **2018**, 348, 438.
- [58] P. Gong, J. Du, D. Wang, B. Cao, M. Tian, Y. Wang, L. Sun, S. Ji, Z. Liu, *J. Mater. Chem. B* **2018**, 6, 2769.
- [59] V. Urbanova, F. Karlicky, A. Matej, F. Sembera, Z. Janousek, J. A. Perman, V. Ranc, K. Cepe, J. Michl, M. Otyepka, R. Zboril, *Nanoscale* **2016**, 8, 12134.
- [60] P. Gong, Q. Zhao, D. Dai, S. Zhang, Z. Tian, L. Sun, J. Ren, Z. Liu, *Chem. - Eur. J.* **2017**, 23, 17531.
- [61] S. Radhakrishnan, A. Samanta, P. M. Sudeep, K. L. Maldonado, S. A. Mani, G. Acharya, C. S. Tiwary, A. K. Singh, P. M. Ajayan, *Part. Part. Syst. Character.* **2017**, 34, 1600221.
- [62] P. Gong, L. Guo, M. Pang, D. Wang, L. Sun, Z. Tian, J. Li, Y. Zhang, Z. Liu, *J. Mater. Chem. B* **2018**, 6, 3068.
- [63] K. Guérin, M. Dubois, A. Houdayer, A. Hamwi, *J. Fluorine Chem.* **2012**, 134, 11.
- [64] H. An, Y. Li, Y. Gao, C. Cao, J. Han, Y. Feng, W. Feng, *Carbon* **2017**, 116, 338.
- [65] H. An, Y. Li, Y. Feng, Y. Cao, C. Cao, P. Long, S. Li, W. Feng, *Chem. Commun.* **2018**, 54, 2727.
- [66] G. Zhong, H. Chen, X. Huang, H. Yue, C. Lu, *Front. Chem.* **2018**, 6, 50.
- [67] H. Cheng, Y. Mao, J. Xie, Y. Lu, X. Zhao, *ACS Appl. Mater. Interfaces* **2019**, 11, 39737.
- [68] Y. Luan, J. Yin, K. Zhu, K. Cheng, J. Yan, K. Ye, G. Wang, D. Cao, *Chem. Eng. J.* **2020**, 392, 123668.
- [69] I. Jeon, M. J. Ju, J. Xu, H. Choi, J. Seo, M. Kim, I. T. Choi, H. M. Kim, J. C. Kim, J. Lee, H. K. Liu, H. K. Kim, S. Dou, L. Dai, J. Baek, *Adv. Funct. Mater.* **2015**, 25, 1170.
- [70] S. Peng, S. Yan, N. Wang, W. Nan, J. Wang, X. Chen, C. Wang, X. Qi, S. Dai, *RSC Adv.* **2018**, 8, 12701.
- [71] M. Mar, M. Dubois, K. Guérin, N. Batisse, B. Simon, P. Bernard, *Carbon* **2019**, 141, 6.
- [72] P. Kovaříček, Z. Bastl, V. Valeš, M. Kalbac, *Chem. - Eur. J.* **2016**, 22, 5404.
- [73] A. Bakandritsos, M. Pykal, P. Błoriski, P. Jakubec, D. D. Chronopoulos, K. Poláková, V. Georgakilas, K. Čépe, O. Tomanec, V. Ranc, A. B. Bourlinos, R. Zbořil, M. Otyepka, *ACS Nano* **2017**, 11, 2982.
- [74] V. Mazánek, A. Libánská, J. Šturala, D. Bouša, D. Sedmidubský, M. Pumera, Z. Janoušek, J. Plutnar, Z. Sofer, *Chem. - Eur. J.* **2017**, 23, 1956.
- [75] D. D. Chronopoulos, A. Bakandritsos, P. Lazar, M. Pykal, K. Čépe, R. Zbořil, M. Otyepka, *Chem. Mater.* **2017**, 29, 926.
- [76] J. Tuček, K. Holá, A. B. Bourlinos, P. Błoriski, A. Bakandritsos, J. Ugolotti, M. Dubecký, F. Karlický, V. Ranc, K. Čépe, M. Otyepka, R. Zbořil, *Nat. Commun.* **2017**, 8, 14525.
- [77] W. Lai, J. Liu, L. Luo, X. Wang, T. He, K. Fan, X. Liu, *Chem. Commun.* **2018**, 54, 10168.
- [78] D. D. Chronopoulos, M. Medved, P. Błoriski, Z. Nováček, P. Jakubec, O. Tomanec, A. Bakandritsos, V. Novotná, R. Zbořil, M. Otyepka, *Chem. Commun.* **2019**, 55, 1088.
- [79] H. Barès, A. Bakandritsos, M. Medved, J. Ugolotti, P. Jakubec, O. Tomanec, S. Kalytchuk, R. Zbořil, M. Otyepka, *Carbon* **2019**, 145, 251.
- [80] W. Lai, C. Wang, Y. Chen, T. He, K. Fan, X. Liu, X. Wang, *Langmuir* **2019**, 35, 6610.
- [81] F. Zhao, B. Pan, Y. Kong, L. Dong, C. Hu, Y. Sang, X. Zhou, B. Zuo, X. Dong, B. Li, W. Li, *Adv. Mater. Interfaces* **2019**, 6, 1801699.
- [82] A. Kouloumpis, D. D. Chronopoulos, G. Potsi, M. Pykal, J. Vlcek, M. Scheibe, M. Otyepka, *Chem. - Eur. J.* **2020**, 26, 6518.
- [83] F. Huang, Y. Li, X. Liu, W. Lai, K. Fan, X. Liu, X. Wang, *Chem. Commun.* **2021**, 57, 351.
- [84] W. Lai, Y. Yuan, X. Wang, Y. Liu, Y. Li, X. Liu, *Phys. Chem. Chem. Phys.* **2018**, 20, 489.
- [85] D. D. Chronopoulos, M. Medved, G. Potsi, O. Tomanec, M. Scheibe, M. Otyepka, *Chem. Commun.* **2020**, 56, 1936.
- [86] R. Stine, J. W. Ciszek, D. E. Barlow, W. Lee, J. T. Robinson, P. E. Sheehan, *Langmuir* **2012**, 28, 7957.
- [87] P. Gong, J. Wang, W. Sun, D. Wu, Z. Wang, Z. Fan, H. Wang, X. Han, S. Yang, *Nanoscale* **2014**, 6, 3316.
- [88] C. Bosch-Navarro, M. Walker, N. R. Wilson, J. P. Rourke, *J. Mater. Chem. C* **2015**, 3, 7627.
- [89] X. Ye, L. Ma, Z. Yang, J. Wang, H. Wang, S. Yang, *ACS Appl. Mater. Interfaces* **2016**, 8, 7483.
- [90] V. Urbanová, K. Holá, A. B. Bourlinos, K. Čépe, A. Ambrosi, A. H. Loo, M. Pumera, F. Karlický, M. Otyepka, R. Zbořil, *Adv. Mater.* **2015**, 27, 2305.
- [91] K. Fan, X. Liu, Y. Liu, Y. Li, Y. Chen, Y. Meng, X. Liu, W. Feng, L. Luo, *Carbon* **2020**, 167, 826.
- [92] S. Deng, D. Rhee, W. Lee, S. Che, B. Keisham, V. Berry, T. W. Odom, *Nano Lett.* **2019**, 19, 5640.
- [93] L. Bao, B. Zhao, V. Lloret, M. Halik, F. Hauke, A. Hirsch, *Angew. Chem., Int. Ed.* **2020**, 132, 6766.
- [94] J. Son, H. Ryu, J. Kwon, S. Huang, J. Yu, J. Xu, K. Watanabe, T. Taniguchi, E. Ji, S. Lee, Y. Shin, J. H. Kim, K. Kim, A. M. van der Zande, G. Lee, *Nano Lett.* **2021**, 21, 891.
- [95] J. Son, N. Buzov, S. Chen, D. Sung, H. Ryu, J. Kwon, S. Kim, S. Namiki, J. Xu, S. Hong, K. Watanabe, T. Taniguchi, W. P. King, G. H. Lee, A. M. van der Zande, *Adv. Mater.* **2019**, 31, 1903424.
- [96] W. H. Lee, J. W. Suk, H. Chou, J. Lee, Y. Hao, Y. Wu, R. Piner, D. Akinwande, K. S. Kim, R. S. Ruoff, *Nano Lett.* **2012**, 12, 2374.
- [97] J. Xie, C. Li, Z. Cui, X. Guo, *Adv. Funct. Mater.* **2015**, 25, 6519.
- [98] Y. Liu, T. Shi, T. Chen, W. He, M. Chen, D. Cao, *Sens. Actuators, B* **2019**, 281, 789.
- [99] A. Mathkar, T. N. Narayanan, L. B. Alemany, P. Cox, P. Nguyen, G. Gao, P. Chang, R. Romero-Aburto, S. A. Mani, P. M. Ajayan, *Part. Part. Syst. Character.* **2013**, 30, 266.
- [100] J. Xu, J. Yu, J. Liao, X. Yang, C. Wu, Y. Wang, L. Wang, C. Xie, L. Luo, *ACS Appl. Mater. Interfaces* **2019**, 11, 21702.
- [101] O. Jankovský, V. Mazánek, K. Klímová, D. Sedmidubský, J. Kosina, M. Pumera, Z. Sofer, *Chem. - Eur. J.* **2016**, 22, 17696.
- [102] C. Sun, Y. Feng, Y. Li, C. Qin, Q. Zhang, W. Feng, *Nanoscale* **2014**, 6, 2634.
- [103] H. Chang, J. Cheng, X. Liu, J. Gao, M. Li, J. Li, X. Tao, F. Ding, Z. Zheng, *Chem. - Eur. J.* **2011**, 17, 8896.
- [104] R. Tian, X. Jia, J. Yang, Y. Li, H. Song, *Chem. Eng. J.* **2020**, 395, 125104.



- [105] M. Zhang, L. Liu, T. He, G. Wu, P. Chen, *Mater. Lett.* **2016**, *171*, 191.
- [106] M. Zhu, X. Xie, Y. Guo, P. Chen, X. Ou, G. Yu, M. Liu, *Phys. Chem. Chem. Phys.* **2013**, *15*, 20992.
- [107] P. Gong, Z. Wang, J. Wang, H. Wang, Z. Li, Z. Fan, Y. Xu, X. Han, S. Yang, *J. Mater. Chem.* **2012**, *22*, 16950.
- [108] X. Wang, Y. Dai, J. Gao, J. Huang, B. Li, C. Fan, J. Yang, X. Liu, *ACS Appl. Mater. Interfaces* **2013**, *5*, 8294.
- [109] S. H. Cheng, K. Zou, F. Okino, H. R. Gutierrez, A. Gupta, N. Shen, P. C. Eklund, J. O. Sofo, J. Zhu, *Phys. Rev. B* **2010**, *81*, 205435.
- [110] Z. Wang, J. Wang, Z. Li, P. Gong, X. Liu, L. Zhang, J. Ren, H. Wang, S. Yang, *Carbon* **2012**, *50*, 5403.
- [111] K. Samanta, S. Some, Y. Kim, Y. Yoon, M. Min, S. M. Lee, Y. Park, H. Lee, *Chem. Commun.* **2013**, *49*, 8991.
- [112] F. Zhao, G. Zhao, X. Liu, C. Ge, J. Wang, B. Li, Q. Wang, W. Li, Q. Chen, *J. Mater. Chem. A* **2014**, *2*, 8782.
- [113] H. Aguilar-Bolados, A. Contreras-Cid, M. Yazdani-Pedram, G. Acosta-Villavicencio, M. Flores, P. Fuentealba, A. Neira-Carrillo, R. Verdejo, M. A. López-Manchado, *J. Colloid Interface Sci.* **2018**, *524*, 219.
- [114] M. Jahanshahi, E. Kowsari, V. Haddadi-Asl, M. Khoobi, B. Bazri, M. Aryafard, J. H. Lee, F. B. Kadumudi, S. Talebian, N. Kamaly, M. Mehrali, A. Dolatshahi-Pirouz, *Appl. Surf. Sci.* **2020**, *515*, 146071.
- [115] Y. Wu, W. Zhao, Y. Qiang, Z. Chen, L. Wang, X. Gao, Z. Fang, *Carbon* **2020**, *159*, 292.
- [116] X. Cai, Y. Luo, B. Liu, H. M. Cheng, *Chem. Soc. Rev.* **2018**, *47*, 6224.
- [117] L. Niu, J. N. Coleman, H. Zhang, H. Shin, M. Chhowalla, Z. Zheng, *Small* **2016**, *12*, 272.
- [118] J. N. Coleman, M. Lotya, A. O'Neill, S. D. Bergin, P. J. King, U. Khan, K. Young, A. Gaucher, S. De, R. J. Smith, I. V. Shvets, S. K. Arora, G. Stanton, H. Y. Kim, K. Lee, G. T. Kim, G. S. Duesberg, T. Hallam, J. J. Boland, J. J. Wang, J. F. Donegan, J. C. Grunlan, G. Moriarty, A. Shmeliov, R. J. Nicholls, J. M. Perkins, E. M. Grieveson, K. Theuvsissen, D. W. McComb, P. D. Nellist, et al., *Science* **2011**, *331*, 568.
- [119] K. Hou, P. Gong, J. Wang, Z. Yang, Z. Wang, S. Yang, *RSC Adv.* **2014**, *4*, 56543.
- [120] F. Zhou, H. Huang, C. Xiao, S. Zheng, X. Shi, J. Qin, Q. Fu, X. Bao, X. Feng, K. Müllen, Z. Wu, *J. Am. Chem. Soc.* **2018**, *140*, 8198.
- [121] P. Gong, Z. Yang, W. Hong, Z. Wang, K. Hou, J. Wang, S. Yang, *Carbon* **2015**, *83*, 152.
- [122] S. Wu, J. Mo, Y. Zeng, Y. Wang, A. Rawal, J. Scott, Z. Su, W. Ren, S. Chen, K. Wang, W. Chen, Y. Zhang, C. Zhao, X. Chen, *Small* **2019**, *16*, 1903397.
- [123] V. Mazanek, O. Jankovsky, J. Luxa, D. Sedmidubsky, Z. Janousek, F. Sembera, M. Mikulics, Z. Sofer, *Nanoscale* **2015**, *7*, 13646.
- [124] P. Meduri, H. Chen, J. Xiao, J. J. Martinez, T. Carlson, J. Zhang, Z. D. Deng, *J. Mater. Chem. A* **2013**, *1*, 7866.
- [125] X. Wang, W. Wang, D. Xu, Y. Liu, W. Lai, X. Liu, *Carbon* **2017**, *124*, 288.
- [126] B. Zhou, X. Qian, M. Li, J. Ma, L. Liu, C. Hu, Z. Xu, X. Jiao, *J. Nanopart. Res.* **2015**, *17*, 130.
- [127] H. Yang, M. Chen, H. Zhou, C. Qiu, L. Hu, F. Yu, W. Chu, S. Sun, L. Sun, *J. Phys. Chem. C* **2011**, *115*, 16844.
- [128] J. Plšek, K. A. Drogowska, M. Fridrichová, J. Vejpravová, M. Kalbáč, *Carbon* **2019**, *145*, 419.
- [129] X. Yu, K. Lin, K. Qiu, H. Cai, X. Li, J. Liu, N. Pan, S. Fu, Y. Luo, X. Wang, *Carbon* **2012**, *50*, 4512.
- [130] R. Jayasinghe, A. K. Thapa, R. R. Dharmasena, T. Q. Nguyen, B. K. Pradhan, H. S. Paudel, J. B. Jasinski, A. Sherehiy, M. Yoshio, G. U. Sumanasekera, *J. Power Sources* **2014**, *253*, 404.
- [131] B. Wang, J. Wang, J. Zhu, *ACS Nano* **2014**, *8*, 1862.
- [132] K. Tahara, T. Iwasaki, A. Matsutani, M. Hatano, *Appl. Phys. Lett.* **2012**, *101*, 163105.
- [133] C. R. Hickenboth, J. S. Moore, S. R. White, N. R. Sottos, J. Baudry, S. R. Wilson, *Nature* **2007**, *446*, 423.
- [134] B. R. Boswell, C. M. F. Mansson, J. M. Cox, Z. Jin, J. A. H. Romaniuk, K. P. Lindquist, L. Cegelski, Y. Xia, S. A. Lopez, N. Z. Burns, *Nat. Chem.* **2021**, *13*, 41.
- [135] J. Li, C. Nagamani, J. S. Moore, *Acc. Chem. Res.* **2015**, *48*, 2181.
- [136] K. Tahara, T. Iwasaki, S. Furuyama, A. Matsutani, M. Hatano, *Appl. Phys. Lett.* **2013**, *103*, 143106.
- [137] X. Wang, W. Wang, Y. Liu, M. Ren, H. Xiao, X. Liu, *Anal. Chem.* **2016**, *88*, 3926.
- [138] J. H. Lee, G. K. W. Koon, D. W. Shin, V. E. Fedorov, J. Choi, J. Yoo, B. Özyilmaz, *Adv. Funct. Mater.* **2013**, *23*, 3329.
- [139] A. B. Bourlinos, K. Safarova, K. Siskova, R. Zbořil, *Carbon* **2012**, *50*, 1425.
- [140] H. F. Bettinger, K. N. Kudin, G. E. Scuseria, *J. Phys. Chem. A* **2004**, *108*, 3016.
- [141] M. Dubecký, E. Otyepková, P. Lazar, F. Karlický, M. Petr, K. Čépe, P. Banáš, R. Zbořil, M. Otyepka, *J. Phys. Chem. Lett.* **2015**, *6*, 1430.
- [142] H. Touhara, F. Okino, *Carbon* **2000**, *38*, 241.
- [143] W. Lai, X. Wang, Y. Li, Y. Liu, T. He, K. Fan, X. Liu, *Carbon* **2018**, *132*, 271.
- [144] R. J. Kashtiban, M. A. Dyson, R. R. Nair, R. Zan, S. L. Wong, Q. Ramasse, A. K. Geim, U. Bangert, J. Sloan, *Nat. Commun.* **2014**, *5*, 4902.
- [145] Y. Sato, T. Kume, R. Hagiwara, Y. Ito, *Carbon* **2003**, *41*, 351.
- [146] Y. Wang, W. C. Lee, K. K. Manga, P. K. Ang, J. Lu, Y. P. Liu, C. T. Lim, K. P. Loh, *Adv. Mater.* **2012**, *24*, 4285.
- [147] V. Mazánek, L. Pavlikova, P. Marvan, J. Plutnar, M. Pumera, Z. Sofer, *Appl. Mater. Today* **2019**, *15*, 343.
- [148] B. Li, K. Fan, X. Ma, Y. Liu, T. Chen, Z. Cheng, X. Wang, J. Jiang, X. Liu, *J. Colloid Interface Sci.* **2016**, *478*, 36.
- [149] S. D. Costa, J. Ek Weis, O. Frank, Z. Bastl, M. Kalbac, *Carbon* **2015**, *84*, 347.
- [150] Y. Sato, K. Itoh, R. Hagiwara, T. Fukunaga, Y. Ito, *Carbon* **2004**, *42*, 3243.
- [151] X. Wang, W. Wang, Y. Liu, M. Ren, H. Xiao, X. Liu, *Phys. Chem. Chem. Phys.* **2016**, *18*, 3285.
- [152] W. Lai, D. Xu, X. Wang, Z. Wang, Y. Liu, X. Zhang, X. Liu, *Phys. Chem. Chem. Phys.* **2017**, *19*, 19442.
- [153] H. Sahin, E. Torun, C. Bacaksiz, S. Horzum, J. Kang, R. T. Senger, F. M. Peeters, *Wiley Interdiscip. Rev.: Comput. Mol. Sci.* **2016**, *6*, 351.
- [154] K. Fan, L. Peng, Y. Liu, Y. Li, Y. Chen, Y. Meng, X. Liu, W. Feng, X. Wang, *ACS Appl. Mater. Interfaces* **2020**, *12*, 40662.
- [155] K. Fan, X. Chen, X. Liu, Y. Liu, W. Lai, Y. Chen, X. Liu, X. Wang, *Carbon* **2020**, *165*, 386.
- [156] F. Karlický, M. Otyepka, *Ann. Phys.* **2014**, *526*, 408.
- [157] Z. Yang, L. Wang, W. Sun, S. Li, T. Zhu, W. Liu, G. Liu, *Appl. Surf. Sci.* **2017**, *401*, 146.
- [158] H. Amii, K. Uneyama, *Chem. Rev.* **2009**, *109*, 2119.
- [159] D. O'Hagan, *Chem. Soc. Rev.* **2008**, *37*, 308.
- [160] T. Chen, X. Wang, Y. Liu, B. Li, Z. Cheng, Z. Wang, W. Lai, X. Liu, *Phys. Chem. Chem. Phys.* **2017**, *19*, 5504.
- [161] M. Ren, X. Wang, C. Dong, B. Li, Y. Liu, T. Chen, P. Wu, Z. Cheng, X. Liu, *Phys. Chem. Chem. Phys.* **2015**, *17*, 24056.
- [162] H. Wang, M. Narasaki, Z. Zhang, K. Takahashi, J. Chen, X. Zhang, *Sci. Rep.* **2020**, *10*, 17562.
- [163] M. Razaghi, A. Ramazani, M. Khoobi, T. Mortezaazadeh, E. A. Aksoy, T. T. Küçükilinc, *J. Drug Delivery Sci. Technol.* **2020**, *60*, 101967.
- [164] X. Zheng, M. Zhang, X. Shi, G. Wang, L. Zheng, Y. Yu, A. Huang, P. K. Chu, H. Gao, W. Ren, Z. Di, X. Wang, *Adv. Funct. Mater.* **2015**, *25*, 1805.
- [165] X. Ding, L. Song, T. He, C. Sun, Y. Cai, C. Zeng, K. Zhang, X. Zhang, X. Zhang, B. Zhang, *Diamond Relat. Mater.* **2020**, *109*, 108010.
- [166] M. Sahoo, J. Wang, Y. Nishina, Z. Liu, J. Bow, C. Lai, *Appl. Surf. Sci.* **2020**, *499*, 143839.

- [167] K. Ho, C. Huang, J. Liao, W. Zhang, L. Li, C. Lai, C. Su, *Sci. Rep.* **2015**, *4*, 5893.
- [168] X. Cui, S. Yang, X. Yan, J. Leng, S. Shuang, P. M. Ajayan, Z. Zhang, *Adv. Funct. Mater.* **2016**, *26*, 5708.
- [169] Y. Liu, Y. Shen, L. Sun, J. Li, C. Liu, W. Ren, F. Li, L. Gao, J. Chen, F. Liu, Y. Sun, N. Tang, H. Cheng, Y. Du, *Nat. Commun.* **2016**, *7*, 10921.
- [170] J. Zhao, C. R. Cabrera, Z. Xia, Z. Chen, *Carbon* **2016**, *104*, 56.
- [171] X. Wang, W. Wang, R. Qin, D. Xu, Y. Li, A. Ou, W. Lai, Y. Liu, X. Liu, *Chem. Eng. J.* **2018**, *354*, 261.
- [172] J. Liu, Z. Bao, Y. Cui, E. J. Dufek, J. B. Goodenough, P. Khalifah, Q. Li, B. Y. Liaw, P. Liu, A. Manthiram, Y. S. Meng, V. R. Subramanian, M. F. Toney, V. V. Viswanathan, M. S. Whittingham, J. Xiao, W. Xu, J. Yang, X. Yang, J. Zhang, *Nat. Energy* **2019**, *4*, 180.
- [173] R. Yazami, A. Hamwi, K. Guérin, Y. Ozawa, M. Dubois, J. Giraudet, F. Masin, *Electrochem. Commun.* **2007**, *9*, 1850.
- [174] G. G. Amatucci, N. Pereira, *J. Fluorine Chem.* **2007**, *128*, 243.
- [175] L. Zhan, S. Yang, Y. Wang, Y. Wang, L. Ling, X. Feng, *Adv. Mater. Interfaces* **2014**, *1*, 1300149.
- [176] H. L. Poh, Z. Sofer, K. Klimova, M. Pumera, *J. Mater. Chem. C* **2014**, *2*, 5198.
- [177] E. C. Vermisoglou, P. Jakubec, A. Bakandritsos, M. Pykal, S. Talande, V. Kupka, R. Zboril, M. Otyepka, *Chem. Mater.* **2019**, *31*, 4698.
- [178] R. Fan, B. Yang, Z. Li, D. Ma, W. Yuan, J. Ma, H. Ren, *RSC Adv.* **2020**, *10*, 31881.
- [179] M. A. Reddy, B. Breitung, M. Fichtner, *ACS Appl. Mater. Interfaces* **2013**, *5*, 11207.
- [180] P. Lam, R. Yazami, *J. Power Sources* **2006**, *153*, 354.
- [181] S. Huang, Y. Li, Y. Feng, H. An, P. Long, C. Qin, W. Feng, *J. Mater. Chem. A* **2015**, *3*, 23095.
- [182] W. Liu, H. Li, J. Xie, Z. Fu, *ACS Appl. Mater. Interfaces* **2014**, *6*, 2209.
- [183] D. Damien, P. M. Sudeep, T. N. Narayanan, M. R. Anantharaman, P. M. Ajayan, M. M. Shaijumon, *RSC Adv.* **2013**, *3*, 25702.
- [184] E. Ranganamy, J. Li, G. Sahu, N. Dudney, C. Liang, *J. Am. Chem. Soc.* **2014**, *136*, 6874.
- [185] F. Jiang, J. Zhang, N. Li, C. Liu, Y. Zhou, X. Yu, L. Sun, Y. Song, S. Zhang, Z. Wang, *J. Chem. Technol. Biotechnol.* **2019**, *94*, 3530.
- [186] A. Vizintin, M. Lozinšek, R. K. Chellappan, D. Foix, A. Krajnc, G. Mali, G. Drazic, B. Genorio, R. Dedryvère, R. Dominko, *Chem. Mater.* **2015**, *27*, 7070.
- [187] R. Yogapriya, K. R. D. Kasibhatta, *ACS Appl. Nano Mater.* **2020**, *3*, 5816.
- [188] K. Jayaramulu, K. K. R. Datta, C. Rösler, M. Petr, M. Otyepka, R. Zboril, R. A. Fischer, *Angew. Chem., Int. Ed.* **2016**, *55*, 1178.
- [189] S. Zhou, W. Li, W. Zhao, Q. Li, C. Liu, Z. Fang, X. Gao, *Prog. Org. Coat.* **2020**, *147*, 105800.
- [190] W. Wang, Z. Xu, X. Zhang, A. Wimmer, E. Shi, Y. Qin, X. Zhao, B. Zhou, L. Li, *Chem. Eng. J.* **2018**, *343*, 61.
- [191] E. Otyepková, P. Lazar, K. Čépe, O. Tomanec, M. Otyepka, *Appl. Mater. Today* **2016**, *5*, 142.
- [192] F. Karlický, E. Otyepková, R. Lo, M. Pitoňák, P. Jurečka, M. Pykal, P. Hobza, M. Otyepka, *J. Chem. Theory Comput.* **2017**, *13*, 1328.
- [193] Q. Li, X. Liu, S. Kim, V. B. Shenoy, P. E. Sheehan, J. T. Robinson, R. W. Carpick, *Nano Lett.* **2014**, *14*, 5212.
- [194] Y. Liu, J. Li, X. Chen, J. Luo, *ACS Appl. Mater. Interfaces* **2019**, *11*, 40470.
- [195] N. Nomedo-Martyr, E. Disa, P. Thomas, L. Romana, J. Mansot, M. Dubois, K. Guérin, W. Zhang, A. Hamwi, *J. Fluorine Chem.* **2012**, *144*, 10.
- [196] K. Delbé, P. Thomas, D. Himmel, J. L. Mansot, M. Dubois, K. Guérin, C. Delabarre, A. Hamwi, *Tribol. Lett.* **2010**, *37*, 31.
- [197] F. Lei, M. Yang, F. Jiang, H. Zhang, Z. Zhang, D. Sun, *Chem. Eng. J.* **2019**, *360*, 673.
- [198] K. Fan, Y. Wang, Y. Liu, Y. Li, Y. Chen, Y. Meng, X. Liu, W. Feng, X. Wang, *Adv. Mater. Interfaces* **2020**, *7*, 2000915.
- [199] T. Bharathidasan, T. N. Narayanan, S. Sathyanarayanan, S. S. Sreejakumari, *Carbon* **2015**, *84*, 207.
- [200] Y. Sin, C. Huang, C. Lin, J. Chih, Y. Hsieh, I. Tsao, J. Li, C. Su, *Carbon* **2020**, *169*, 248.
- [201] A. L. Moore, L. Shi, *Mater. Today* **2014**, *17*, 163.
- [202] H. Chen, V. V. Ginzburg, J. Yang, Y. Yang, W. Liu, Y. Huang, L. Du, B. Chen, *Prog. Polym. Sci.* **2016**, *59*, 41.
- [203] W. Dai, T. Ma, Q. Yan, J. Gao, X. Tan, L. Lv, H. Hou, Q. Wei, J. Yu, J. Wu, Y. Yao, S. Du, R. Sun, N. Jiang, Y. Wang, J. Kong, C. Wong, S. Maruyama, C. Lin, *ACS Nano* **2019**, *13*, 11561.
- [204] J. Chen, X. Huang, B. Sun, P. Jiang, *ACS Nano* **2018**, *13*, 337.
- [205] Y. Yao, X. Zeng, F. Wang, R. Sun, J. Xu, C. Wong, *Chem. Mater.* **2016**, *28*, 1049.
- [206] X. Zeng, J. Sun, Y. Yao, R. Sun, J. Xu, C. Wong, *ACS Nano* **2017**, *11*, 5167.
- [207] H. Cheng, X. Sha, L. Chen, A. C. Cooper, M. Foo, G. C. Lau, W. H. Bailey III, G. P. Pez, *J. Am. Chem. Soc.* **2009**, *131*, 17732.
- [208] W. Kang, S. Li, *RSC Adv.* **2018**, *8*, 23459.
- [209] Y. H. Kim, J. S. Park, Y. Choi, S. Y. Park, S. Y. Lee, W. Sohn, Y. Shim, J. Lee, C. R. Park, Y. S. Choi, B. H. Hong, J. H. Lee, W. H. Lee, D. Lee, H. W. Jang, *J. Mater. Chem. A* **2017**, *5*, 19116.
- [210] W. Zhang, G. Xu, L. Chen, S. Pan, X. Jing, J. Wang, S. Han, *Int. J. Hydrogen Energy* **2017**, *42*, 15262.
- [211] J. Schrier, *ACS Appl. Mater. Interfaces* **2011**, *3*, 4451.
- [212] H. Zhang, L. Fan, H. Dong, P. Zhang, K. Nie, J. Zhong, Y. Li, J. Guo, X. Sun, *ACS Appl. Mater. Interfaces* **2016**, *8*, 8652.
- [213] T. Wu, Q. Xue, C. Ling, M. Shan, Z. Liu, Y. Tao, X. Li, *J. Phys. Chem. C* **2014**, *118*, 7369.
- [214] P. Kumar, V. Sharma, F. A. Reboledo, L. Yang, R. Pushpa, *Sci. Rep.* **2016**, *6*, 31841.
- [215] Q. Feng, Y. Zheng, J. Li, L. Jiang, Y. Lin, Q. Ye, L. Chen, Z. Huang, *Carbon* **2018**, *132*, 691.
- [216] Y. Zheng, X. Wan, N. Tang, Q. Feng, F. Liu, Y. Du, *Carbon* **2015**, *89*, 300.
- [217] X. Hong, S. H. Cheng, C. Herding, J. Zhu, *Phys. Rev. B* **2011**, *83*, 085410.
- [218] I. V. Antonova, I. I. Kurkina, A. K. Gutakovskii, I. A. Kotin, A. I. Ivanov, N. A. Nebogatikova, R. A. Soots, S. A. Smagulova, *Mater. Des.* **2019**, *164*, 107526.
- [219] X. Wang, Y. Dai, W. Wang, M. Ren, B. Li, C. Fan, X. Liu, *ACS Appl. Mater. Interfaces* **2014**, *6*, 16182.
- [220] F. Withers, T. H. Bointon, M. Dubois, S. Russo, M. F. Craciun, *Nano Lett.* **2011**, *11*, 3912.
- [221] S. Hajian, X. Zhang, P. Khakbaz, S. Tabatabaei, D. Maddipatla, B. B. Narakathu, R. G. Blair, M. Z. Atashbar, *IEEE Sens. J.* **2020**, *20*, 7517.
- [222] M. Kolešnik-Gray, V. I. Sysoev, S. Gollwitzer, D. V. Pinakov, G. N. Chekhova, L. G. Bulusheva, A. V. Okotrub, V. Krstić, *Adv. Electron. Mater.* **2018**, *4*, 1800073.
- [223] X. Ye, P. Gong, J. Wang, H. Wang, S. Ren, S. Yang, *Composites, Part A* **2015**, *75*, 96.
- [224] F. Withers, M. Dubois, A. K. Savchenko, *Phys. Rev. B* **2010**, *82*, 073403.
- [225] W. Lee, J. T. Robinson, D. Gunlycke, R. R. Stine, C. R. Tamanaha, W. P. King, P. E. Sheehan, *Nano Lett.* **2011**, *11*, 5461.
- [226] A. L. Walter, H. Sahin, K. Jeon, A. Bostwick, S. Horzum, R. Koch, F. Speck, M. Ostler, P. Nagel, M. Merz, S. Schupler, L. Moreschini, Y. J. Chang, T. Seyller, F. M. Peeters, K. Horn, E. Rotenberg, *ACS Nano* **2014**, *8*, 7801.
- [227] F. Withers, S. Russo, M. Dubois, M. F. Craciun, *Nanoscale Res. Lett.* **2011**, *6*, 526.
- [228] C. Su, C. Yang, B. Jhang, Y. Hsieh, Y. Sin, C. Huang, *ACS Appl. Mater. Interfaces* **2020**, *12*, 10233.

- [229] X. Yin, Y. Feng, Q. Zhao, Y. Li, S. Li, H. Dong, W. Hu, W. Feng, *J. Mater. Chem. C* **2018**, *6*, 6378.
- [230] Y. Li, X. Wang, W. Wang, R. Qin, W. Lai, A. Ou, Y. Liu, X. Liu, *J. Phys. Chem. C* **2019**, *123*, 584.
- [231] S. Feng, Z. Zhong, Y. Wang, W. Xing, E. Drioli, *J. Membr. Sci.* **2018**, *549*, 332.
- [232] G. Guenoun, J. Faou, G. Régnier, N. Schmitt, S. Roux, *Polymer* **2020**, *193*, 122333.
- [233] J. M. Cox, B. A. Wright, W. W. Wright, *J. Appl. Polym. Sci.* **1964**, *8*, 2935.
- [234] X. Cai, Z. Jiang, X. Zhang, T. Gao, K. Yue, X. Zhang, *RSC Adv.* **2018**, *8*, 11367.
- [235] P. Lazar, C. K. Chua, K. Holá, R. Zbořil, M. Otyepka, M. Pumera, *Small* **2015**, *11*, 3790.
- [236] F. Marsusi, N. D. Drummond, M. J. Verstraete, *Carbon* **2019**, *144*, 615.
- [237] P. V. Bakharev, M. Huang, M. Saxena, S. W. Lee, S. H. Joo, S. O. Park, J. Dong, D. C. Camacho-Mojica, S. Jin, Y. Kwon, M. Biswal, F. Ding, S. K. Kwak, Z. Lee, R. S. Ruoff, *Nat. Nanotechnol.* **2020**, *15*, 59.
- [238] W. Lee, M. Haydell, J. T. Robinson, A. R. Laracuente, E. Cimpoiasu, W. P. King, P. E. Sheehan, *ACS Nano* **2013**, *7*, 6219.
- [239] N. A. Nebogatikova, I. V. Antonova, A. I. Ivanov, V. A. Demin, D. G. Kvashnin, A. Olejniczak, A. K. Gutakovskii, K. A. Kornieieva, P. L. J. Renault, V. A. Skuratov, L. A. Chernozatonskii, *Nanotechnology* **2020**, *31*, 295602.
- [240] R. D. Yamaletdinov, Y. A. Nikiforov, L. G. Bulusheva, A. V. Okotrub, *Nanoscale* **2021**, *13*, 1206.
- [241] O. Y. Posudievsky, A. S. Kondratyuk, O. A. Kozarenko, V. V. Cherepanov, G. I. Dovbeshko, V. G. Koshechko, V. D. Pokhodenko, *Carbon* **2019**, *152*, 274.
- [242] D. Voylov, T. Saito, B. Lokitz, D. Uhrig, Y. Wang, A. Agapov, A. Holt, V. Bocharova, A. Kisliuk, A. P. Sokolov, O. R. T. U. Oak Ridge National Laboratory ORNL, *ACS Macro Lett.* **2016**, *5*, 199.
- [243] X. Liu, X. Li, Y. Li, R. Qin, F. Huang, X. Wang, X. Liu, *Ind. Eng. Chem. Res.* **2021**, *60*, 875.
- [244] J. Yang, Z. Zeng, J. Kang, S. Betzler, C. Czarnik, X. Zhang, C. Ophus, C. Yu, K. Bustillo, M. Pan, J. Qiu, L. Wang, H. Zheng, *Nat. Mater.* **2019**, *18*, 970.
- [245] L. Yang, R. Zhang, B. Liu, J. Wang, S. Wang, M. Han, Z. Zhang, *Angew. Chem., Int. Ed.* **2014**, *53*, 10109.
- [246] Z. Komeily-Nia, L. Qu, J. Li, *Small Sci.* **2021**, *1*, 2000026.
- [247] M. Medved, G. Zoppellaro, J. Ugolotti, D. Matochova, P. Lazar, T. Pospisil, A. Bakandritsos, J. Tucek, R. Zboril, M. Otyepka, *Nanoscale* **2018**, *10*, 4696.
- [248] W. Lai, D. Xu, X. Wang, Z. Wang, Y. Liu, X. Zhang, Y. Li, X. Liu, *Phys. Chem. Chem. Phys.* **2017**, *19*, 24076.
- [249] T. He, Z. Xing, Y. Wang, D. Wu, Y. Liu, X. Liu, *Polym. Chem.* **2020**, *11*, 5693.
- [250] T. He, X. Liu, Y. Wang, D. Wu, Y. Liu, X. Liu, *Appl. Surf. Sci.* **2020**, *529*, 147017.
- [251] J. Lv, Z. Cheng, H. Wu, T. He, J. Qin, X. Liu, *Composites, Part B* **2020**, *182*, 107608.
- [252] Y. Que, Z. Huang, C. Feng, Y. Yang, X. Huang, *ACS Macro Lett.* **2016**, *5*, 1339.
- [253] P. H. Tan, W. P. Han, W. J. Zhao, Z. H. Wu, K. Chang, H. Wang, Y. F. Wang, N. Bonini, N. Marzari, N. Pugno, G. Savini, A. Lombardo, A. C. Ferrari, *Nat. Mater.* **2012**, *11*, 294.
- [254] X. Liu, Z. Hao, E. Khalaf, J. Y. Lee, Y. Ronen, H. Yoo, D. Haei Najafabadi, K. Watanabe, T. Taniguchi, A. Vishwanath, P. Kim, *Nature* **2020**, *583*, 221.
- [255] H. Zhu, Z. Lai, Y. Fang, X. Zhen, C. Tan, X. Qi, D. Ding, P. Chen, H. Zhang, K. Pu, *Small* **2017**, *13*, 1604139.
- [256] Y. Yan, J. Gong, J. Chen, Z. Zeng, W. Huang, K. Pu, J. Liu, P. Chen, *Adv. Mater.* **2019**, *31*, 1808283.
- [257] X. Hong, K. Zou, B. Wang, S. Cheng, J. Zhu, *Phys. Rev. Lett.* **2012**, *108*, 226602.
- [258] G. Potsi, A. B. Bourlinos, V. Mouselimis, K. Poláková, N. Chalmpes, D. Gournis, S. Kalytchuk, O. Tomanec, P. Błóński, M. Medved, P. Lazar, M. Otyepka, R. Zbořil, *Appl. Mater. Today* **2019**, *17*, 112.
- [259] I. Papadakis, D. Kyrginas, A. Stathis, S. Couris, G. Potsi, A. B. Bourlinos, O. Tomanec, M. Otyepka, R. Zboril, *J. Phys. Chem. C* **2019**, *123*, 25856.
- [260] A. Stathis, I. Papadakis, N. Karampitsos, S. Couris, G. Potsi, A. B. Bourlinos, M. Otyepka, R. Zboril, *ChemPlusChem* **2019**, *84*, 1288.



**Xinyu Chen** received his B.S. in 2020 in polymer science and engineering from Sichuan University, China. Afterward, he has been pursuing his Ph.D. degree under the supervision of Dr. Xu Wang at the College of Polymer Science and Engineering, Sichuan University. His research interests cover the application of fluorinated graphene materials and the organic synthesis of graphene nanoribbons.





**Kun Fan** has been a Ph.D. student in Dr. Xiangyang Liu's group at Sichuan University since 2017. His current research is focused on the preparations and derivative modifications of fluorinated carbon nanomaterials and their potential applications in photoelectricity, lubrication, energy conversion, and polymer-based nanocomposites.



**Xiangyang Liu** is currently a full professor at the College of Polymer Science and Engineering, Sichuan University. He received his Ph.D. in 2006 for high-performance heat-resistant polymer materials from Sichuan University. His current scientific interests are developing novel fluorinated nanomaterials, high-performance heat-resistant polymer materials and their composite materials, and new technologies for the surface/interfacial modification of polymer materials.



**Wei Feng** received his Ph.D. in 2000 from the Xi'an Jiaotong University of China after studying the optical–electrical properties and device applications of novel conducting polymers, and then worked at Osaka University and Tsinghua University as a JSPS fellow and postdoctoral researcher, respectively. In 2004, he became a full professor at Tianjin University, where he works on functional nanocarbon materials.



**Xu Wang** is now an associate professor at the College of Polymer Science and Engineering, Sichuan University. He received his Ph.D. degree in materials science in 2014 from Sichuan University and then worked at the University of New Brunswick and Technische Universitaet Dresden as a postdoctoral researcher and visiting scholar, respectively. His current scientific interests include the synthesis of novel nanocarbon material fluorides, high-performance polymers, and their nanocomposites.